LEVEL II

THE DESIGN AND ANALYSIS OF TURBOMACHINERY IN AN INCOMPRESSIBLE, STEADY FLOW USING THE STREAMLINE CURVATURE METHOD

Mark W. McBride

Technical Memorandum
File No. TM 79-33
February 13, 1979
Contract No. N00024-79-C-6043

Copy No. 6

The Pennsylvania State University
APPLIED RESEARCH LABORATORY
Post Office Box 30
State College, Pa. 16801

Approved for Public Release
Distribution Unlimited

NAVY DEPARTMENT

NAVAL SEA SYSTEMS COMMAND

UNCLASSIFIED

SECURITY CLASSIFICATION OF THIS PAGE (When Date Entered)

REPORT DOCUMENTATION PAGE

READ INSTRUCTIONS BEFORE COMPLETING FORM

1. REPORT NUMBER: TM 79-33

2. GOVT ACCESSION NO.

3. RECIPIENT'S CATALOG NUMBER

4. TITLE (and Subtitle): THE DESIGN AND ANALYSIS OF TURBOMACHINERY IN AN INCOMPRESSIBLE, STEADY FLOW USING THE STREAMLINE CURVATURE METHOD

5. TYPE OF REPORT & PERIOD COVERED: Technical Memorandum memo

6. PERFORMING ORG. REPORT NUMBER

7. AUTHOR(s): Mark W. McBride

8. CONTRACT OR GRANT NUMBER(s): N00024-79-C-6043

9. PERFORMING ORGANIZATION NAME AND ADDRESS
Applied Research Laboratory
Post Office Box 30
State College, PA 16801

10. PROGRAM ELEMENT, PROJECT, TASK AREA & WORK UNIT NUMBERS

11. CONTROLLING OFFICE NAME AND ADDRESS
Naval Sea Systems Command, Code 0351, Washington, DC 20362 and Naval Ocean Systems Command, San Diego, CA 92152

12. REPORT DATE: February 13, 1979

13. NUMBER OF PAGES: 161

14. MONITORING AGENCY NAME & ADDRESS (if different from Controlling Office)

15. SECURITY CLASS (of this report): UNCLASSIFIED

15a. DECLASSIFICATION/DOWNGRADING SCHEDULE

16. DISTRIBUTION STATEMENT (of this Report)
Approved for public release. Distribution unlimited.
Per NAVSEA - March 30, 1979

17. DISTRIBUTION STATEMENT (of the abstract entered in Block 20, if different from Report)

ARL/PSU/TM-79-33

18. SUPPLEMENTARY NOTES

19. KEY WORDS (Continue on reverse side if necessary and identify by block number)
turbomachinery
streamline
hydrodynamics
curvature

20. ABSTRACT (Continue on reverse side if necessary and identify by block number)

The design of new and more efficient turbomachinery requires an improved understanding of the fluid flow phenomena associated with the duct and blading required for the operation of such devices. In recent years, the digital computer has made possible the solution of equations of motion pertinent to this field. The study described here deals with the design and analysis of turbomachinery in an incompressible, steady flow, such as hydraulic pumps

DD FORM 1 JAN 73 1473 EDITION OF 1 NOV 65 IS OBSOLETE

UNCLASSIFIED

SECURITY CLASSIFICATION OF THIS PAGE (When Data Entered)

391 007

and turbines. The basic numerical approach used in the analysis of these devices is the Streamline Curvature Method.

The development of a turbomachine design method requires an accurate model of the through-flow describing the spatial variation of the velocity and pressure in the fluid. Equations of motion are developed in a way that allows the modeling of the blade row spanwise and chordwise loading distributions on a blade row and determination of their effect on the through-flow. The equations are solved using the Streamline Curvature Method with the effects of viscosity and turbulence included in an empirical fashion due to the complexity of the governing equations.

Once the turbomachine performance and the subsequent through-flow solutions have been determined, the airfoil-shaped blades must be specified to produce the prescribed flow field. An empirical method of designing airfoils has been developed by G. F. Wislicenus. This method, the Mean Streamline Method, relies on correlations of performance data of blades tested as two-dimensional cascades to construct a blade camber line using the theoretical mean flow streamline and an offset distribution. The offset distribution is dependent on a number of geometric and flow variables. An analysis was performed to extend the range of applicability of the Mean Streamline Method on a new correlation developed to aid in the design of airfoil sections.

Further improvement of turbomachine performance and the development of a rational three-dimensional solution of a turbomachine through-flow requires an analytical approach to blade section design. A Streamline Curvature Method was developed to solve the indirect or design problem for blades in a cascade. The properties of the flow at the blade row inlet and exit are specified along with the loading distribution along the blade chord that is desired. A blade-to-blade analysis is performed that satisfies the equations of motion and iteratively determines an airfoil shape that will perform as specified. The effects of the blade surface boundary layers on the flow are included in an empirical fashion. A result of this procedure is a blade-to-blade flow solution that can be used to construct a three-dimensional representation of the velocity and pressure fields in the turbomachine.

Experimental investigations were performed to validate each of the analysis and design methods described. In general, the performance of the various test articles was in agreement with predictions. It is apparent, however, that phenomena associated with turbulent and viscous flows require more sophisticated modeling than those used in this study.

ABSTRACT

The design of new and more efficient turbomachinery requires an improved understanding of the fluid flow phenomena associated with the duct and blading required for the operation of such devices. In recent years, the digital computer has made possible the solution of equations of motion pertinent to this field. The study described here deals with the design and analysis of turbomachinery in an incompressible, steady flow, such as hydraulic pumps and turbines. The basic numerical approach utilized in the analysis of these devices is the Streamline Curvature Method.

The development of a turbomachine design method requires an accurate model of the through-flow describing the spatial variation of the velocity and pressure in the fluid. Equations of motion are developed in a way that allows the modeling of the blade row spanwise and chordwise loading distributions on a blade row and determination of their effect on the through-flow. The equations are solved using the Streamline Curvature Method with the effects of viscosity and turbulence included in an empirical fashion due to the complexity of the governing equations.

Once the turbomachine performance and the subsequent through-flow solutions have been determined, the airfoil-shaped blades must be specified to produce the prescribed flow field. An empirical method of designing airfoils has been developed by G. F. Wislicenus. This method, the Mean Streamline Method, relies on correlations of performance data of blades tested as two-dimensional cascades to construct a blade camber line using the theoretical mean flow streamline and an offset

distribution. The offset distribution is dependent on a number of geometric and flow variables. An analysis was performed to extend the range of applicability of the Mean Streamline Method on a new correlation developed to aid in the design of airfoil section

Further improvement of turbomachine performance and the development of a rational three-dimensional solution of a turbomachine through-flow requires an analytical approach to blade section design. A Streamline Curvature Method was developed to solve the indirect or design problem for blades in a cascade. The properties of the flow at the blade row inlet and exit are specified along with the loading distribution along the blade chord that is desired. A blade-to-blade analysis is performed that satisfies the equations of motion and iteratively determines an airfoil shape that will perform as specified. The effects of the blade surface boundary layers on the flow are included in an empirical fashion. A result of this procedure is a blade-to-blade flow solution that can be used to construct a three-dimensional representation of the velocity and pressure fields in the turbomachine.

Experimental investigations were performed to validate each of the analysis and design methods described. In general, the performance of the various test articles was in agreement with predictions. It is apparent, however, that phenomena associated with turbulent and viscous flows require more sophisticated modeling than those used in this study.

TABLE OF CONTENTS

	Page
ABSTRACT	iii
LIST OF FIGURES	vii
NOMENCLATURE	xii
ACKNOWLEDGEMENTS	xv
I. A GENERAL STATEMENT OF THE PROBLEM AND ITS SOLUTION	1
II. STATE OF THE ART	7
III. ANALYSIS AND DESIGN TECHNIQUE	14
IV. THE STREAMLINE CURVATURE METHOD OF THROUGH-FLOW ANALYSIS	17
4.1 Development of the Equations of Motion	18
4.2 The Effects of Blade Rows	27
4.3 The Effects of Viscosity and Turbulence	31
4.4 Use of the Streamline Curvature Method	32
V. THE CORRELATIONAL MEAN STREAMLINE METHOD	37
5.1 Introduction	38
5.2 The Computerized Analysis of Cascade Data	39
5.3 Evaluation of the Cascade Data	43
5.4 Computation of the Offset Distribution	51
5.5 Numerical Description of the Offset Distribution	52
5.6 Estimation of the Blade Pressure Distribution	55
5.7 Summary	57
VI. AXIAL FLOW PUMP DESIGN EXAMPLE	58
6.1 Flow Field Calculations Through the Axial Flow Pump	59

Page

6.2 Detailed Blade Section Design 66

6.3 Axial Flow Pump Tests 66

6.4 Test Procedure 70

6.5 Test Results 73

6.6 Summary 73

VII. CASCADE BLADE SECTION DESIGN USING THE STREAMLINE CURVATURE METHOD--GENERAL STATEMENT 79

VIII. CASCADE BLADE SECTION DESIGN USING THE STREAMLINE CURVATURE METHOD--THE NUMERICAL METHOD 85

8.1 Development of the Numerical Method 85

8.2 Definition of a Cascade Design Test Case 105

8.3 Results of Cascade Airfoil Design Calculations . . . 107

IX. EXPERIMENTAL PERFORMANCE VERIFICATION OF THE STREAMLINE CURVATURE CASCADE BLADE DESIGN METHOD 109

9.1 Cascade Blade Test Experimental Apparatus 111

9.2 Comparison of the Analytical and Experimental Pressure Distribution 124

9.3 Comparison of the Analytical and Experimental Flow Fields 130

9.4 Summary of the Analytical and Experimental Comparisons 150

X. SUMMARY, CONCLUSIONS, AND RECOMMENDATIONS FOR FURTHER RESEARCH 152

10.1 Summary and Conclusions 152

10.2 Recommendations for Further Research 156

REFERENCES 159

LIST OF FIGURES

Figure	Title	Page
1	Basic Turbomachine Types	2
2	Generalized Velocity Components in an Axisymmetric Duct	4
3	General Description of Computation Planes in a Turbomachine Blade Row	9
4	General Reference Station Parameters (Meridional Plane)	19
5	Differential Streamtube Element	21
6	Blade Force Components	29
7	Detail View of the Streamlines Calculated Through Two Blade Rows	33
8	Streamlines in a Francis-Type Turbine	34
9	Comparison of Theoretical and Experimental Velocities Behind a Blade Row as Solved by the Direct (Specified Angularity) Method	36
10	Example of the Output of the Cascade Analysis (Positive Incidence Case)	41
11	Example of the Output of the Cascade Analysis (Zero Incidence Case)	42
12	Normalized Maximum Offset, $\Delta N/C \cdot C_L$, vs Vane Stagger Angle, β_v	45
13	Normalized Maximum Offset, $\Delta N/C \cdot \sigma$, vs Vane Lift Coefficient, C_L	46
14	Least Squared Error Curve Fit of the Normalized Maximum Offset, $\Delta N/C$, vs the Vane Lift Coefficient, C_L	48
15	Loading Parameter, ℓ, vs the Location of the Maximum Offset, $C_{o_{max}}$	50

Figure	Title	Page
16	Parameters Defining the Nondimensionalized Offset Distribution	54
17	General Layout of the Axial Flow Pump Design Example	61
18	Velocity Profile in Duct Upstream of Rotor	62
19	Distribution of Peripheral Velocity at Rotor Exit	63
20	Computed Streamlines for the Axial Flow Pump Design Example	64
21	Computed Blade Row Velocity Profiles	65
22	Rotor Cylindrical Design Sections	67
23	Stator Cylindrical Design Sections	68
24	View of the Axial Flow Pump Rotor and Stator	69
25	Overview of the Axial Flow Pump Installed in the Six-Inch Water Tunnel (Flow is from Right to Left)	71
26	Close-up View of the Axial Flow Pump Rotor and Stator Installed in the Test Section of the Six-Inch Water Tunnel (Flow is from Left to Right)	72
27	Experimental and Theoretical Velocity Profiles Immediately Upstream of the Axial Flow Pump Rotor	74
28	Comparison of the Theoretical and Experimental Total Pressure Rise Across the Axial Flow Pump at Design Flow Rate	75
29	Performance Data for the Axial Flow Pump	76
30	Major Phenomena Affecting the Work Done by a Cascade of Blades	80
31	Schematic Representation of Camber Line Corrected to Account for Potential and Real Flow Effects in a Cascade	81
32	Design Boundary Conditions Input to the Two-Dimensional Cascade Design Procedure	86
33	Initial Solution Geometry Consisting of a Number of Parallel Mean Streamlines Between Ideal, Zero Thickness Blades	88
34	Generalized Cascade Flow Field Geometry	91

Figure	Title	Page
35	Geometric and Physical Variables Required for the Integration of the Momentum Equation	93
36	Initial Differences Between the One-Dimensional or Averaged Flow and the Results of the Exact Integration of the Momentum Equation	96
37	The Effects of the Gradual Addition of Blade Thickness to the Analytical Solution	99
38	Illustration of Singular Point at Blade Leading Edge .	100
39	Modification of the Stagnation Streamline to Account for Boundary Layer Displacement Thickness and the Blade Wake	103
40	Prescribed Performance Requirements for the Design Cascade Blade Analysis	106
41	Computer Generated Plot of the Initial and Final Analytical Solution for the Cascade Blade Test Case	108
42	Theoretical Streamline Distribution and Blade Shape Determined by the Streamline Curvature Blade Design Method	110
43	Photograph of Cascade Tunnel with Test Blades and Three-Hole Probe Mounted	112
44	Detail of Airfoil Section Shape and Location of Holes for Surface Pressure Measurements	113
45	Three-Hole Probe and Cascade Blade Test Geometry . . .	115
46	Expanded View of Three-Hole Probe Tip	116
47	Three-Hole Probe Calibration in Open Jet Tunnel	117
48	Three-Hole Probe Calibration (C_{p_α} vs α)	119
49	Three-Hole Probe Calibration (C_{p_t} vs α)	120
50	Three-Hole Probe Calibration (C_{p_s} vs α)	122
51	Theoretical Cascade Blade Pressure Distribution from the Streamline Curvature Analysis	125
52	Theoretical Cascade Blade Pressure Distribution from the Douglass-Neumann Potential Flow Analysis	128

Figure	Title	Page
53	Experimental Cascade Blade Pressure Distribution . . .	129
54	Experimentally Determined Velocity Field in the Test Cascade	131
55	Comparison of the Theoretical and Experimental Velocity Profiles in the Test Cascade Reference Station 20 Percent Blade Chord Upstream	132
56	Comparison of the Theoretical and Experimental Velocity Profiles in the Test Cascade Reference Station Coincident with Leading Edge	133
57	Comparison of the Theoretical and Experimental Velocity Profiles in the Test Cascade Reference Station at 10 Percent of the Blade Chord	134
58	Comparison of the Theoretical and Experimental Velocity Profiles in the Test Cascade Reference Station at 20 Percent of the Blade Chord	135
59	Comparison of the Theoretical and Experimental Velocity Profiles in the Test Cascade Reference Station at 30 Percent of the Blade Chord	136
60	Comparison of the Theoretical and Experimental Velocity Profiles in the Test Cascade Reference Station at 40 Percent of the Blade Chord	137
61	Comparison of the Theoretical and Experimental Velocity Profiles in the Test Cascade Reference Station at 50 Percent of the Blade Chord	138
62	Comparison of the Theoretical and Experimental Velocity Profiles in the Test Cascade Reference Station at 60 Percent of the Blade Chord	139
63	Comparison of the Theoretical and Experimental Velocity Profiles in the Test Cascade Reference Station at 70 Percent of the Blade Chord	140
64	Comparison of the Theoretical and Experimental Velocity Profiles in the Test Cascade Reference Station at 80 Percent of the Blade Chord	141
65	Comparison of the Theoretical and Experimental Velocity Profiles in the Test Cascade Reference Station at 90 Percent of the Blade Chord	142

Figure	Title	Page
66	Comparison of the Theoretical and Experimental Velocity Profiles in the Test Cascade Reference Station Coincident with Trailing Edge	143
67	Comparison of the Theoretical and Experimental Velocity Profiles in the Test Cascade Reference Station 20 Percent Blade Chord Downstream	144
68	Comparison of the Theoretical and Experimental Velocity Profiles in the Test Cascade Reference Station 50 Percent Blade Chord Downstream	145
69	Cascade Turning Angle as a Function of Blade Chord Reynolds Number	148
70	Experimental Cascade Blade Pressure Distribution as a Function of Blade Chord Reynolds Number	149

NOMENCLATURE

Symbol	Definition
A, B, C, D, E	polynomial coefficients
a, b, c, d, e	polynomial coefficients
C_L	blade lift coefficient
$C_{o_{max}}$	percent of blade chord, where ΔN is a maximum
C_P	pressure coefficient
c	blade chord length
k	streamline curvature = (R_k^{-1})
L	integrated total blade force
ℓ	percent of blade chord where one-half of total turning occurs
N	revolutions per second
ΔN	offset or distance between the mean streamline and the blade camber line
n	ordinate normal to a streamline
P	pressure
ΔP	pressure difference across a blade
R	radius
R_k	radius of curvature of a streamline
r	ordinate along a radial line
S	spacing of two blades in a cascade
s	ordinate parallel to a streamline
t	projected length of a blade in the (x) direction

Symbol	Definition
U	blade peripheral velocity
u	velocity component in (x) direction
V	velocity
$\dot{V}$	volume flow rate per unit depth
v	velocity component in (r) or (y) direction
x	axial coordinate
y	radial coordinate
α	angle between a streamline and a path of integration
α	relative flow angle
α_i	incidence angle
β	angle between a blade force vector and a streamsurface
β	dummy variable of integration
β_v	stagger angle, angle between the blade chord line and axial or (x) direction
η	axis coincident with a path of integration
θ	ordinate in peripheral direction
ξ	ordinate on η axis
ρ	fluid density
σ	cascade solidity (S/C)
ϕ	angle between a streamline and the (x) direction

Subscript

1	uniform upstream or leading edge conditions
2	uniform downstream or trailing edge conditions
a	axial or (x) component
i	denotes an integration starting point
ℓ	local condition

Symbol	Definition
m	meridional component, parallel to ϕ direction
o	denotes an integration end point
S	reference static condition
s	local static condition
T	reference total condition
T	blade thickness
t	local total condition
x	component in (x) direction
x	partial differential W. R. T. (x)
y	component in (y) direction
y	partial differential W. R. T. (y)
ps	pressure surface
ss	suction surface
α	function of flow angle
η	function of η
θ	peripheral component
ξ	denotes a property of a streamline coincident with a value of ξ on η
∞	denotes a reference condition

ACKNOWLEDGEMENTS

The author wishes to express his gratitude to the following institutions and persons who supported the work reported in this thesis.

Direct support for the various works described in this thesis was furnished by the Naval Sea Systems Command Code 0351. Funding for the design, fabrication, and testing of the axial flow pump described herein was furnished by the Naval Oceans Systems Center, San Diego, California.

Dr. Robert E. Henderson and Prof. Walter S. Gearhart provided inspiration and technical assistance throughout the investigations reported here. Many members of the staff of the Fluids Engineering Department contributed technical assistance to these projects. The author is a full-time member of the staff of the Applied Research Laboratory of The Pennsylvania State University and is very grateful for the opportunity to pursue the work reported herein under the support of the Applied Research Laboratory.

CHAPTER I

A GENERAL STATEMENT OF THE PROBLEM AND ITS SOLUTION

The problem addressed in this study is the development of a rational engineering solution to the design of turbomachinery that operate in an incompressible, steady flow. The types of turbomachines considered include axial, mixed, and radial flow pumps, fans, and turbines. Schematic examples of these types of machines are shown in Figure 1. All turbomachines require rotating rows of airfoil-shaped blades. Geometrically, blade row shapes can be quite complex, and their shape is closely related to the exact flow field in the turbomachine. The performance of a turbomachine is defined relative to the amount of fluid passing through the machine in a given time and the change in energy, or total pressure, that the fluid experiences. The indirect or design problem is one of specifying a geometric shape of duct and blading that will deliver the desired flow parameters either at a single operating point or over a continuous range of operating conditions. The direct or analysis problem considers a given blade row shape and determines the operating points of the machine. Both problems require methods to determine the exact nature of the flow field in the turbomachine.

A number of additional considerations must be made during a design, all of which affect both the machine's performance and geometry. These considerations include efficiency requirements, constraints due to cavitation or fluid vaporization in low pressure regions, unsteady flow effects, two- and three-dimensional effects of viscosity, and

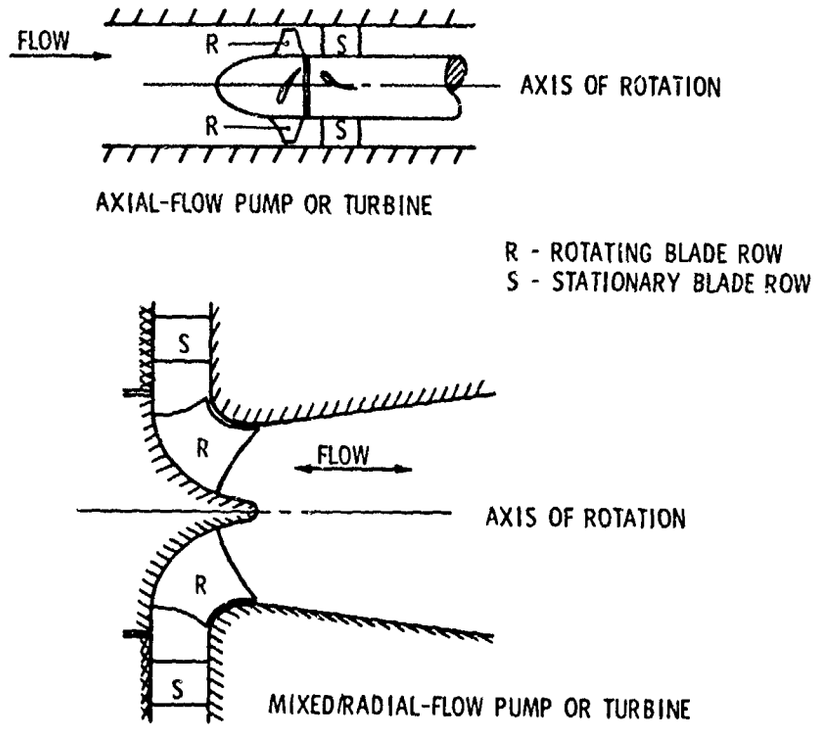

Figure 1. Basic Turbomachine Types.

manufacturing limitations. All of these constraints and effects must be considered in a sound, analytical design procedure.

The design of a turbomachine can be traced through three basic phases. The first is the preliminary design phase in which the type of machine to be employed is determined. Additionally, the size, speed, and over-all geometry are determined. Since the entire design process is iterative, the preliminary design parameters and shapes are always subject to modification. Many aspects of this preliminary design process are empirical and/or arbitrary and are based on engineering experience, system or installation limitations, costs, and other factors of which the designer must be aware. However, to be able to proceed with a detailed design, a fairly complete conceptual form of the machine must be generated.

The second phase is the detailed design of the machine duct and blade shapes. A design that is based on the equations of fluid motion requires the development of a mathematical description or model of the flow field and the machine geometry. This phase requires computerized methods to solve the equations of motion while accounting for as many of the physical properties and boundary conditions as possible. Since the direct solution of the equations of motion for viscous, turbulent flow is impossible, it becomes necessary to approximate some of the physics of the flow. However, the exact solution of the nonviscous or ideal flow field with forces due to fluid accelerations, rotation, and nonuniform flows taken into account is possible. Figure 2 helps to visualize these various aspects of the flow geometry. The usual approach used is to solve for the inviscid flow field and superimpose the effects of real fluid flow which are difficult to treat analytically.

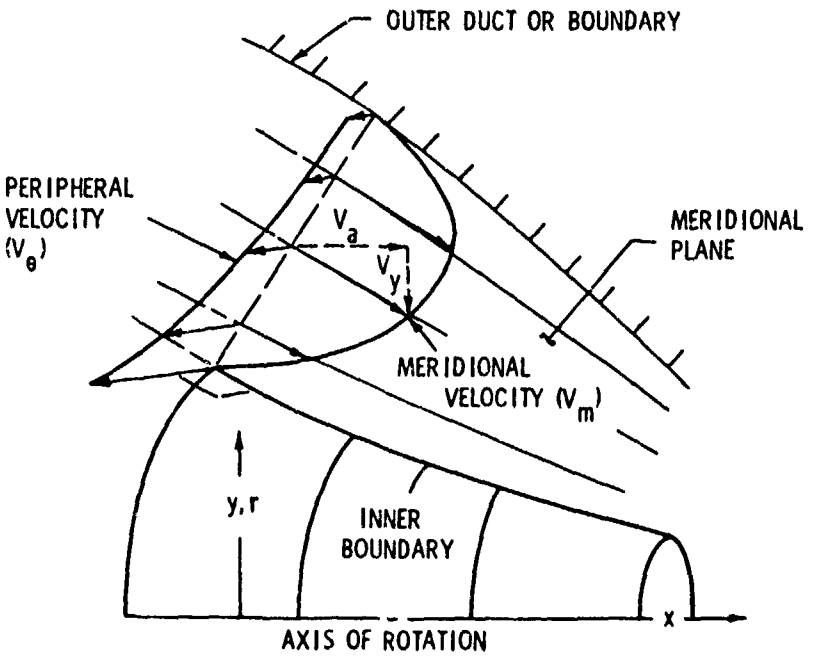

Figure 2. Generalized Velocity Components in an Axisymmetric Duct.

The solution must include physical effects peculiar to each type of machine. Generally, the inflow conditions to the turbomachine will be nonuniform in velocity and pressure. The chordwise and spanwise loading or pressure on the blade rows will be nonuniform as is the blockage due to blade thickness and boundary layer growth. If the flow field is unbounded, as for a nonducted fan, additional boundary conditions are necessary to perform a flow analysis. The effects of viscosity in the blade row passages must be modeled accurately to achieve the design performance requirements.

The second phase culminates in an actual blade shape design that will produce the flow field specified by the analysis. Determination of this shape is difficult as there are a number of boundary conditions that it must satisfy, and the performance of a blade row is highly subject to real flow phenomena which are not easily approached analytically. Again, a combination of ideal flow theory and empirical corrections are required to specify a blade row with desired performance.

The third phase is essentially similar to the analysis and blade design except that the geometry of the system is fixed and it is desired to determine the effect of a blade row on the flow field. This should give the same solution as the original analysis at the design point. However, the results of performance testing and, in particular, measured velocity and pressure profiles in the vicinity of the blade row may be used to test the theoretical analysis and design. Where differences are found, corrections to the mathematical models or to the hardware may be required.

In summary, the design and analysis of a turbomachine requires an accurate description of the internal flow field. A numerical simulation

of the turbomachine, including the various components of the equations of motion in either exact or approximate (empirical) form, must be constructed. This simulation consists of two basic parts, a meridional plane or through-flow solution and a blade design method that includes an analytical blade-to-blade flow solution. Each of these solutions affects the other and must be developed iteratively to produce a consistent model of the flow. Once a model is generated, a check against the design requirements must be made to assure that no part of it fails the design requirements. Once complete, the model must be compatible with mechanical limitations and manufacturing capabilities. An additional iteration with the design constraints may be necessary to finally arrive at an acceptable engineering solution to the design of the turbomachine.

CHAPTER II

STATE OF THE ART

Before the advent of the digital computer, turbomachine design relied on experience and intuition more than on theoretical analysis. The inefficiency of early gas turbines pointed to the need to study the aerodynamics of turbomachines in depth. To accomplish this end, a succession of analysis techniques have been developed, used, and, in some cases, discarded as not being accurate enough. A basic understanding of the flows in the complicated passages and blading was obtained through experiment and, in many cases, these data were applied directly to design problems. Historically, the methods that were evolving started as an analysis of tested hardware and were extended to the design of new machines. Numerical methods have been developed that aid in the design of compressible flows in turbines and compressors, though, at present, a great deal of designer's art is still required. Attention has not been so great in the area of hydrodynamic turbomachines, such as hydroturbines and pumps. Improvements in the design of these machines require better analysis tools to be developed--the purpose of this study.

The equations of motion for a viscous, turbulent, compressible flow in a turbomachine are impossible to solve even with the help of the largest computers. This has required a reduction of their complexity and the approximation of various terms, particularly with respect to viscosity and turbulence. These two phenomena are strongly interrelated and are caused in part by molecular forces associated with the fluid itself.

As such, it has been necessary to reduce the complexity of the flow mathematically by introducing concepts of macroscopic regions for flow where simplified equations of motion, coupled with models for turbulent and viscous effects, work with sufficient accuracy. To reduce the computation requirements, time and spatial averaging of the equations, coupled with simple models of real fluid effects, make it possible to obtain engineering data for various types of flows.

In the early 1950's, Wu [1] recognized these problems and formulated a set of equations which had the possibility of a solution. He broke the problem of the three-dimensional flow into a set of coupled two-dimensional solutions. Figure 3 helps to explain Wu's analysis in which he broke the problem into two planes generally perpendicular to each other. One, the meridional plane, describes the flow on hub-to-tip stream surfaces. The other, the blade-to-blade solution, describes the flow on planes generally parallel to the hub surface of the machine and perpendicular to the blading. A complete solution by Wu's method would require a number of both parallel meridional and parallel blade-to-blade solutions. The solutions are coupled and must be solved iteratively to simultaneously satisfy the equations on all of the solution planes.

At the time of formulation of Wu's analysis, computational methods and machines were not large or fast enough to give a comprehensive solution. As a result, many approximate methods evolved. Wislicenus [2] summarized many of the design techniques in use at the time. Most of these techniques relied heavily on experimental data to be useful. NASA [3] also compiled detailed design methods and data available for the design of compressors.

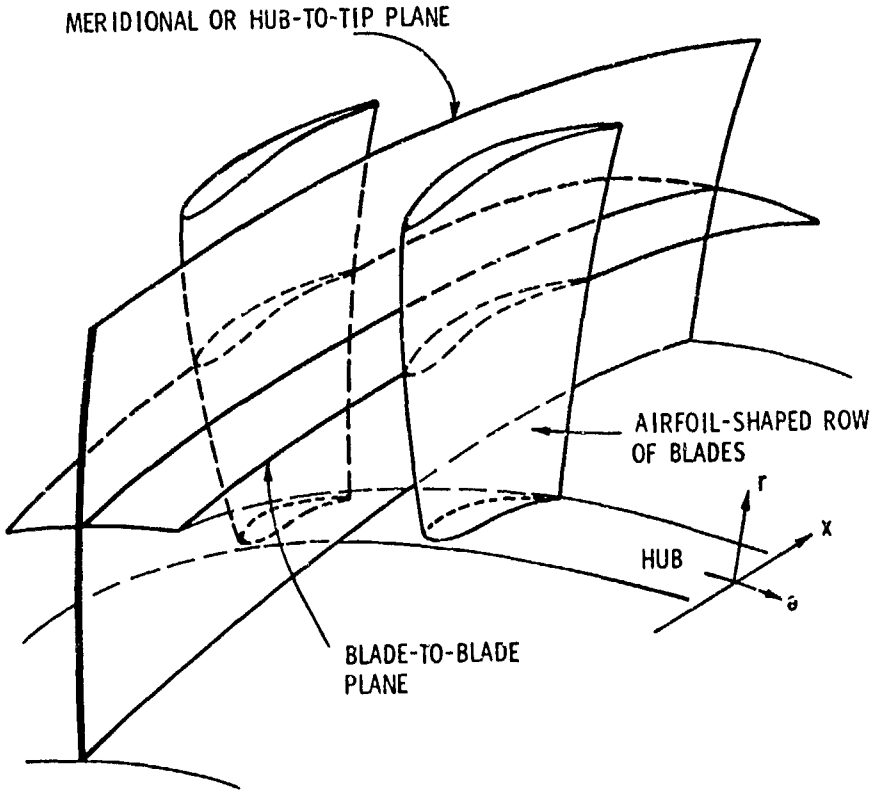

Figure 3. General Description of Computation Planes in a Turbomachine Blade Row.

Smith [4] rearranged the equations of motion in the meridional plane to give a time and spatially averaged picture of the flow in a blade row. At the same time, additional computerized techniques were developed to solve the through-flow problem. Marsh [5] and Katsanis [6] developed a solution (the Matrix Through-Flow Method) where the Meridional plane was divided into a grid of roughly square blocks. The equations for the stream function at every grid point were solved by the finite difference method, an approximation to the actual differential equations. These solutions are all basically inviscid and nonturbulent. Novak [7] formulated a solution (the Streamline Curvature Method) that solved for the velocities and streamlines rather than the stream functions. Again, the solution was basically inviscid and nonturbulent. The problem of losses due to viscosity and turbulence was addressed by Bosman and Marsh [8], but in general, experimental data are always required to adequately model the real fluid effects encountered in a turbomachine. Davis and Millar [9] made comparisons of the usefulness of the Matrix Through-Flow and the Streamline Curvature Methods of through-flow predictions. They arrived at several conclusions which are important in the selection of a method for various problem types. Computationally, both methods require approximately the same amount of computer time. However, due to very large matrix operations involved, a much larger computer memory is required for the Matrix Through-Flow Method.

The Streamline Curvature Method offers an advantage in that the equations and solution are in terms of physical variables of velocity and pressure rather than those of a stream function. Additionally, viscous and turbulence effects are much easier to incorporate into the

Streamline Curvature Method because their models are developed in terms of physical variables.

A Streamline Curvature Method specifically designed for hydrodynamic applications is reported in McBride [10]. This analysis is important because the effects of the chordwise and spanwise loading and thickness distributions in blade rows are included, and specific loss correlations for various turbomachine types are easily included. The through-flow analysis is also designed to be linked to a blade element analysis yielding an inviscid solution of the three-dimensional flow in a turbomachine. An interesting capability of this analysis method is its application to the analysis of unbounded turbomachine flows as reported by Billet [11]. A feature of the analysis is that a free streamline through a nonducted blade row tip is calculated. An additional extension of this Streamline Curvature Method analysis is reported in Brophy [12], where the analysis was used to form the basis of a design procedure for radial flow pumps.

Where the three-dimensional nature of the flow field is required, determination of the effects of the blading on the meridional flow requires flow field solutions on the blade-to-blade surfaces. The design of blade sections also requires an accurate analysis technique. Katsanis [13] was one of the first to successfully compute the velocity and pressure distribution on the blade-to-blade plane. He used a method very similar to the Matrix Through-Flow Method. Wilkenson [14] adapted the Streamline Curvature Method to the analysis of blade-to-blade flows. Thompson [15] used the finite element method, similar to the finite difference method, to analyze the flow field. None of these methods was

adapted to the design problem; all were used for analysis of existing geometries.

Wislicenus [2] developed the Mean Streamline Method of blade section design. This method is based on experimental correlations of fluid turning and the blade pressure distribution. A relationship between the average or mean streamline on the blade-to-blade surface and the blade section camber line was developed. Reference of this approach is reported in McBride [16], where two-dimensional cascade data were analyzed parametrically and the design method revised based on the acquired correlational data.

None of the above methods incorporates sufficient modeling of the turbulent boundary layer flow associated with turbomachine blade rows. Raj and Lakshminarayana [17] conducted experiments which gave insight into the nature of the blade boundary layers and the structure of the wake shed from the trailing edge of a blade. These data will help in the formulation of more accurate models of this flow phenomenon.

The availability of the various through-flow and blade-to-blade solutions leads to the possibility of synthesizing a three-dimensional model of the turbomachine flow field. The interaction of the flow on the meridional plane and on the blade-to-blade planes becomes important in this case. The result of blade-to-blade analysis is that forces due to the geometry of the blading may be determined. Smith and Yeh [18] and Lewis and Hill [19] formulated analyses which predict the effect of these forces on the through-flow. Howells and Lakshminarayana [20] obtained experimental data regarding the effects of these body forces on the through-flow in a turbomachine. Katsanis and McNally [21] and Katsanis [22] used the Matrix Through-Flow Method as the basis of

estimating the three-dimensional velocity field in blade rows. Novak and Hearsey [23] utilized the Streamline Curvature Method in a similar manner to generate a quasi-three-dimensional analysis. It should be stressed that the above techniques are for analysis of already designed blade rows and do not apply to the actual determination of a blade shape, i.e., the design problem. This paper will address the design problem by using the Streamline Curvature Method to construct an averaged through-flow picture that satisfies the general design requirements. Then two methods, the Mean Streamline Method and the Streamline Curvature Method, will be used to actually define blading that generates the flow field prescribed by the through-flow analysis. Combining the through-flow analysis and the blade-to-blade analysis, a quasi-three-dimensional analytical representation of the flow field is generated.

CHAPTER III

ANALYSIS AND DESIGN TECHNIQUE

The fundamental problem in the design of a turbomachine is the specification of a blade row that produces a desired energy or total pressure change with a given fluid flow rate. Due to possible restrictions on the size, efficiency, operating characteristics, and cost of the turbomachine, additional constraints on the size, speed, and type of blade row may be necessary. The problem the designer faces is the optimization of the blade row with respect to these constraints while still achieving the desired over-all performance.

The design of a turbomachine blade row is accomplished in several fairly distinct but interactive phases. As progress from one step to the next is made, the possibility of iterations and back steps is always at hand if it becomes obvious that some portion of the design will not fit the performance specifications.

With the specification of the performance parameters and design constraints, the first phase, the preliminary design, is started. In this step, the over-all design and dimensions of the blade row are determined. The performance specifications will determine if axial, mixed, or radial flow blading is required. The basic blade row sizes and speed will be determined, and a preliminary layout of the duct geometry is made.

At this point, the second phase, which is the detailed specification of the blade spanwise loading distribution, is performed. Empirical

data place limits on the amount of work a single blade row can perform without severely affecting the blade's efficiency by causing stall or flow separation. An iteration with the initial design phase may be necessary to assure that the blade row will not be overloaded and perform poorly.

The third phase of the design is the development of an axisymmetric, numerical model of the flow through the duct and blade row. Here, consideration is made of the exact inflow conditions to the blade row. The Streamline Curvature Method of through-flow analysis reported in a later chapter is used to develop the numerical model, solving the inviscid equations of motion for the flow and correcting the solution for the flow losses due to viscosity and turbulence that are expected. The detailed velocity and pressure fields are calculated, and by examination of these and the power requirements, corrections can be made either to the preliminary design, if necessary, or to the spanwise loading distribution. The result of this phase is a two-dimensional model of the turbomachine that satisfies all of the design restraints and requirements and the laws of fluid motion.

The final phase in the design is the specification of an actual blade geometry that will give the flow field specified by the through-flow analysis. This is the most difficult phase of the design problem as the real fluid effects of viscosity and turbulence play a very important role in the actual performance of the blade row. The real flow is highly three-dimensional in a rotating blade row, but because of the complexity of the flows, the best models that can be used in the design are two-dimensional. Two methods of specifying the blade geometry are reported in later chapters.

The first method is the Mean Streamline Method, which is basically empirical and relies on correlation data developed from two-dimensional tests of blade sections. The second is the Streamline Curvature Method, which is basically theoretical but relies on correlational data to calculate the viscosity and turbulence effects. The Streamline Curvature Method, while specifying the blade shape, also calculates the flow field around the blade sections.

With the blade geometry in hand, examination of the flow field may reveal areas prone to separation or cavitation, indicating that adjustments must be made in the earlier phases of the design process. The final acceptance of the design is then based on the mechanical strength of the blade and on its suitability for manufacture. Again, additional iterations, going as far back as the preliminary design, may be necessary.

An additional input to the design process is the actual tested performance of another turbomachine blade row designed by the process. The Streamline Curvature Method of through-flow analysis may take measured data and reconstruct numerically the measured flow field. Comparison with the design data helps to improve the quality of the necessary correlational data used in the design process, both in the through-flow analysis and in the blade section design process. This final iteration is necessary to strengthen the design process and to improve understanding of the highly complex nature of turbomachine flows.

CHAPTER IV

THE STREAMLINE CURVATURE METHOD OF THROUGH-FLOW ANALYSIS

The Streamline Curvature Method refers to a solution technique for determining the flow on the meridional plane of a turbomachine (the through-flow problem) or on the blade-to-blade planes of the turbomachine. The method relies on the ability to define accurately the streamlines on the meridional plane as shown in Figure 3 and to subsequently determine the convective and streamwise normal fluid accelerations based on their geometry. The Streamline Curvature Method has been used successfully for the determination of the through-flow solution for axial flow pumps, compressors, and turbines, utilizing equations of motion written in orthogonal or intrinsic coordinate systems. Approximations are often made that limit the accuracy of the analysis, particularly with regard to the influence of blade rows on the through-flow. Blade rows have been treated as thick actuator disks with the effects of chordwise loading, solid blockage, and body forces internal to the blade row ignored. This chapter serves to document a Streamline Curvature analysis that addresses the problems described.

Improvement of the SCM requires that the equations of motion used in the solution be written such that reference stations in the turbomachine take arbitrary paths through the machine. This allows the modeling of the blade row loading distribution. Blade-to-blade effects may be included as circumferentially-averaged body forces. The equations are general enough that axial, mixed, and radial flows may be calculated.

Proper choice of the boundary conditions allows both the indirect (design) case and the direct (analysis) problem to be calculated.

The analysis has been used to design axial and radial flow pumps and has performed the direct analysis of a nonducted rotor in an infinite medium, all with good success. Some examples of the use of this analysis will be presented at the conclusion of this chapter.

4.1 Development of the Equations of Motion

In the axisymmetric inviscid analysis, Euler's equations of motion are written in a radial equilibrium equation that forms the essence of the Streamline Curvature Method. The additional equations used are those which express the conservation of mass: total energy, or pressure, and angular momentum. The method of solution of these equations requires that they be solved by successive approximations with the necessary data taken from the iteratively determined velocity field and streamline pattern.

Let x and y be rectangular coordinates in a meridional plane, Figure 3, as illustrated in Figure 4. Euler's equations in these rectangular coordinates for an axisymmetric, steady, incompressible flow are

$$u \frac{\partial v}{\partial x} + v \frac{\partial v}{\partial y} = - \frac{1}{\rho} \frac{\partial P}{\partial y}$$

and (4.1)

$$u \frac{\partial u}{\partial x} + v \frac{\partial u}{\partial y} = - \frac{1}{\rho} \frac{\partial P}{\partial x} \quad .$$

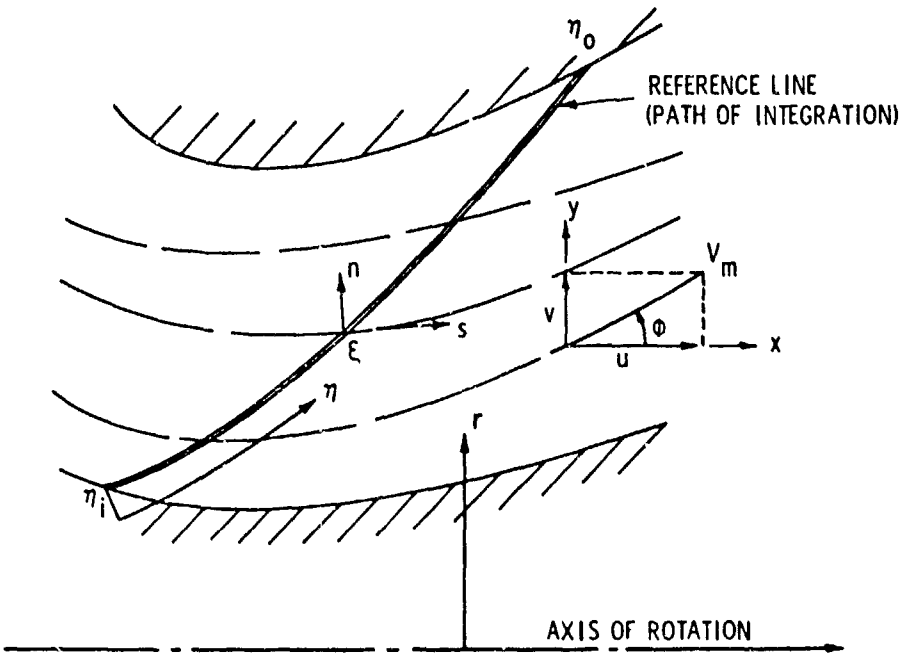

Figure 4. General Reference Station Parameters (Meridional Plane).

Figures 4 and 5 represent the meridional plane of the solution, and geometric quantities used in the following equations are shown on these figures.

The pressure gradient between points a and b, Figure 5, can be represented by

$$\left.\frac{\partial P}{\partial \eta}\right|_a^b = \left.\frac{\partial P}{\partial s}\frac{\partial s}{\partial \eta}\right|_a^b + \left.\frac{\partial P}{\partial \eta}\frac{\partial \eta}{\partial \eta}\right|_a^b \quad . \tag{4.2}$$

To compute the pressure gradient along η requires the partial derivatives in Equation (4.2) to be determined.

In the streamwise direction, one has

$$\frac{\partial P}{\partial s} = \frac{\partial P}{\partial y}\sin\phi + \frac{\partial P}{\partial x}\cos\phi \quad . \tag{4.3}$$

Combining Equations (4.1) and (4.3), we have

$$-\frac{1}{\rho}\frac{\partial P}{\partial s} = \left[u\frac{\partial v}{\partial x} + v\frac{\partial v}{\partial y}\right]\sin\phi + \left[u\frac{\partial u}{\partial x} + v\frac{\partial u}{\partial y}\right]\cos\phi \quad . \tag{4.4}$$

Note that

$$v = V_m \sin\phi \tag{4.5}$$

and

$$u = V_m \cos\phi \quad .$$

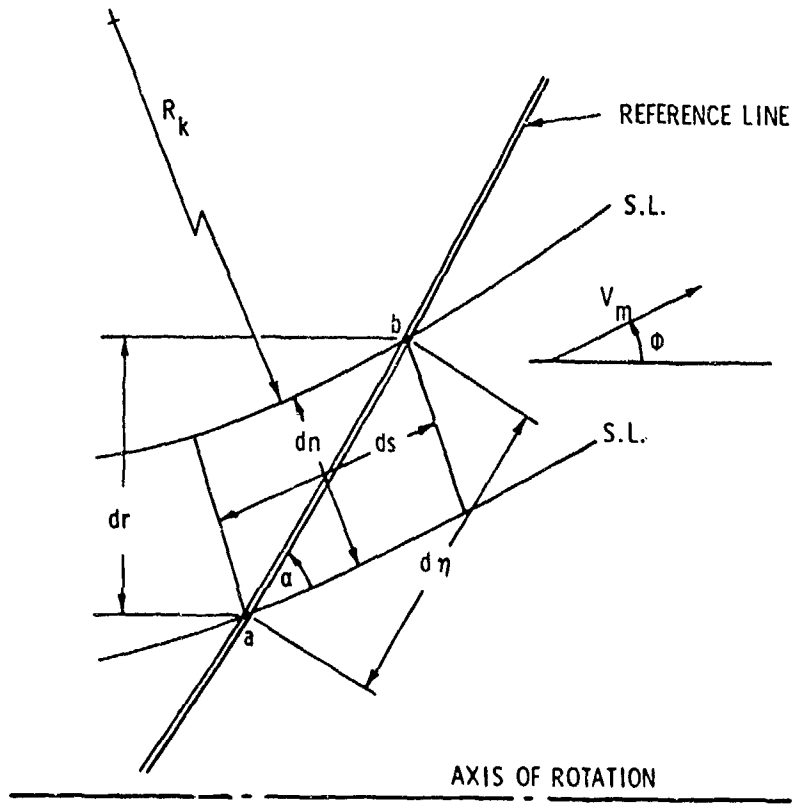

Figure 5. Differential Streamtube Element.

The following derivatives are determined by the chain rule

$$\frac{\partial v}{\partial x} = V_m \cos \phi \, \phi_x + \sin \phi \, V_{m_x} \quad ,$$

$$\frac{\partial u}{\partial x} = -V_m \sin \phi \, \phi_x + \cos \phi \, V_{m_x} \quad ,$$

$$\frac{\partial v}{\partial y} = V_m \cos \phi \, \phi_y + \sin \phi \, V_{m_y} \quad , \tag{4.6}$$

and

$$\frac{\partial u}{\partial y} = -V_m \sin \phi \, \phi_y + \cos \phi \, V_{m_y} \quad .$$

The quantities determined in Equations (4.5) and (4.6) are substituted into Equation (4.4) and, after reduction, the result is

$$-\frac{1}{\rho} \frac{\partial P}{\partial s} = V_m \cos \phi \, V_{m_x} + V_m \sin \phi \, V_{m_y} \quad . \tag{4.7}$$

Equation (4.7) reduces to

$$-\frac{1}{\rho} \frac{\partial P}{\partial s} = V_m \frac{\partial V_m}{\partial s} \quad , \tag{4.8}$$

which is seen to be the differential form of the steady Bernoulli's equation for an incompressible flow.

The streamwise normal component of Equation (4.2) is developed in a similar manner by noting that

$$\frac{\partial P}{\partial n} = \frac{\partial P}{\partial y} \cos \phi - \frac{\partial P}{\partial x} \sin \phi \tag{4.9}$$

and

$$-\frac{1}{\rho}\frac{\partial P}{\partial n} = \left[u\frac{\partial v}{\partial x} + v\frac{\partial v}{\partial y}\right]\cos\phi - \left[u\frac{\partial u}{\partial x} + v\frac{\partial u}{\partial y}\right]\sin\phi \quad . \tag{4.10}$$

After combining Equations (4.5), (4.6), and (4.10), we obtain the following result:

$$-\frac{1}{\rho}\frac{\partial P}{\partial n} = V_m^{\,2}\cos\phi\,\phi_x + V_m^{\,2}\sin\phi\,\phi_y \quad , \tag{4.11}$$

which is equivalent to

$$-\frac{1}{\rho}\frac{\partial P}{\partial n} = V_m^{\,2}\left\{\frac{\partial x}{\partial s}\phi_x + \frac{\partial y}{\partial s}\phi_y\right\} \quad . \tag{4.12}$$

The quantity in the brackets in Equation (4.12) is recognized to be equivalent to $\partial\phi/\partial s$, the curvature (k) or $(R_k)^{-1}$ of the streamline.

Finally, Equation (4.12) becomes

$$-\frac{1}{\rho}\frac{\partial P}{\partial n} = k\,V_m^{\,2} \quad . \tag{4.13}$$

Combining Equations (4.2), (4.8), and (4.10), we determine the radial equilibrium equation for nonswirling flow to be

$$\frac{\partial P}{\partial \eta} = \frac{\partial P}{\partial s}\frac{\partial s}{\partial \eta} + \frac{\partial P}{\partial n}\frac{\partial n}{\partial \eta}$$

and, finally,

$$-\frac{1}{\rho}\frac{\partial P}{\partial \eta} = k\,V_m^{\,2}\sin\alpha + V_m\frac{\partial V_m}{\partial s}\cos\alpha \quad . \tag{4.14}$$

The pressure gradient due to swirl is determined in a similar manner and leads to the term

$$-\frac{1}{\rho}\frac{\partial P}{\partial r} = \frac{1}{R} V_\theta^2 \quad , \tag{4.15}$$

where there are no circumferential derivatives; i.e., the flow is assumed to be uniform in the circumferential direction. The computational form of the radial equilibrium is

$$-\frac{1}{\rho}\frac{\partial P}{\partial \eta} = k\, V_m^2 \sin\alpha + \frac{1}{R} V_\theta^2 \sin(\phi+\alpha) + V_m \frac{\partial V_m}{\partial s} \cos\alpha \quad . \tag{4.16}$$

The three terms on the right-hand side of Equation (4.16) represent the meridional curvature, the radial and the convective accelerations, respectively. Integration of the equation will yield the static pressure difference between any two points in the flow field.

From Equation (4.16), the static pressure difference relative to some point, say η_i, in the flow to another point, ξ, along the reference line may be found. To satisfy conservation of mass and energy across the reference line, an absolute value of static pressure must be found at the reference point, η_i. The following direct solution for this value is an improvement over other procedures which are iterative in nature.

A continuity equation may be written for every station in the problem:

$$\rho \int_{\eta_i}^{\eta_o} V_m(\eta)\, r(\eta)\, \sin(\alpha_\eta)\, d\eta = \text{const} \quad , \tag{4.17}$$

where η_i and η_o are defined in Figure 4. In words, the mass flow across a reference line, regardless of its path between two streamlines, is constant, assuming an incompressible fluid. Bernoulli's equation may be written along a streamline between a particular point, ξ, on the reference line and the upstream reference conditions:

$$\left\{P_{\infty_\xi} + \frac{1}{2}\rho V_{\infty_\xi}^2 - \frac{1}{2}\rho V_{\theta_\xi}^2 - P_{\eta_i} - \int_{\eta_i}^{\xi} \left(-\frac{1}{\rho}\frac{\partial P}{\partial \eta}\right) d\eta\right\} = \frac{1}{2}\rho V_{m_\xi}^2 \quad (4.18)$$

The first two terms on the left-hand side represent the total pressure (static plus dynamic) available at the point ξ. The term P_{∞_ξ} contains all head loss and rotor energy changes between the upstream reference condition and the station of interest. The sum of the fourth and fifth terms is the static pressure at ξ. The term in the integral is the static pressure difference between η_i and the point ξ along the reference line from Equation (4.16).

Equations (4.17) and (4.18) may be combined and integrated between the two flow boundaries to give

$$\int_{\eta_i}^{\eta_o} \left\{P_{\infty_\eta} + \frac{1}{2}\rho V_{\infty_\eta}^2 - \frac{1}{2}\rho V_{\theta_\eta}^2 - P_{\eta_i} - \int_{\eta_i}^{\eta} \left(-\frac{1}{\rho}\frac{\partial P}{\partial \beta}\right) d\beta\right\}^{1/2} r_\eta \sin(\alpha_\eta)\, d\eta =$$

$$\int_{\eta_i}^{\eta_o} \frac{1}{2}\rho V_{m_\eta} r_\eta \sin(\alpha_\eta)\, d\eta \quad . \quad (4.19)$$

Because P_{η_i} is a constant, Equation (4.19) may be rearranged to give

$$\int_{\eta_i}^{\eta_o} P_{\eta_i} W^2 d\eta = \int_{\eta_i}^{\eta_o} \left\{ P_{\infty_\eta} + \frac{1}{2}\rho V_{\infty_\eta}^2 - \frac{1}{2}\rho V_{\theta_\eta}^2 - \left\{ \int_{\eta_i}^{\eta} \left(-\frac{1}{\rho} \frac{\partial P}{\partial \beta} \right) d\beta \right\} - \frac{1}{2}\rho V_{m_\eta}^2 \right\} W^2 d\eta \quad , \tag{4.20}$$

where

$$W = r_\eta \sin(\alpha_\eta) \quad ,$$

and, finally,

$$P_{\eta_i} = \frac{\int_{\eta_i}^{\eta_o} \left\{ P_{\infty_\eta} + \frac{1}{2}\rho (V_{\infty_\eta}^2 - V_{\theta_\eta}^2) - \frac{1}{2}\rho V_{m_\eta}^2 - \int_{\eta_i}^{\eta} \left(-\frac{1}{\rho} \frac{\partial P}{\partial \beta} \right) d\beta \right\} W^2 d\eta}{\int_{\eta_i}^{\eta_o} W^2 d\eta} \quad . \tag{4.21}$$

The static pressure at any point ξ along a reference line is then

$$P_\xi = P_{\eta_i} + \int_{\eta_i}^{\xi} \left(-\frac{1}{\rho} \frac{\partial P}{\partial n} \right) dn \quad . \tag{4.22}$$

The velocity profile which satisfies conservation of angular momentum and continuity and satisfies Bernoulli's equation along all streamlines is given by rearranging Equation (4.18).

$$V_{m_\xi} = \frac{2}{\rho}\left\{P_{\infty_\xi} + \frac{1}{2}\rho(V_{\infty_\xi}{}^2 - V_{\theta_\xi}{}^2) - P_{\eta_i} - \int_{\eta_i}^{\xi} \left(-\frac{1}{\rho}\frac{\partial P}{\partial \eta}\right) d\eta\right\}^{1/2} . \quad (4.23)$$

The flow field is solved by marching downstream to each station in turn and integrating Equation (4.16). The static pressure is then obtained from Equation (4.22). The improved velocity profiles are generated by Equation (4.23) until the changes in the velocity profiles and streamline locations are small between two successive passes.

4.2 The Effects of Blade Rows

In an inviscid solution of the turbomachine through-flow, the effect of a blade row is to change the angular momentum distribution in the flow as it passes the blade row. In the case of a rotating blade row, the total energy or total pressure of the fluid is changed in a manner proportional to the blade row chordwise loading distribution. In a case where the spanwise loading or work distribution is not uniform, the total energy will be changed in a nonuniform way in the spanwise direction as well. The effect of the blade row is then to change the through-flow velocity profiles and the streamline pattern.

A rotating blade row changes the total pressure in proportion to the change in angular momentum of the fluid passing through the rotor. The total pressure is increased between the points 1 and 2 along a streamline

(or, in the case of a turbine, decreased) in an inviscid fluid in accordance with the equation

$$\Delta P_{\infty_\eta} = \frac{1}{2}\rho(U_2 V_{\theta_2} - U_1 V_{\theta_1}) \quad , \tag{4.24}$$

where V_θ is positive in the direction of rotation.

The effect of an airfoil-shaped blade in a flow is to produce a lifting force perpendicular to the blade surface. For the purpose of this discussion, it will be assumed that the force can be integrated over the surface of an airfoil section and concentrated at some point on the blade surface. This force can be seen as the force L in Figure 6. The airfoil cross section of interest lies on the streamsurface that is defined by the axisymmetric through-flow solution. The three components of the coordinate system are shown as the circumferential direction (θ), the streamwise direction (s), and the streamsurface normal direction (n). In general, a blade surface is not perpendicular to the streamsurface defined in the (s, θ) plane, and therefore the lifting force L will not lie on this plane. The lift force can be resolved into components along the axes as shown in Figure 6. The two components of the lift force that are of principle importance are accounted for by the equations already discussed; namely, Equation (4.24). These are the circumferential force L_θ and the streamwise force L_s. The third force cannot be computed without foreknowledge of the geometric shape of the blade surface, which is required in the determination of the angle β shown in Figure 6. As can be inferred from the figure, in the case of blading that is perpendicular to the streamsurfaces, which is true for most radial blade rows, the angle β is small and the resultant force L_n normal to the

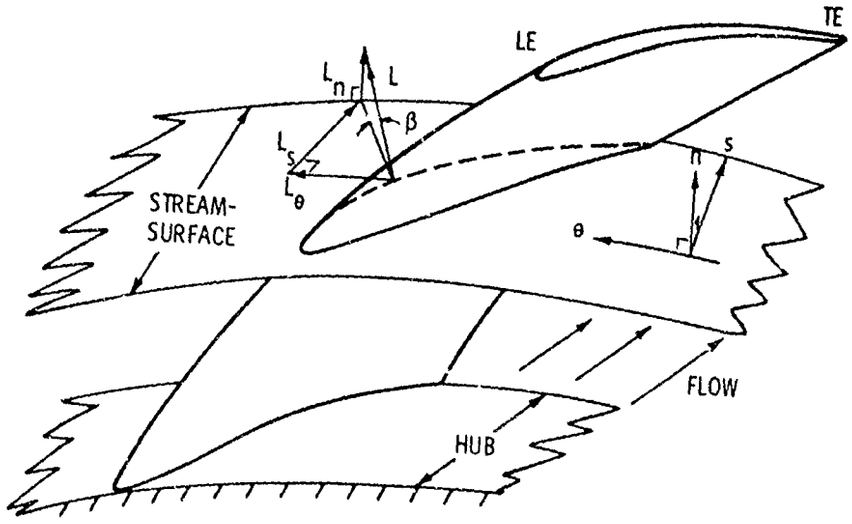

Figure 6. Blade Force Components.

streamsurface can be neglected. Occasionally, either due to design or as a result of the mechanical arrangement of a blade shape, the angle β can attain significant values and the result of the action of the streamsurface normal force is to change the through-flow in the blade row, which in turn affects the blade row performance. When this case is encountered, an adjustment must be made to the radial equilibrium equation to account for this force.

The forces shown in Figure 6 are not concentrated but are actually blade body forces distributed over the entire blade surface. The radial equilibrium Equation (4.16) requires an additional term where a significant body force component perpendicular to the streamsurface is present. This term is a pressure gradient due to the normal component of the blade force along the path of integration. Because the path of integration is generally perpendicular to the streamsurfaces, the magnitude of the term is that of the normal blade body force and is usually small.

Calculation of the streamsurface normal body force is difficult because of its dependence on the geometry of the blading involved. This implies that a detailed through-flow analysis and blade section design must be performed before the term can be computed. Additionally, the force is distributed both in the circumferential direction and along the streamwise direction. To be properly included in the radial equilibrium equation, the force must be integrated and averaged in the circumferential direction to determine its axisymmetric value. Obtaining the data necessary to generate the term for the radial equilibrium equation requires determination of the blade-to-blade flow solutions on a number of streamsurfaces. Once accomplished, the streamsurface normal pressure gradient along a path of integration within the blade row may be

determined by use of finite difference differentiation of the pressures existing on successive streamsurfaces at constant circumferential locations. The determined pressure gradients may then be averaged in the circumferential direction and applied to the radial equilibrium equation.

4.3 The Effects of Viscosity and Turbulence

Viscosity and turbulence are a result of molecular properties of a fluid and have profound influences on some regions of a flow. Because of this, equations describing their effects are extremely difficult to solve, in particular, where flows have a three-dimensional nature. This is the case with turbomachinery. The average effect of viscosity and turbulence on turbomachine flows can be established, however. In general, a turbomachine flow will experience a total pressure reduction and a redistribution of velocity as it passes through a duct or blade row. The magnitude of these effects can be determined experimentally by acquiring certain data frc testing of a turbomachine. In the case of a blade row, circumferentially-averaged spanwise (axisymmetric) traverses of the velocity and pressure field up and downstream of the blade row are required. By use of the previously described inviscid flow analysis, a comparison of the tested data and ideal flow characteristics can be made. This comparison will reveal the magnitude and distribution of the loss in total pressure that the flow experiences. If a correlation is developed and applied to the analysis, the result is a model of the real flow field. In the development of new designs, it must be assumed that the loss correlations are similar for blade rows of similar characteristics.

4.4 Use of the Streamline Curvature Method

To help clarify the nature of the information that can be obtained from the axisymmetric through-flow analysis described in this chapter, several examples of calculated flow fields are presented. An actual design is presented in detail in a later chapter.

The first two examples are indicative of the type of data that must be generated to begin the detailed design of a blade row. They are the calculated axisymmetric velocity and pressure fields in the vicinity of rotating blade rows. In Figure 7 is a plot of the streamline pattern around two nonducted blade rows set in an approximately infinite medium. Both blade rows are adding total pressure to the flow as it passes through them, and the result is a flow contraction through each in a manner similar to that calculated by actuator disk theory. The velocity and pressure field is calculated for each of the reference stations shown in the figure. The data at the stations corresponding to the blade row leading and trailing edges are required to begin the detailed design of blading to produce the calculated flow field.

The second example shown in Figure 8 is a simulation of the axisymmetric flow field in a Francis-type turbine. In this example, computing stations internal to the blade row are required to model the blade loading distribution accurately. Again, the velocity and pressure distribution at each reference station is calculated. This data may be used in a design method, such as that of Brophy [12], to calculate an actual vane shape.

The final example is a demonstration of the direct problem, where an existing blade row shape is analyzed to determine the flow field produced for a specified inflow. The method of Billet [11] was utilized

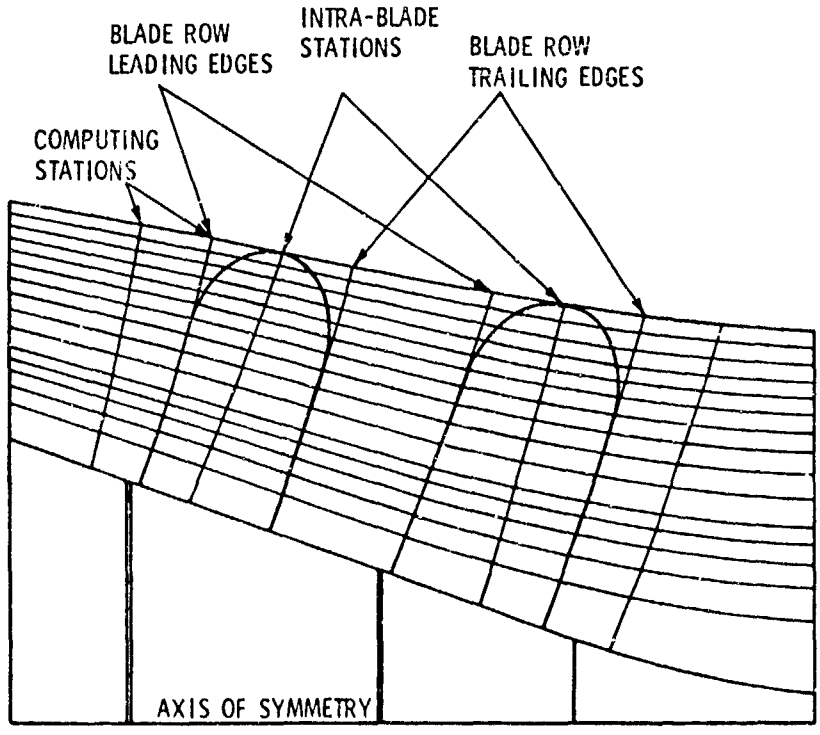

Figure 7. Detail View of the Streamlines Calculated Through Two Blade Rows.

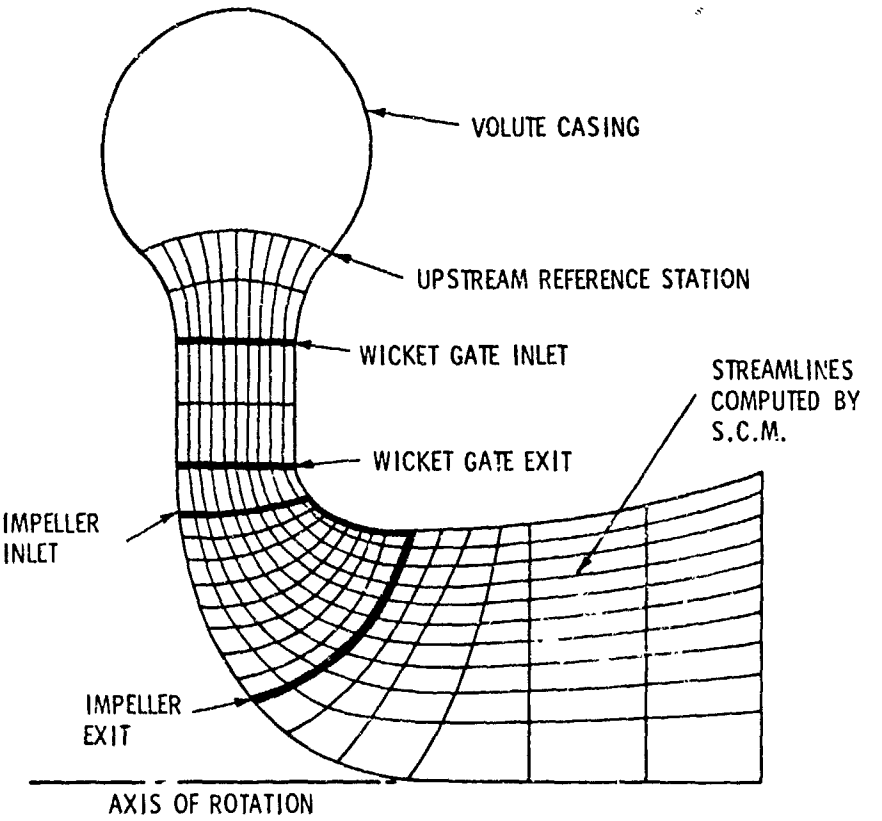

Figure 8. Streamlines in a Francis-Type Turbine.

to determine the angularity distribution behind a given blade row. The angularity boundary condition was applied in the Streamline Curvature Method at the blade row exit plane and the flow field determined satisfied the flow angularity. Figure 9 is a plot of experimental data and a comparison with calculated velocities at a blade row exit plane.

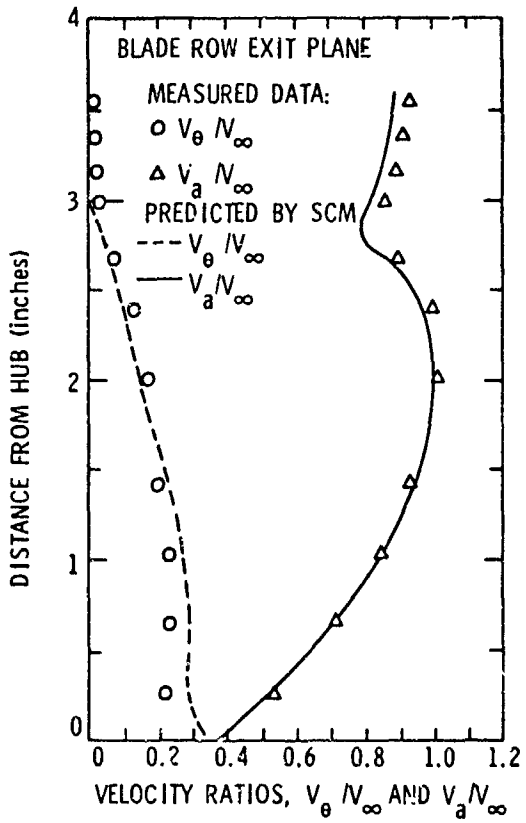

Figure 9. Comparison of Theoretical and Experimental Velocities Behind a Blade Row as Solved by the Direct (Specified Angularity) Method.

CHAPTER V

THE CORRELATIONAL MEAN STREAMLINE METHOD

The Mean Streamline Method of cascade blade section design developed by Wislicenus [2] correlates the differences in the shape of the blade camber line and the one-dimensional mean flow streamline. By accounting for the effects of blade thickness, the boundary layer growth, lift coefficient, solidity, and loading distribution, blade sections with good performance have been designed.

Effort has been directed toward the extension of this design method to cover a wider range of loading distributions, including trailing edge loaded blades and blades with higher than usual solidities (C/S). A computer analysis was made of experimental data for many available blade shapes with differing loading distributions. Relations were determined for the differences or deviations between the camber line and the mean flow streamline as a function of the lift coefficient, solidity, a loading distribution parameter, and blade stagger angle.

Using these correlations, a computerized design method was developed which rapidly produces blade shapes with specified design characteristics. A radial equilibrium theory is utilized to compute the actual blade surface pressure distribution. When a blade is to be designed which is similar to existing designs, the method has proven very reliable.

5.1 Introduction

The Mean Streamline Method of blade section design due to Wislicenus [2] is a semi-empirical method of designing a cascade airfoil section having prescribed fluid turning angle, thickness, and chordwise loading distribution. The Mean Streamline Method is capable of accounting for blade thickness and boundary layer blockage and the effects of nonuniform pressure and velocity profiles at the blade row inlet and exit. This design method relies on the ability to determine the departure of the mean flow streamline from the actual airfoil camber line and thus, account for the underturning exhibited by blade rows due to viscous and potential flow effects. This departure or offset which is usually small may be measured experimentally and may be correlated with design parameters, such as lift coefficient, solidity, loading distribution, and cascade stagger angle.

The original correlations used in the Mean Streamline Method covered a rather narrow range of lift coefficient and studied primarily leading edge loaded configurations. Where cavitation resistance is a primary consideration, a trailing edge loaded blade is desirable. The trailing edge loaded blade tends to minimize local blade surface velocities near the leading edge where the static pressure is low. In the present study, emphasis has been placed on extending the range of this design technique by correlating a larger range of lift coefficient and data on trailing edge loaded blades tested by Erwin [24].

A computer program was developed to analyze available experimental cascade data. The measured pressure distribution, cascade geometry, and loading distribution are input to the program. The mean flow streamline is constructed and compared to the camber line to obtain the offset

distribution. The output is in the form of a graphic representation of the input data and provides the resultant offset distribution and numerical results.

The resulting data relating the magnitude and shape of the offset distribution to the cascade flow parameters were analyzed in several ways. Direct comparisons were made to the original data of Reference [2]. Additional correlations were made and, finally, a statistical method was used to analyze the data. The results indicated that the offset was more dependent on the lift coefficient and less on the stagger angle than previously reported. The data also indicate that, in most cases, extrapolated sections designed using the original data would have been somewhat over-designed, giving more than the prescribed turning.

This chapter will summarize the computer analysis of the cascade data and the various correlations derived, and, finally, suggest a method by which these new data may be utilized in a design process.

5.2 The Computerized Analysis of Cascade Data

A computerized procedure was devised to quickly analyze the results of previous cascade testing. The input to this procedure is the blade geometry and the measured blade static pressure distribution, incidence, and turning angle. The pressure distribution is prescribed as a function of the chord and then transformed into a function of projected length in the axial direction for the purpose of computing the mean flow streamline.

The mean streamline is computed by the following procedure. Since the inlet and exit flow angles are known from the test data, the total turning is known. Additionally, upstream and downstream axial velocities

are assumed constant and continuity is preserved, assuming an incompressible fluid. In the blade passage, blockage due to blade thickness and the displacement thickness of an assumed boundary layer are used to extimate the mean axial velocity.

At any given position in the blade passage, the normal velocity component is computed by the following momentum balance equation:

$$Vy(x) = Vy(1) + \frac{\int_{1}^{x} \Delta P_x \, dx}{t \int_{1} \Delta P_x \, d_x} , \qquad (5.1)$$

where the subscripts (x) apply to a given chordwise position along the blade, (1) applies to that at the blade row inlet, and t is the projected length of the blade row. Knowing the distribution of both the axial and normal velocities as a function of the chord position, the mean streamline may be computed by using the tangents of the flow angle at each axial station. Usually, ten axial stations are used for this purpose. Once the mean streamline is determined and spline curve fitted, the offset distribution is computed by geometrically comparing the mean streamline to the blade camber line. The offset distribution is nondimensionalized by its maximum value and plotted as in Figures 10 and 11 by a Calcomp 718 flatbed plotter driven by an IBM 1130 computer system. The mean streamline is also used to compute the mean static pressure line, which is also plotted in Figures 10 and 11. The computation of this mean static pressure is based on the local mean streamline

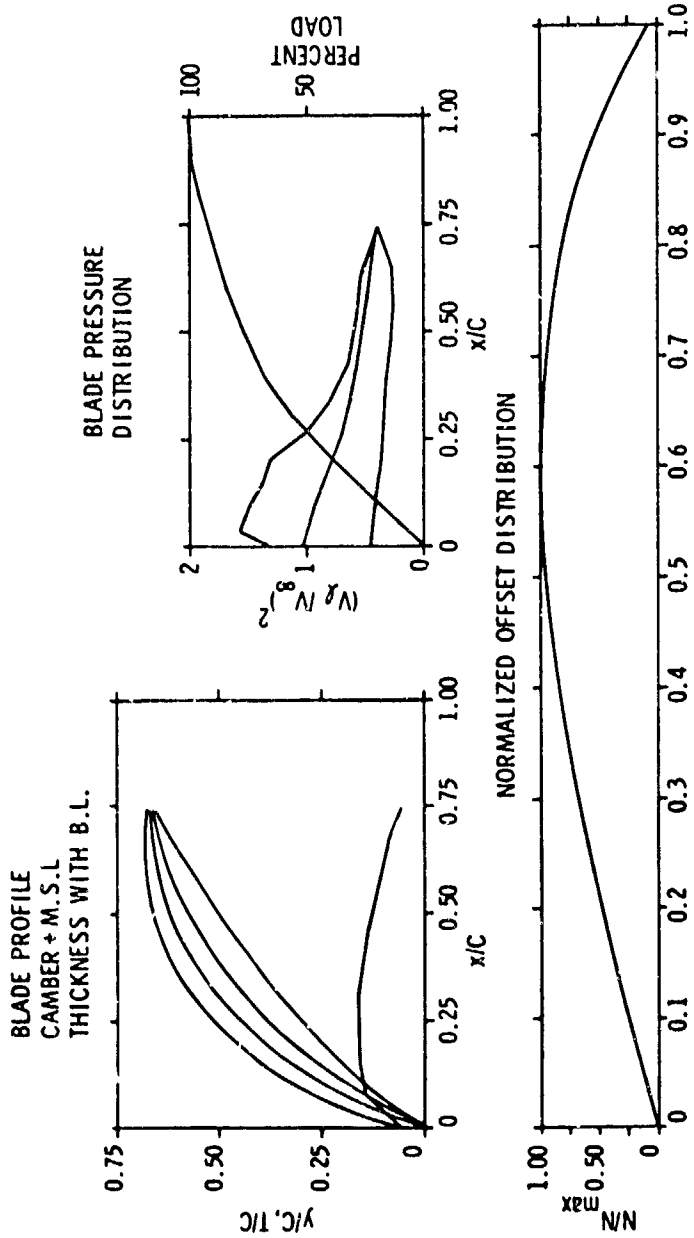

Figure 10. Example of the Output of the Cascade Analysis (Positive Incidence Case).

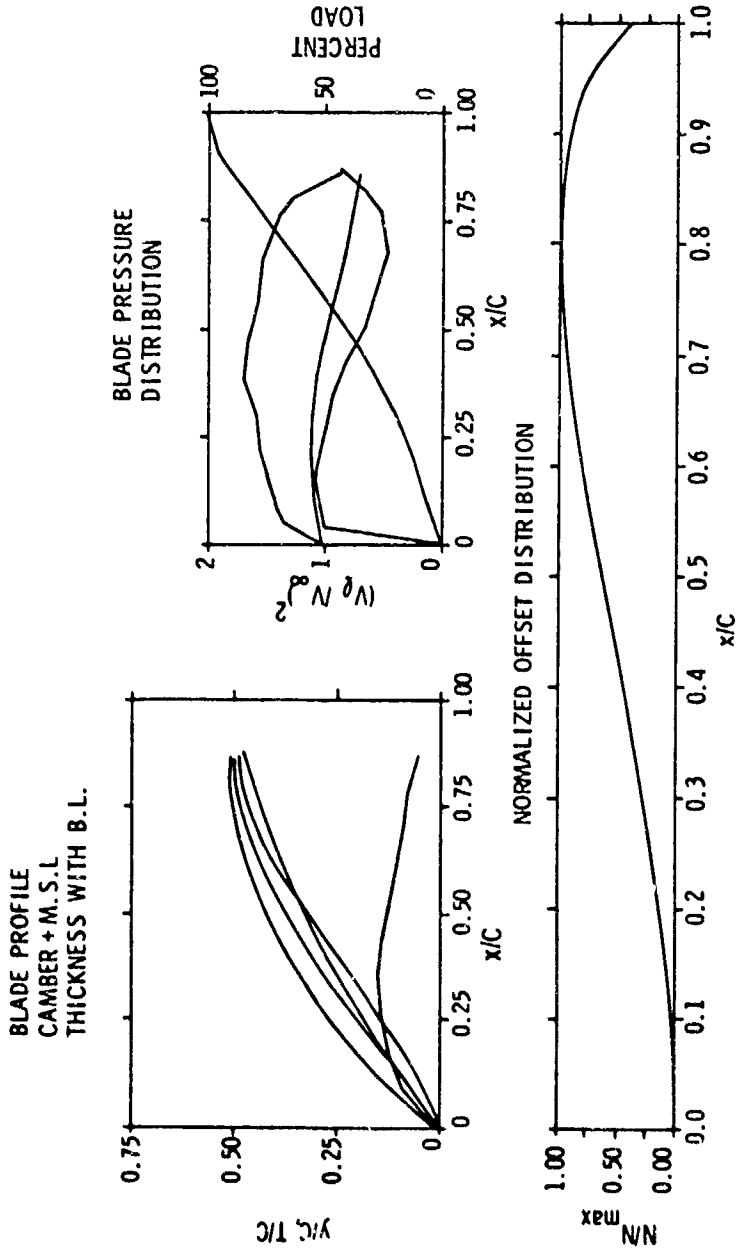

Figure 11. Example of the Output of the Cascade Analysis (Zero Incidence Case).

velocities existing at a given percent of the chord and assuming that the total pressure relative to the blade is a constant.

5.3 Evaluation of the Cascade Data

Cascade data from several sources were used in the effort to extend the range of applicability of the Mean Streamline Method. Two sources were used to generate the majority of these data, however. The data originally used by Wislicenus [2] were used to verify that the computerized procedure yielded the same results that he originally obtained. These data agree when reduced by the computerized procedure. NACA 65 series data documented in Reference [24] were used to obtain information over an extended range of lift coefficient for trailing edge loaded blades. This source documented six pressure distributions at different angles of attack for each cascade geometry. The zero incidence condition was found and a pressure distribution interpolated to match this condition.

Data generated at the Applied Research Laboratory, Reference [25], were utilized to both verify the computerized procedure and to provide data points similar to ARL blade designs which often exhibit very high solidity and use the ARL thickness distribution with the maximum thickness at 60 percent of the chord. Theoretical results of Reference [26] were used to verify trends and upper limits of camber line offset.

The resulting data relating the magnitude and shape of the camber line offset distributions to the experimental cascade geometries were analyzed in several ways. The term ΔN_{max} is defined as the maximum measured offset minus the offset at the trailing edge. The quantity $(\Delta N/C_{max})/C_L$ was plotted against the cascade stagger angle. This is

identical to the original correlation of Reference [2]. This plot, Figure 12, indicates that there is a great deal of variation of the data. By using the original correlation, a design should be produced that would generate more than the desired turning in the cascade.

When the quantity $(\Delta N/C_{max} \cdot C_L) \cdot \sigma$ is plotted against the lift coefficient, Figure 13 results. This figure shows a reasonably good correlation with larger offsets associated with the higher lift coefficients. Theoretical results of Reference [24] fall reasonably close to the experimental points, and as an upper limit, the isolated airfoil data line shown also looks reasonable. However, there is still significant dispersion of the data and only slight correlation with the stagger angle.

None of the correlations tried yielded definitive results, indicating a much more complex interaction was occurring between four primary cascade variables. The variables chosen were the lift coefficient (C_L), the solidity (σ), a loading parameter (ℓ), and the stagger angle (β_v). The loading parameter was defined as the percent of blade chord where one-half of the total turning was accomplished. A high loading parameter infers that the blade is trailing edge loaded.

A least squared error curve fit was used to determine the nature of the dependency of the offset on the four cascade variables. A curve fit of the following form was assumed:

$$\frac{\Delta N}{C} \text{ max} = a + b \cdot C_L^c \cdot \sigma^d \cdot \ell^e \cdot \beta_v^f \quad , \tag{5.2}$$

and a computer program utilizing an iterative technique was used to solve for the six coefficients while minimizing the total error in predicting the maximum offset. This error was defined by the relation

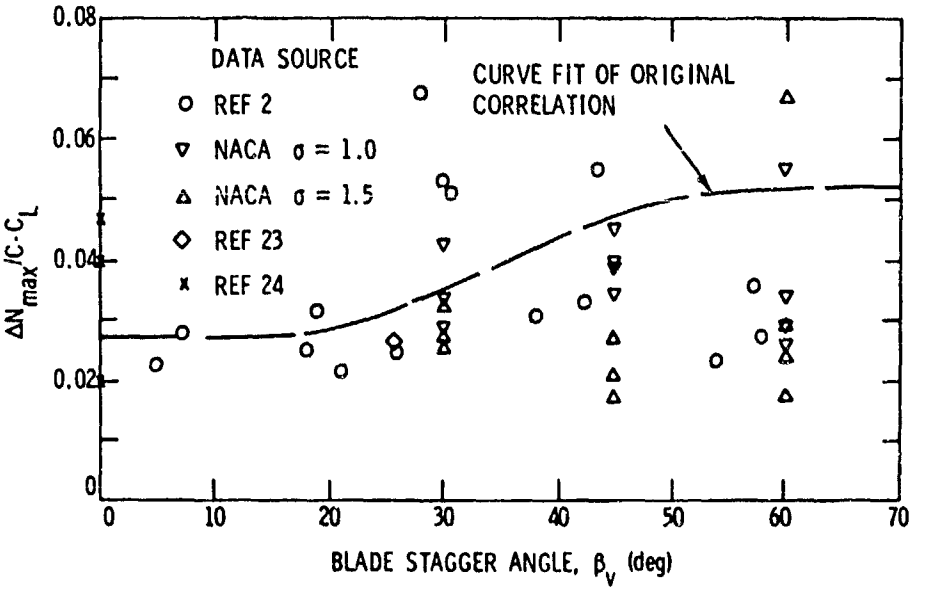

Figure 12. Normalized Maximum Offset, $\Delta N/C \cdot C_L$, vs Vane Stagger Angle, β_v.

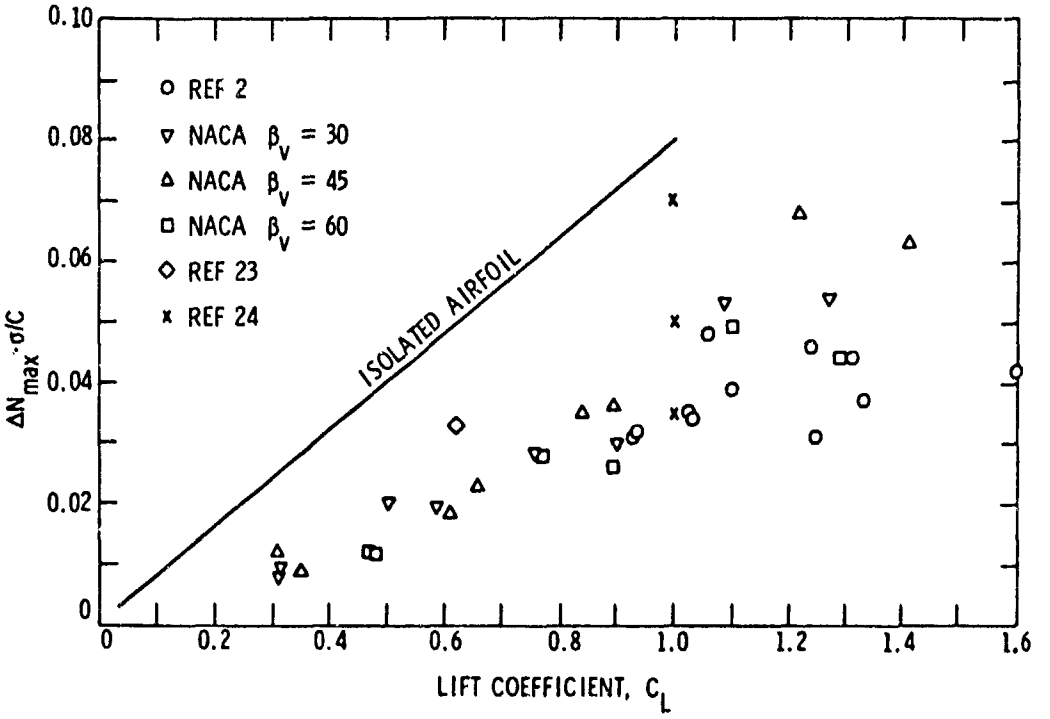

Figure 13. Normalized Maximum Offset, $\Delta N/C \cdot \sigma$, vs Vane Lift Coefficient, C_L.

$$\text{ERROR} = \frac{1}{n} \sum_{i=1}^{n} \left\{ \left\{ \frac{\Delta N}{C} \max_i - (a + b \cdot C_{L_i}^{c} \cdot \sigma_i^{d} \cdot \ell_i^{e} \cdot \beta_{v_i}^{f}) \right\}^2 \right\}^{1/2} , \quad (5.3)$$

where n is the number of cases being considered.

To solve this equation, reasonable values of the coefficients were chosen, then each in turn was varied to find the minimum error with respect to that coefficient. The process was repeated until convergence occurred. The final results, eliminating several data points which probably represented geometries that exhibited separation, were

$$\frac{\Delta N}{C} \max = 0.0018 + 0.0345\ C_L^{1.508}\ \sigma^{-0.4779}\ \ell^{0.0086}\ \beta_v^{0.1250} . \quad (5.4)$$

The magnitude of ℓ in this equation varies from zero to one, while the vane angle is measured in radians. The most important observation to be drawn from this equation is that the loading parameter and the vane angle appear to be insignificant and may be readily eliminated from this relation. The small positive constant (0.0018) is in general agreement with data published in Reference [27] which indicates that for staggered, flat plate cascades at zero incidence, there is a small negative lift, requiring a positive offset for correction. The magnitude of the exponents of the lift coefficient and solidity are in general agreement with observations made on the other correlations. The results of this equation are plotted in Figure 14. On this plot, the value derived from the fit and experimental values of the nondimensional offset are plotted against the lift coefficient. The (+) sign represents the experimental value of the offset, while the (x) represents the curve fit value and the vertical line represents the error in the curve fit. The solid curve

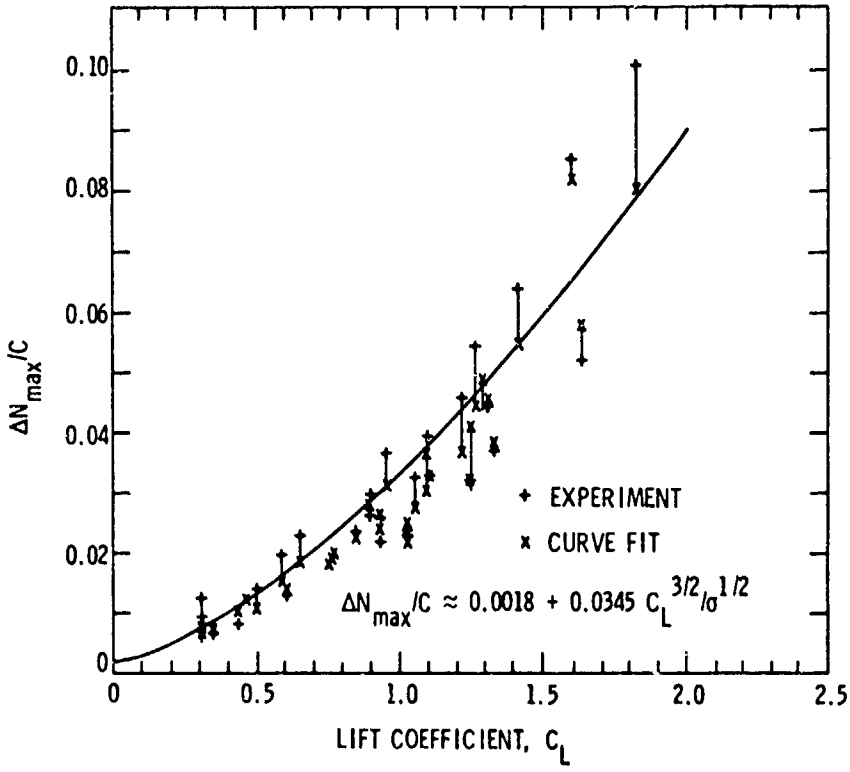

Figure 14. Least Squared Error Curve Fit of the Normalized Maximum Offset, $\Delta N/C$, vs the Vane Lift Coefficient, C_L.

represents a curve fit for a condition of unit solidity and a symmetrical loading distribution. The mean error in $(\Delta N/C_{max})$ for these data was less than 0.005, less than 10 percent of the usual offset values used in a design. Some divergence is seen at higher lift coefficients, which would be expected due to flow separations.

Finally, a curve fit of the form

$$\frac{\Delta N}{C}\ \text{max} = 0.002 + 0.035\ C_L^{3/2}/\sqrt{\sigma} \tag{5.5}$$

closely approximates the derived curve fit and would lead to slightly more than the desired turning angle in a design process.

The actual shape of the offset distribution varies considerably and is highly dependent on the incidence angle of the cascade. The NACA data used specified an incidence of 0 degrees and results in a cusp in the leading edge of the cascade as seen in Figure 11. The data of Wislicenus [2], however, are not specified at the zero incidence condition and results in an offset distribution similar to Figure 10. Here, the deviation caused by the offset decreases the effective incidence angle and should be helpful in reducing the possibility of leading edge suction face cavitation. The data analysis indicated that the shape of the offset distribution on the trailing edge side of the maximum point was fairly consistent, while the shape and magnitude of the leading edge varied considerably, an observation also made in Reference [2].

In a design exercise, the location of the maximum offset should be important and prehaps related to the loading distribution shape. Figure 12 was an attempt to make this correlation. The loading parameter is plotted against the percent chord of the maximum offset. Although there is considerable dispersion of the data, the straight line is a reasonable

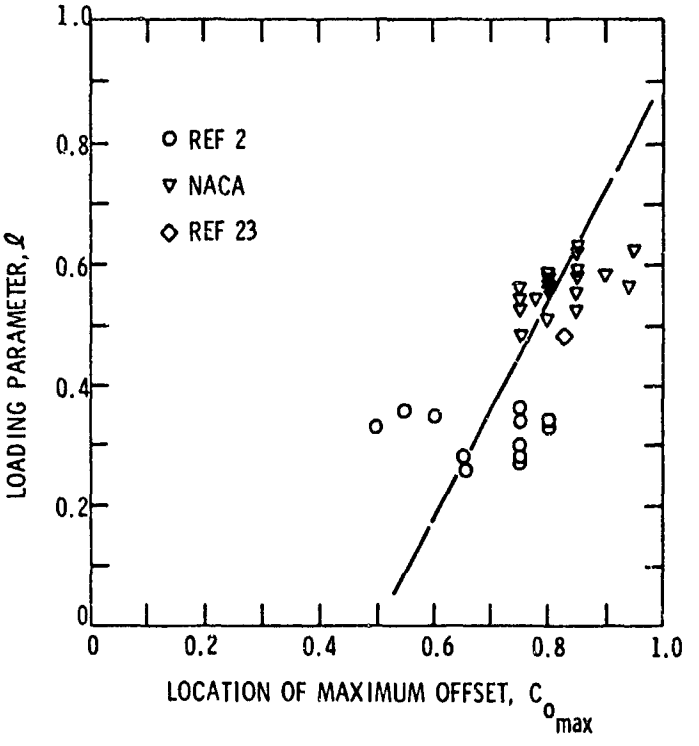

Figure 15. Loading Parameter, ℓ, vs the Location of the Maximum Offset, $C_{o_{max}}$.

fit and indicates that the maximum offset is generally toward the trailing edge and shifts toward the trailing edge as the loading shifts rearward, again as would be expected.

There is no apparent correlation for the leading edge offset distribution, leaving the designer relatively free to choose this shape, either for cavitation resistance or zero incidence.

5.4 Computation of the Offset Distribution

The designer is free to choose the loading distribution to be used for a particular cascade. This distribution is integrated to determine the loading parameter, ℓ, which is related to the position of the chord at which one-half the total work of the blade is accomplished. In more precise terms,

$$\int_{1}^{\ell \cdot t} \Delta P(x)dx = \frac{1}{2} \int_{1}^{2} \Delta P(x)dx \quad , \tag{5.6}$$

solving for ℓ. This can easily be done graphically or numerically, or if a symmetrical loading is used, the loading parameter is 50 percent. This is substituted into the relation

$$C_{o_{max}} = 0.5 + 0.525 \cdot \ell \quad , \tag{5.7}$$

where $C_{o_{max}}$ is the percent chord at which the maximum offset exists. This relation is derived from Figure 15. The lift coefficient (C_L) is known from the through-flow analysis and is substituted into the approximate relation for the maximum offset, along with the solidity, which is known from the chord length and the blade spacing. Then,

$$\frac{\Delta N}{C} \text{ max} = 0.002 + 0.035\ C_L^{3/2}/\sqrt{\sigma} \quad . \tag{5.8}$$

When the computerized Mean Streamline Method of Reference |28| is used, the lift coefficient, solidity, and chord length are determined iteratively and the above relations for $C_{o_{max}}$ and $\Delta N/C_{max}$ must be used within the process.

The shape of the offset distribution is determined as follows. An incidence at the leading edge is chosen, such as zero, for shock free entry or more probably a small negative incidence, usually about 1 degree for cavitation suppression.

The offset distribution must be determined as a continuous, smooth function of the chord position. In the computerized design that is described later in chis chapter, a polynominal curve fit is made to the necessary boundary conditions. Alternate methods may be used even to the extent of laying out a distribution using mechanical spline curves.

5.5 Numerical Description of the Offset Distribution

The information generated by the correlation relations is sufficient to numerically describe an offset distribution. A polynomial may be generated that satisfies the following boundary conditions:

$$Y/C(C_{o_{max}}) = \frac{\Delta N}{C} \text{ max} \quad ,$$

$$Y'/C(C_{o_{max}}) = 0.0 \quad ,$$

$$Y/C(100\%\ C) = 0.0 \quad ,$$

$$Y'/C(0.0\%) = \text{TAN}(\alpha_i) \quad ,$$

and

$$Y/C(0.0\%) = YLE \quad ,$$

where (Y/C) is the value of the offset and (Y'/C) is the slope of the offset distribution. The last parameter is arbitrary and may be adjusted to prevent reverse camber or obviously undesirable offset shapes from being determined. Usually, YLE may be set to zero.

A polynomial of the form

$$Y/C = A(x/c)^4 + B(x/c)^3 + C(x/c)^2 + D(x/c) + E \qquad (5.9)$$

will satisfy all of the above boundary conditions. Some design intuition must be used, especially when selecting the incidence angle. The quantities used above are shown graphically in Figure 16.

The coefficients may readily be determined:

$$E = YLE \quad ,$$

$$D = TAN(\alpha_i) \quad ,$$

$$A = (TAN(\alpha_i)(\frac{2}{C_{o_{max}}} - 3) + YLE(\frac{1}{C_{o_{max}}^2} - 3. - \frac{\frac{\Delta N}{C}_{max}}{C_{o_{max}}^2})/(1-C_{o_{max}}) \quad ,$$

$$B = (TAN(\alpha_i)(\frac{1}{C_{o_{max}}} - 1) + YLE(\frac{1}{C_{o_{max}}^2} - 1) - \frac{\frac{\Delta N}{C}_{max}}{C_{o_{max}}^2})/(1-C_{o_{max}})$$

$$- A(1 + C_{o_{max}}) \quad ,$$

and

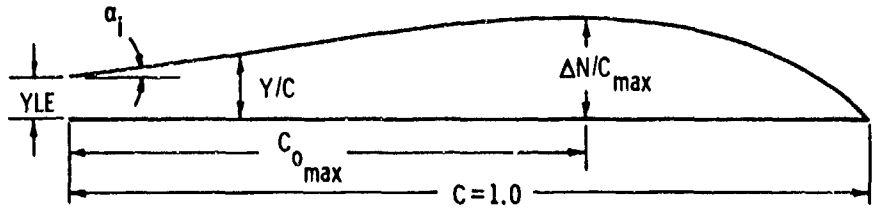

Figure 16. Parameters Defining the Nondimensionalized Offset Distribution.

$$C = - (+TAN(\alpha_1)+YLE+A+B) \quad .$$

These results are applied directly to the computerized design procedure.

5.6 Estimation of the Blade Pressure Distribution

The design process develops, at a certain percentage of the chord, the static pressure difference across the blade and the average through-flow velocity. Additionally, the total pressure of the f'ow is known from consideration of inlet conditions, the change in angular momentum, and the rotational speed, if any. An approximate solution for the surface static pressures may be developed from this information.

The average total pressure at any point in the blade row may be expressed as

$$P_{t_x} = P_{s_1} + \frac{1}{2}\rho\{(V_{m_x}+\Delta V_{m_x})^2 + (V_{\theta_x}-U_x)^2\} \quad . \qquad (5.10)$$

This quantity is assumed to be constant across the channel from the suction to the pressure surface. It is necessary to find the variation of relative velocity across the channel and at the same time assure that the volume flow rate is conserved.

The static pressure difference between the suction surface (ss) and the pressure surface (ps) is known (ΔP), and the gradient is assumed to vary as the square of the local velocity. This is equivalent to assuming that the curvature of the streamlines is uniform across the channel. Therefore,

$$\Delta P = \frac{1}{2}\rho \int_{ss}^{ps} \text{Const } W(y)^2 \cos(\gamma)\, dy \quad , \qquad (5.11)$$

where (γ) is the local flow angle and W is the local relative velocity. The volume flow rate per unit depth may be expressed as

$$\dot{V} = \int_{ss}^{ps} W(y) \cos(\gamma)\, dy \quad , \tag{5.12}$$

and, combining the three previous equations,

$$\dot{V} = \frac{2}{\rho} \int_{ss}^{ps} (P_t - P_{ss} - \Delta P(y))^{1/2} \cos(\gamma)\, dy \quad , \tag{5.13}$$

where P_{ss} is the suction surface static pressure and $\Delta P(y)$ is the pressure difference between the suction surface and some point in the channel. Knowing the distributions of local relative velocity W(y) and static pressure, the suction surface static pressure may be determined:

$$P_{ss} = \int \{P_t - W(y)^2 - \Delta P(y)\}\, dy \quad . \tag{5.14}$$

Once the suction surface static pressure is known, the velocity and static pressure gradients may be reevaluated in an iterative procedure which will converge in about five steps. As an initial guess of the velocity and pressure distributions, a uniform velocity and linear pressure are used. In each step of the cycle, the velocity distribution is checked for volume flow and corrected to match the proper valve.

This method produces a pressure distribution quite similar to the estimation method used in Reference [2] but is slightly less

conservative in predicting the minimum pressure, i.e., the minimum pressure is slightly higher than that found by the method of Wislicenus [2].

5.7 Summary

A significant range of cascade data was analyzed to provide refined input to the Mean Streamline Method of blade section design of Reference [2]. The maximum deviation or offset of the camber line from the mean flow streamline has been shown to be primarily a function of the blade lift coefficient and solidity. The loading distribution and vane stagger angle are shown to have only a small effect on this deviation. The shape of the offset distribution is influenced to a degree by the loading distribution.

A method of computing offset distributions for pumps or subsonic compressors has been presented that is valid for a wide range of lift coefficient and loading parameter. In all cases, the offset correction is small compared to the chord length, and the error in specifying this offset may be considered insignificant. The shape of the leading edge of the offset distribution is poorly correlated with any of the blade parameters, and it is apparent that the designer is free to adjust this shape for shock free entry or cavitation suppression on the suction surface as desired.

An approximate method of determining the blade pressure distribution has been presented. The method satisfies the pressure difference required by the loading distribution and conservation of mass and total pressure. The method is based on a simplified radial equilibrium approach, and it is felt to be more accurate than previous methods of approximation used with the Mean Streamline Method.

CHAPTER VI

AXIAL FLOW PUMP DESIGN EXAMPLE

A simple axial flow pump was designed by the use of the Streamline Curvature Method and the Mean Streamline Method of blade section design. The flow geometry was simple enough that a one-dimensional through-flow analysis would have sufficed, except that, due to blade geometry problems, a rotor with nonuniform spanwise loading was required. This in turn causes a radial displacement of the streamlines which in turn requires the use of a radial equilibrium theory to predict the through-flow. Because the inflow is a fully developed boundary layer flow, the Streamline Curvature Method must be used for the solution in lieu of simpler radial equilibrium approaches.

The design requirements of the axial flow pump are:

Volume flow rate	Q	= 1000 gpm
Head rise	H	= 36 ft of water
Shaft speed	N	= 6000 rpm
Rotor tip diameter	D_t	= 0.312 ft
Rotor hub diameter	D_h	= 0.12 ft
Casing diameter	D_c	= 0.315 ft
Inlet head	H_{sv}	= 150 ft

The suction specified speed is

$$S = \frac{N(rpm)\sqrt{Q(gpm)}}{H_{sv}^{3/4}} = 3829 \quad . \tag{6.1}$$

In Reference [29], it is indicated that cavitation inception should not occur until values of S approaching 6300 are obtained. The head coefficient, ψ, for the pump rotor is defined as

$$\psi = \frac{gH}{U_t^2} = 0.121 \quad , \tag{6.2}$$

where U_t is blade speed at the blade tip. In Reference [2], it is shown that values of ψ as high as 0.2 can be handled by a single stage axial flow pump. On the basis of the above, a single stage axial flow pump is selected.

From Reference [30], the specific speed of the pump indicates a hydraulic efficiency of approximately 0.80. An estimate of horsepower required and the shaft torque can now be made, where

$$\text{Shaft Horsepower} = \frac{\gamma H\ Q(cfs)}{550} = 11.36 \text{ HP}$$

and

$$\text{Shaft Torque} = \text{Power}/2\pi N = 9.94 \text{ ft lbs} \quad ,$$

where N is the rotational speed in revolutions per second.

6.1 Flow Field Calculations Through the Axial Flow Pump

The Streamline Curvature Method of through-flow analysis presented in an earlier chapter was used to obtain the flow field solution used in

the design of the axial flow pump. This technique assumes the flow to be axisymmetric and requires as input the radial distribution of velocity and energy at some station upstream of the pump, as well as the radial distribution of peripheral turning to be placed in the flow by the blade rows. The meridional velocity at station (1), indicated on Figure 17, was estimated based on the Blasius seventh-root law for turbulent flow in smooth pipes and modified as recommended in Reference [31] to correct for the higher Reynolds number effects incurred for this particular application. The velocity profile is influenced by the presence of a diffuser and bends located in the pipe upstream of station (1), but there is no means of predicting their effect. The velocity profiles at station (1), based on the seventh-root law for boundary layers and also modified for Reynolds number effect, are shown in Figure 18. The modified profile was assumed to apply in this design.

The radial forced vortex distribution of peripheral velocity selected to impart the required energy to the flow is shown by Figure 19. Also plotted is a distribution for a free vortex radial loading distribution, and it is apparent that less turning is required near the root sections if the forced vortex loading is used. The reduced turning near the blade root is desired to prevent the possibility of flow separation from the blade surface and to ease manufacturing problems.

The axisymmetric streamline solution derived for the pump is shown in Figure 20. The velocity profiles obtained at the rotor inlet and exit, as well as those at stator inlet and exit, are shown in Figure 21.

The integrated value of head based on a mass average equals 36 feet, if the peripheral velocity and meridional velocities of Figures 19 and 21 are used.

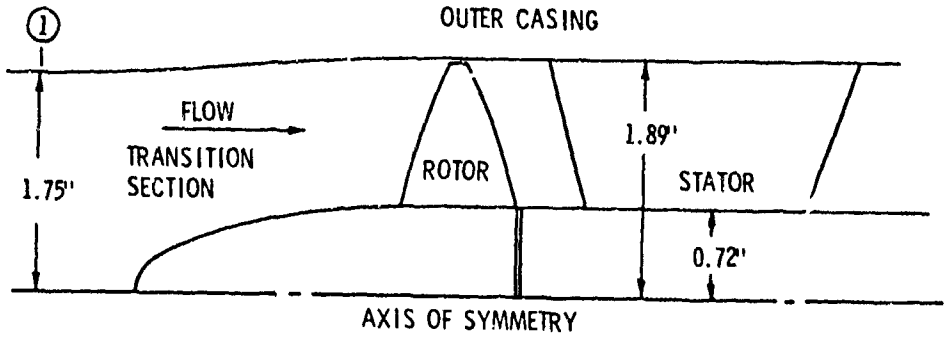

Figure 17. General Layout of the Axial Flow Pump Design Example.

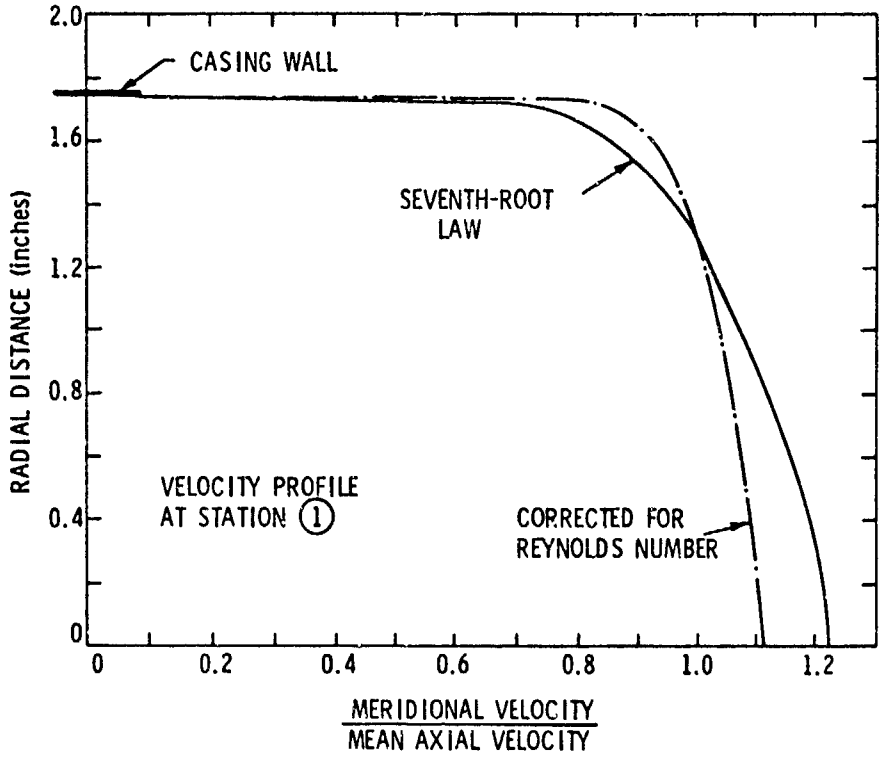

Figure 18. Velocity Profile in Duct Upstream of Rotor.

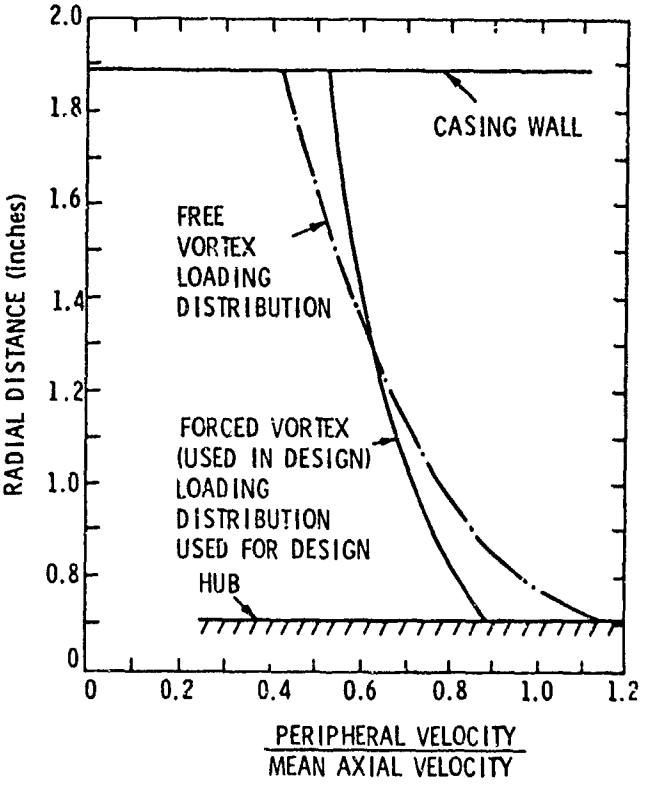

Figure 19. Distribution of Peripheral Velocity at Rotor Exit.

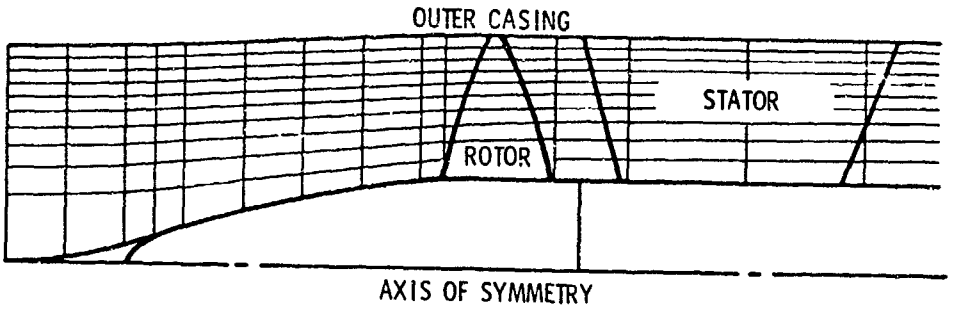

Figure 20. Computed Streamlines for the Axial Flow Pump Design Example.

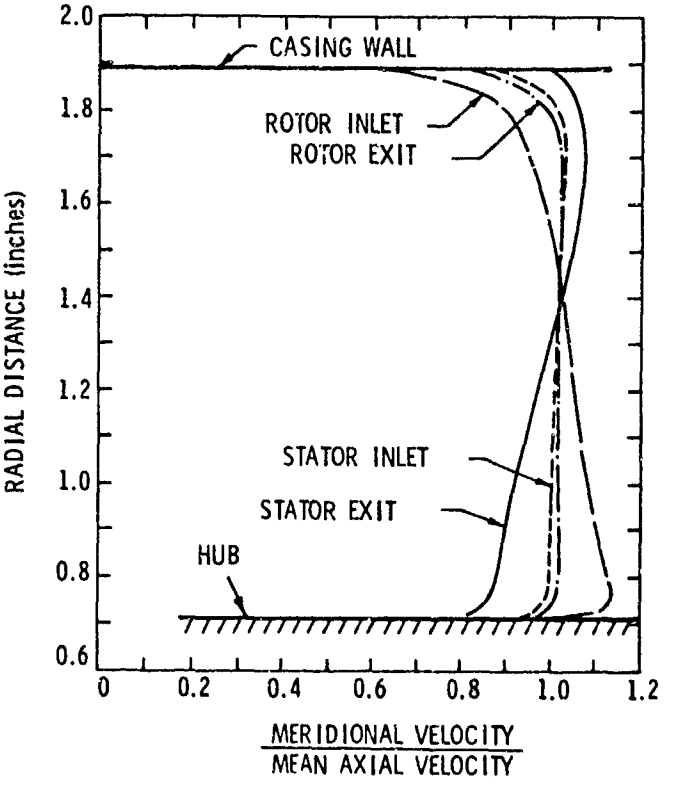

Figure 21. Computed Blade Row Velocity Profiles.

6.2 Detailed Blade Section Design

The velocity profile data developed by the Streamline Curvature Method was used as input to the Mean Streamline Method of blade section design. Cylindrical sections at five equally spaced radii were designated for both the rotor and stator. Preliminary considerations of blade loading were used to determine the projected length of each section to give a lift coefficient of approximately 0.7. This distribution of blade length was modified slightly to ease problems of manufacture and the physical constraints imposed by the duct and resulted in the blade planform depicted in Figure 17. The streamline representing the pump casing has a theoretical zero velocity. To aid convergence of the Streamline Curvature Method, the velocity at the wall is given an initial value of one-half the mass averaged duct velocity. In the design of the blade tip section, the velocity associated with the streamline 2 percent inside the casing is used to represent the tip flow condition.

The developed cylindrical sections for the rotor and stator are plotted in Figures 22 and 23, respectively.

Once the blade section shapes were finalized, the lofting procedure of Reference [32] was used to develop rectangular sections for each blade. The rectangular blade sections are input to a series of computer programs that produce data necessary to operate a numerically controlled milling machine with the blade surfaces numerically machined. The fillet area at the hub is machined by conventional methods. A photograph of the finished pump blading is shown by Figure 24.

6.3 Axial Flow Pump Tests

The axial flow pump was installed in the ARL/PSU six-inch water tunnel. An adapting collar and nozzle mated the smaller diameter rotor

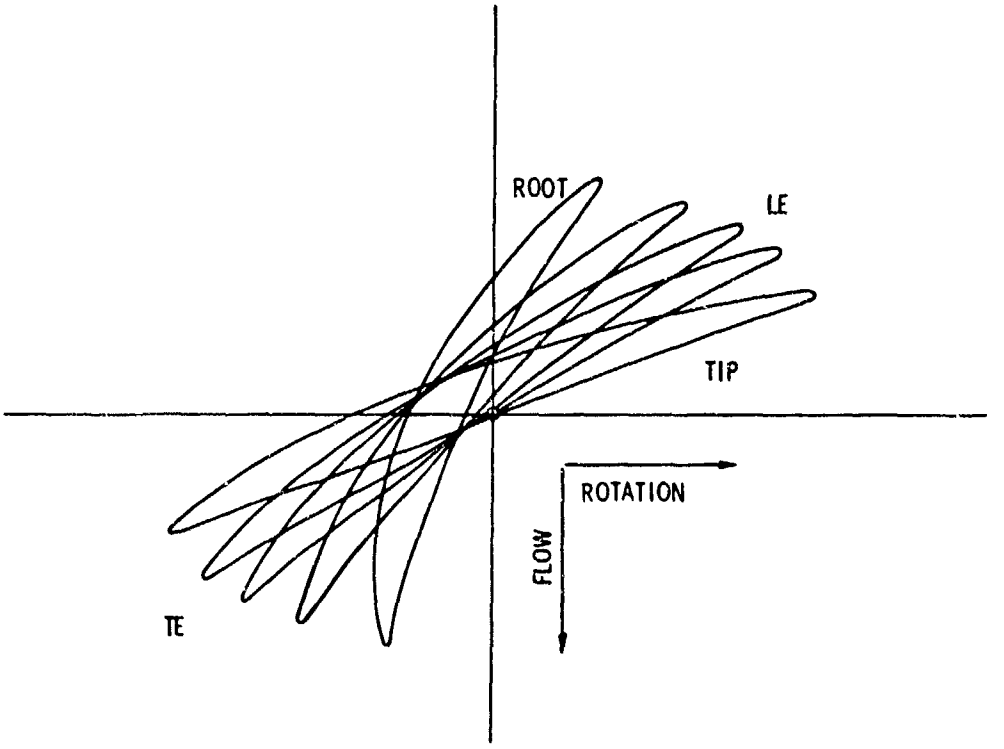

Figure 22. Rotor Cylindrical Design Sections.

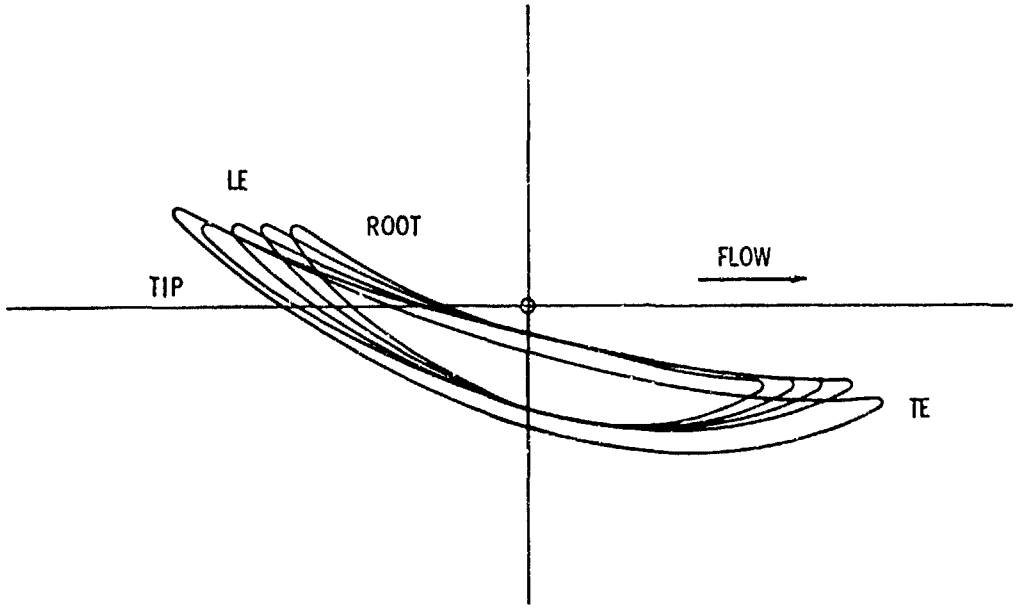

Figure 23. Stator Cylindrical Design Sections.

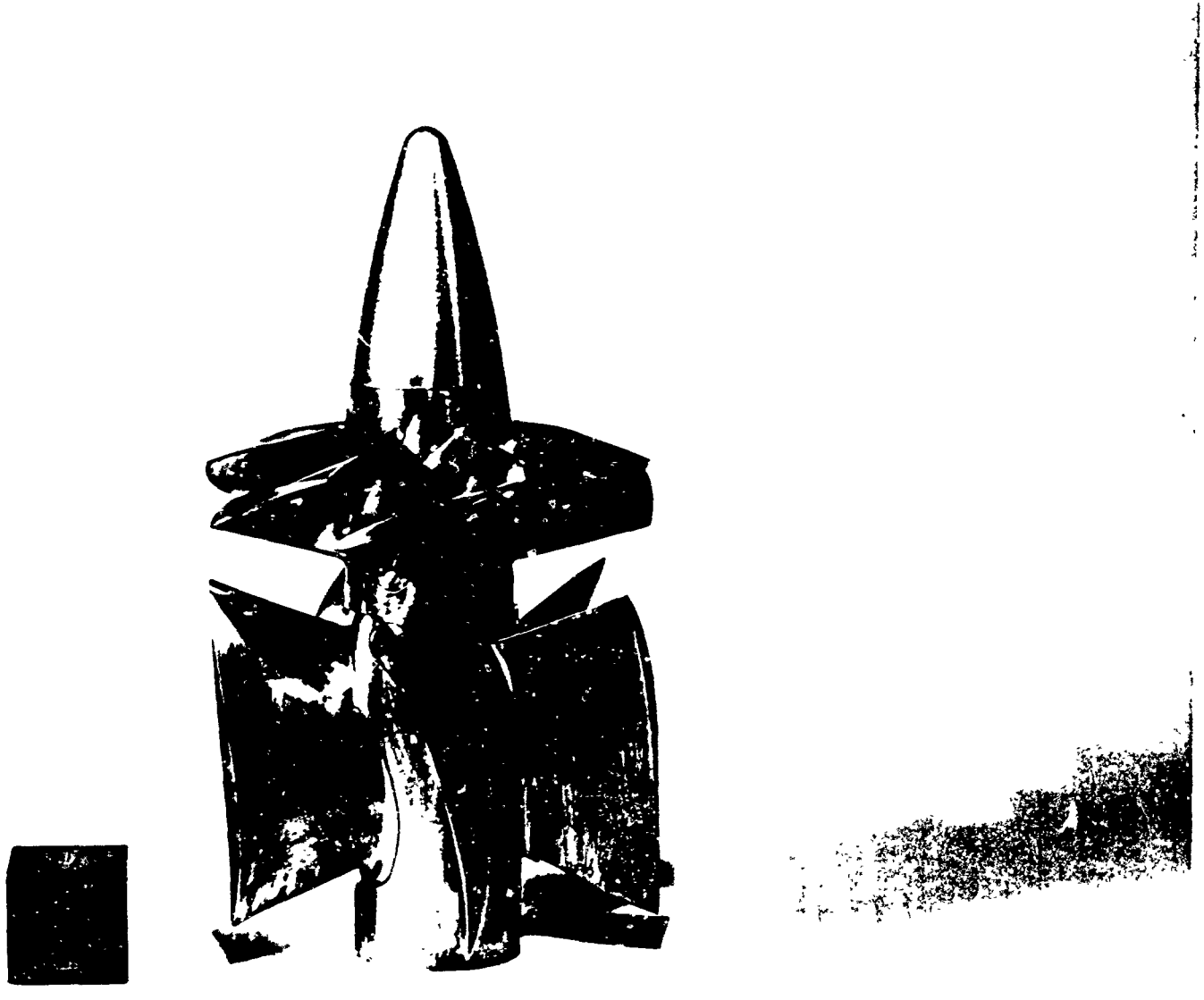

Figure 24. View of the Axial Flow Pump Rotor and Stator

and stator (3.78 inches) to the six-inch diameter water tunnel test section. Orifice plates installed in the legs of the water tunnel provided the necessary pressure drop to test the pump from 50 percent to 150 percent of its design capacity. The water tunnel main drive pump was used to control the flow rate through the pump.

Surveys of velocity and total pressure just upstream and downstream of the pump were used to determine the flow rate and total head rise of the pump. A torque cell was used to determine input power to the rotor. Cavitation performance was noted using the tunnel pressure system, but the validity of the results is limited due to the slow response of the tunnel pressure system and the uncontrolled high air content in the water.

6.4 Test Procedure

The axial flow pump was installed in the six-inch water tunnel as shown in the photographs of Figures 25 and 26. The flow field through the pump was measured with a wedge probe installed approximately 2 inches upstream of the rotor and a Kiel total pressure probe installed approximately 1 inch downstream of the stator. A four and one-half inch orifice plate was installed in the downstream vertical leg. A three-inch orifice plate was installed in the upstream vertical leg.

The upstream wedge probed was nulled before true readings of total pressure were made. The downstream Kiel probe was designed to read total pressure while eliminating any effects of rotation in the flow. The data taken over several tests indicated that over-all the data were repeatable to within 3 percent.

The upstream and downstream probes were set at 0.7 of the blade span and a setting of the water tunnel pump was determined that yielded the correct total pressure rise for the corresponding RPM of the pump. At

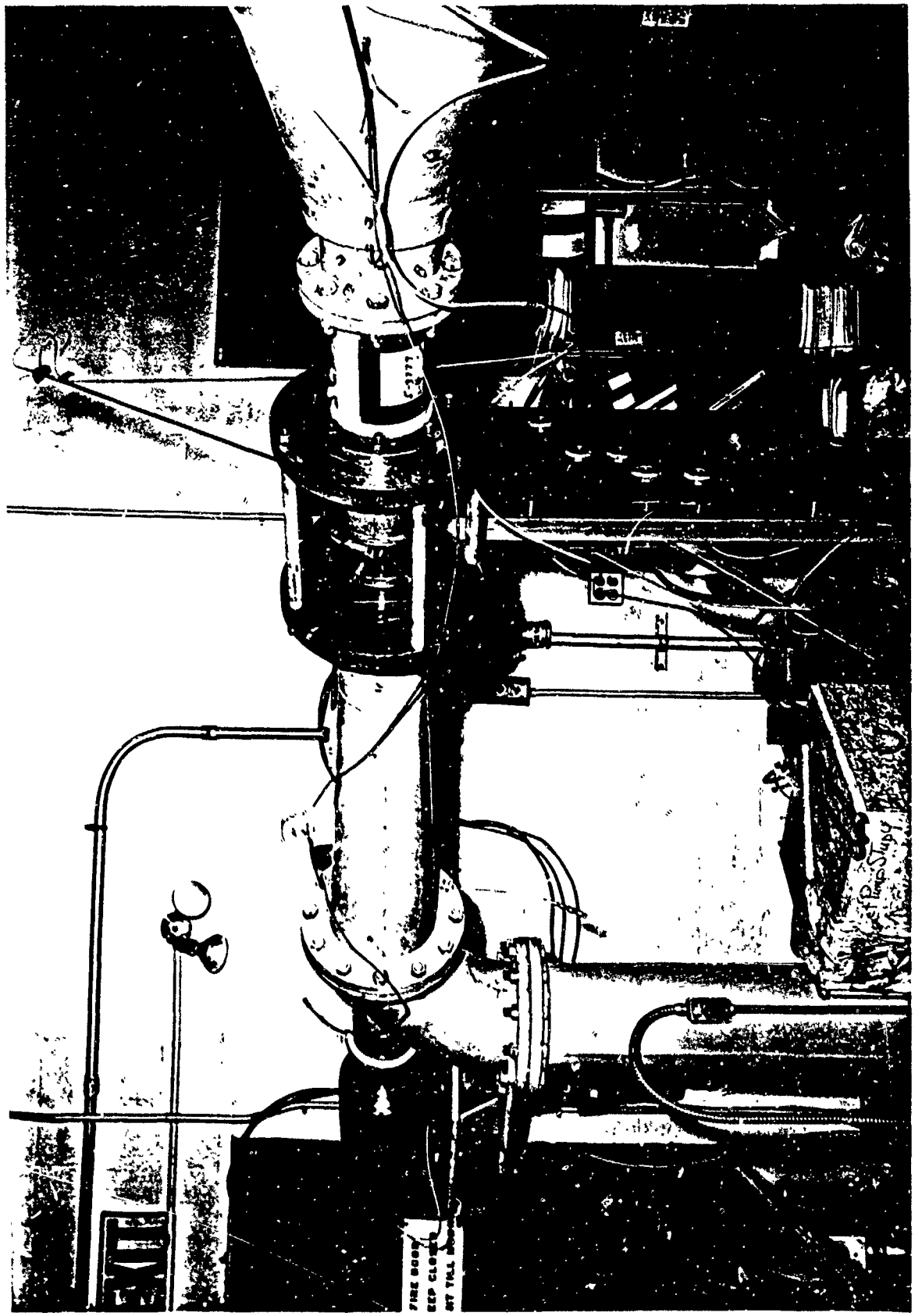

Figure 25. Overview of the Axial Flow Pump Installed in the Six-Inch Water Tunnel (Flow is from Right to Left).

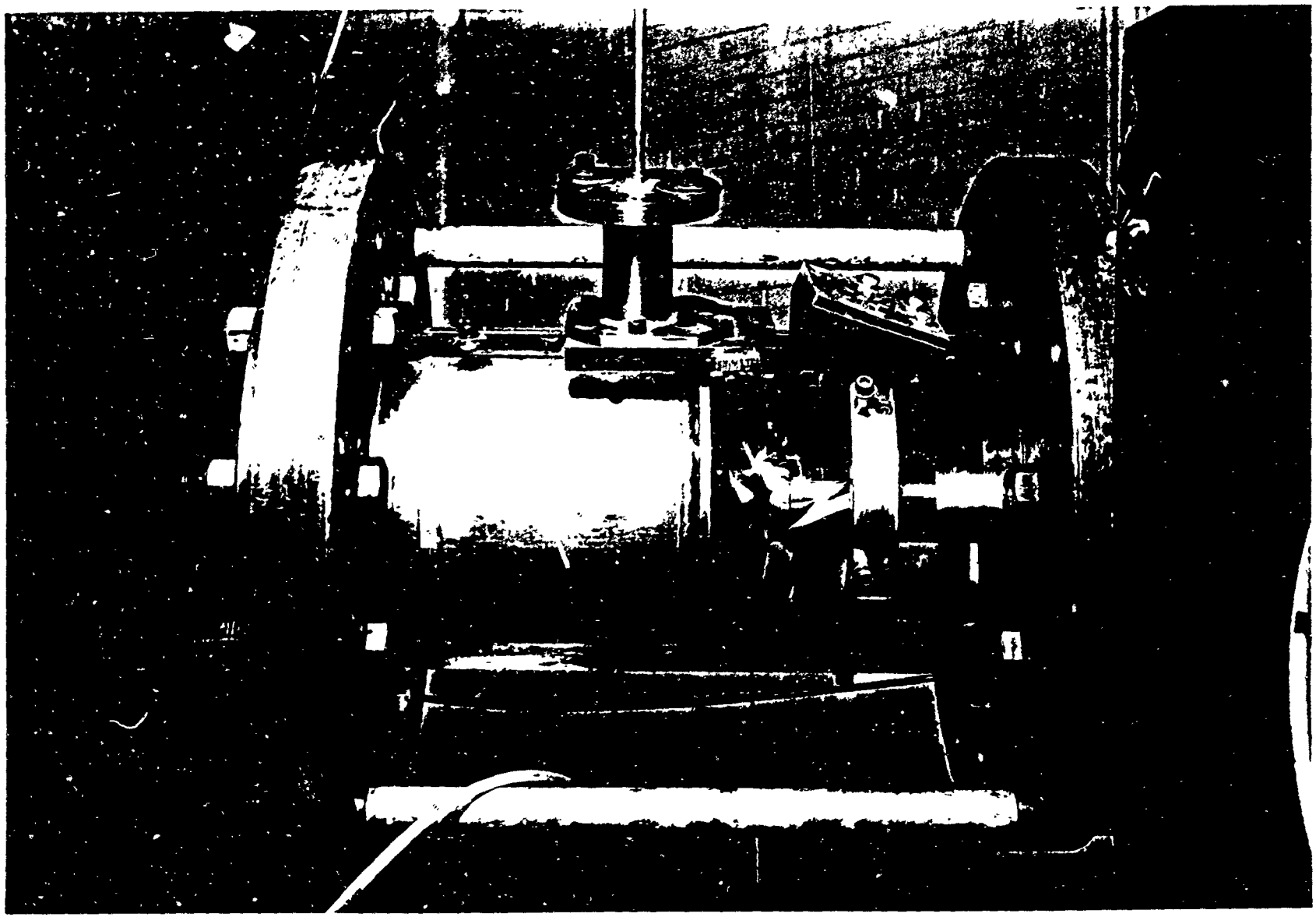

Figure 26. Close-up View of the Axial Flow Pump Rotor and Stator Installed in the Test Section of the Six-Inch Water Tunnel (Flow is from Left to Right).

these settings, the upstream velocity profile and the downstream total pressure profile were obtained as a function of radius.

Both profiles were integrated to give the mass-averaged velocity at the pump inlet and the mass-averaged total pressure at the stage exit. The upstream velocity probe and the downstream total pressure probe were set at a radius that corresponded to the mass-averaged values. It was assumed that the shape of the velocity and total pressure curves did not change appreciably with flow coefficient and the main tunnel pump was used to systematically vary the flow coefficient. The average velocity, average total pressure rise, and shaft torque were recorded for a range of flow coefficients.

6.5 Test Results

The upstream velocity profile and probe location which corresponds to the mass-averaged velocity for the rotor are presented in Figure 27. The total pressure survey data are shown in Figure 28. With the probes located as shown in Figurew 27 and 28, the total pressure coefficient and powering requirements obtained are presented in Figure 29. Some care must be used in interpreting the efficiency curves since very large (40 percent) bearing torque values were measured, decreasing the accuracy of the powering data.

6.6 Summary

The axial flow pump was tested in the ARL/PSU six-inch water tunnel from 50 percent to 150 percent of its design capacity. Tests indicated that the design placed 13 percent too much total pressure rise into the fluid and, hence, required more power to drive than anticipated.

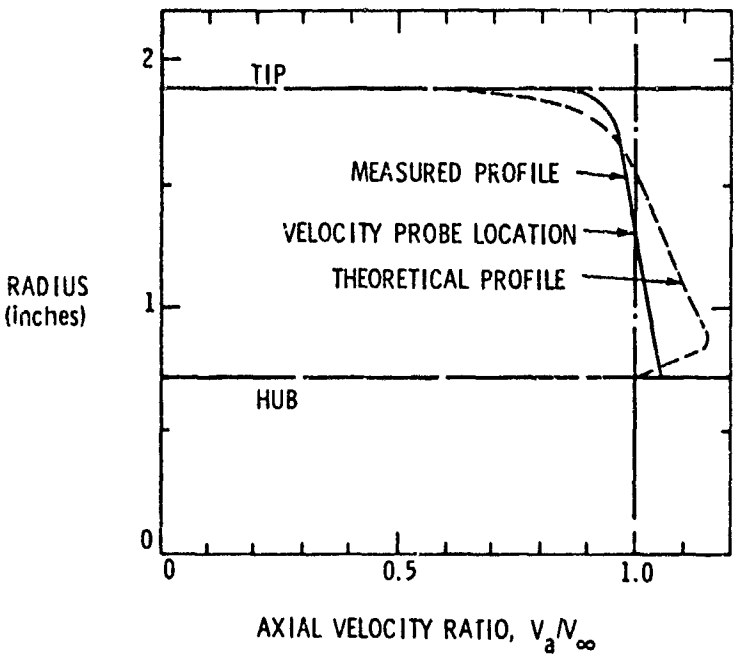

Figure 27. Experimental and Theoretical Velocity Profiles Immediately Upstream of the Axial Flow Pump Rotor.

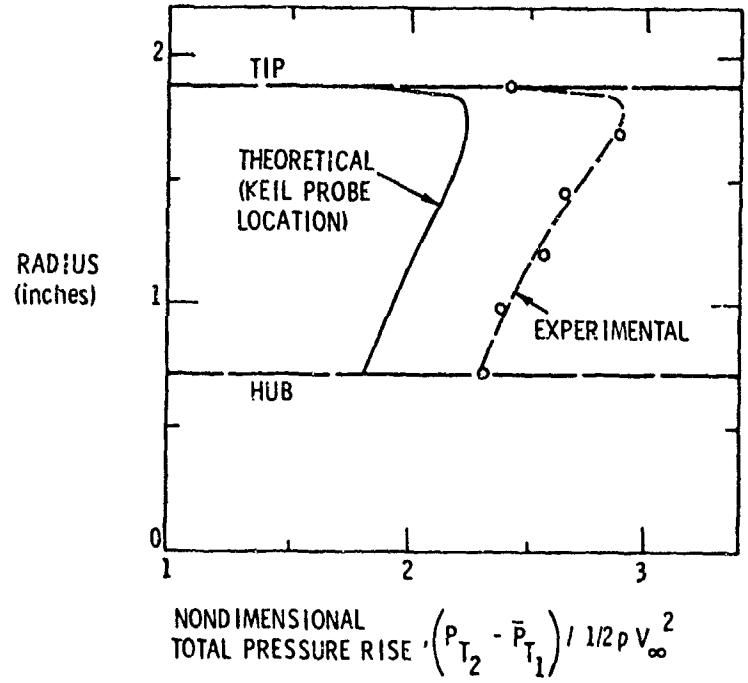

Figure 28. Comparison of the Theoretical and Experimental Total Pressure Rise Across the Axial Flow Pump at Design Flow Rate.

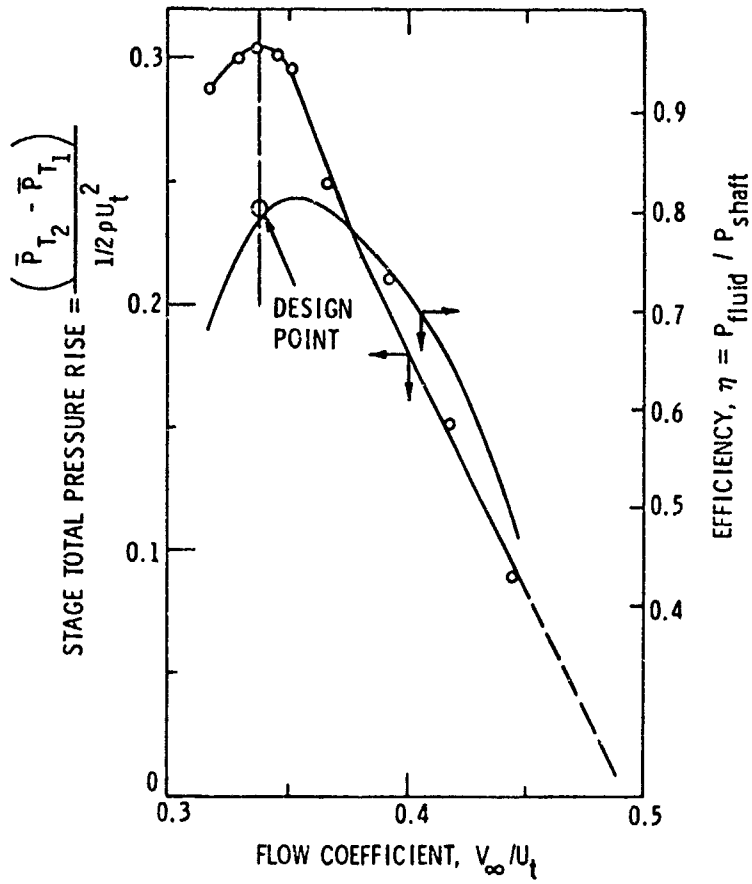

Figure 29. Performance Data for the Axial Flow Pump.

Analysis of the results of the axial flow pump design and test reveals several possible explanations for the differences between the design specifications and the test results. First, the inlet velocity profile in the test facility was different than that anticipated for the design application. Figure 27 reveals this difference. At the tip of the rotor, the blade incidence was considerably higher than anticipated and could have contributed to the increased torque and pressure rise noted. Additionally, the original estimation of the stage efficiency ($\eta = 0.80$) was conservatively low by at least 5 percent for this particular application. Because of this low estimate, higher than required blade loading would be specified. An accurate indication of the actual rotor efficiency could have been obtained experimentally if velocity and angularity measurements could have been made between the rotor and the stator. However, due to the proximity of the two blade rows, a probe could not be placed in a position adequate for the required measurements. It is apparent from Figure 28 that the distribution of the total pressure rise is correct but that a uniform increment has been added, supporting the argument that the estimated design value of efficiency was too low. A modification to the trailing edge of the rotor was necessary to bring the pump to its design point and also indicated that too much loading was specified in the preliminary design.

The design point efficiency as derived from powering data in Figure 29 is 0.78. However, considerable error may be present in this figure due to bearing tare forces of at least 40 percent of the total shaft torque. This situation was caused by a bearing and shaft requirement for the test which could not be altered.

It is not apparent that these test results support the use of the design procedures described, although the performance problems seemed to be a result of the preliminary design rather than the detailed analysis. Because of the boundary conditions imposed by the preliminary design, a simplified through-flow analysis could not have been used. While agreement of the theoretical and experimental flow fields was not as good as anticipated in this case, other design examples of a more complex nature have shown excellent agreement as can be seen in Figure 9.

CHAPTER VII

CASCADE BLADE SECTION DESIGN USING THE STREAMLINE CURVATURE METHOD--GENERAL STATEMENT

An empirical method of satisfying an airfoil section with a prescribed loading distribution was explained previously. This method, the Mean Streamline Method, relied on correlational data to correct a theoretical blade shape based on the mean flow streamline to account for the effects of potential flow interactions and viscous losses encountered in a cascade of blades. The correlations geometrically increase the camber of the airfoil section in such a way as to compensate for the underturning experienced by the airfoil in actual operation. Figure 30 shows the major causes of cascade blade performance degradation.

In the Mean Streamline Method, all of the geometric and flow effects are lumped into a single correlation or camber line curvature correction as shown in Figure 31. A large number of airfoils were found in the literature which had substantial test data available. New correlations were developed which separated the major physical parameters in such a way as to show how each contributed to the design of the airfoil. The interesting results of this study were that only section lift coefficient and cascade solidity had any important effect on the airfoil performance or on the geometric shape of the theoretical camber line.

The direct theoretical determination of the required blade camber line is of great practical interest, as the effect of various geometric and fluid parameters can be determined separately. Additionally,

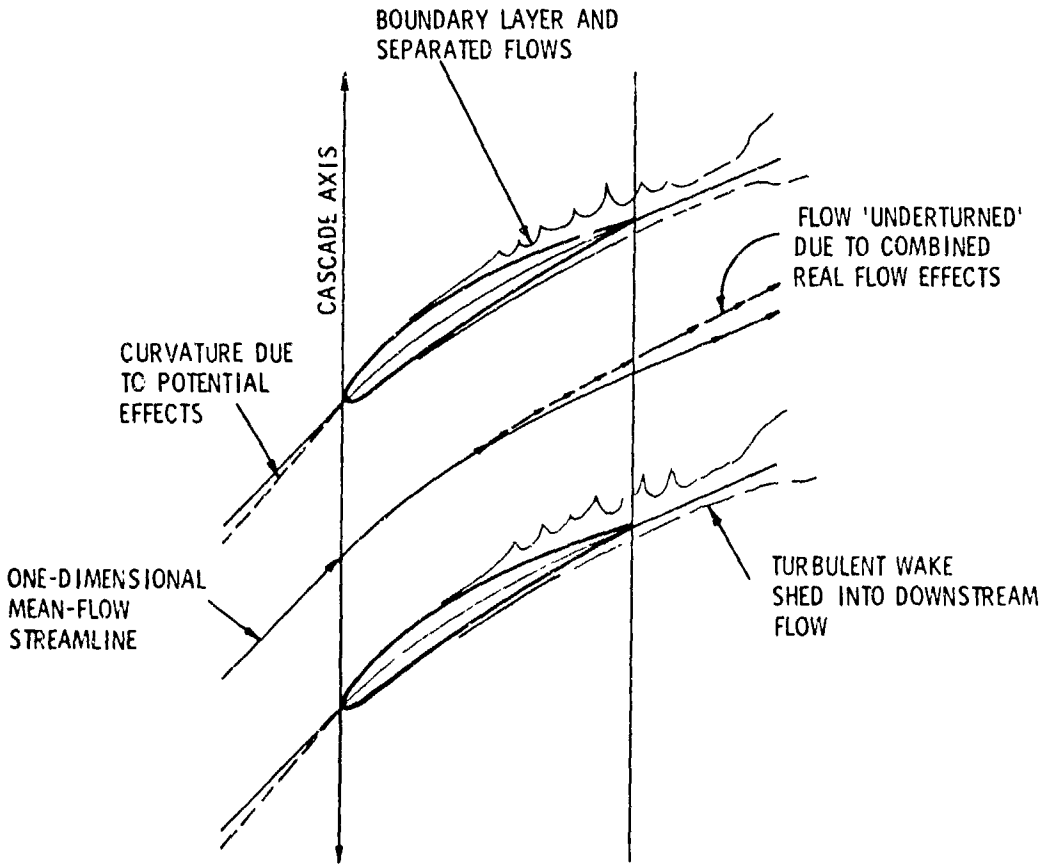

Figure 30. Major Phenomena Affecting the Work Done by a Cascade of Blades.

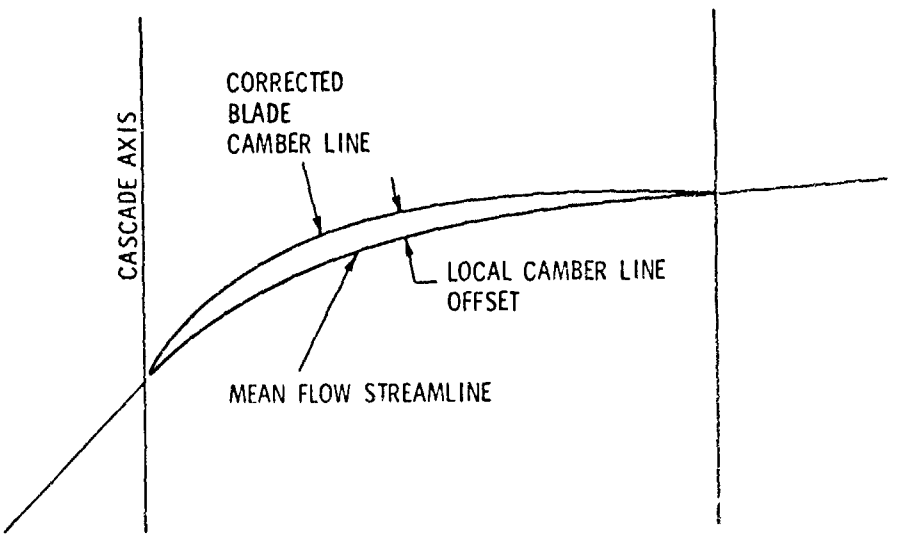

Figure 31. Schematic Representation of Camber Line Corrected to Account for Potential and Real Flow Effects in a Cascade.

correlation data are incomplete for two-dimensional sections and nonexistent for conformal sections or two-dimensional sections with variations in stream sheet thickness. Earlier investigators have explored the problem of designing arbitrary blade sections for compressors and turbines, Reference [3], some using the Matrix Through-Flow Method, others using the Streamline Curvature Method.

The unique solution of a blade shape for arbitrary loading and thickness distribution requires satisfaction of a variety of physical constraints. The majority of these are embodied in the laws of motion and are mentioned here. Each of the three equations of motion for incompressible, steady flow have several boundary conditions which must be satisfied.

The changes in fluid momentum through a cascade of airfoils, both parallel to the cascade axis and normal to it, must be balanced by blade surface pressure forces. For a cascade that is two-dimensional with no stream sheet thickness variation, there is essentially no net momentum change normal to the cascade axis. However, due to the thickness and boundary layer blockage, there are local momentum changes internal to the blade row. Additionally, the specification of the blade loading distribution requires a scheduled change in the average momentum parallel to the cascade axis as the fluid passes through the system. An additional constraint is that there can be no net momentum change anywhere outside the cascade boundaries. Local perturbations are required due to pressure effects propagated upstream and downstream of each blade section. This notion leads to another important requirement, that the periodic nature of the flow through an infinite row of blades in cascade be conserved. The flow at points on any line parallel to the cascade axis and spaced by

an integral number of blade spaces must be identical to conserve the periodicity of the flow field.

The momentum equation is required to satisfy all of these criteria, as well as to account for acceleration effects normal to the streamlines caused by the substantial streamline curvatures encountered in cascade flows, particularly those with closely spaced, highly loaded blading.

Conservation of total pressure in a cascade flow is fairly simple except that, for viscous flows, the losses caused by boundary layer growth and separation play a dominant role in causing changes in the blade row performance. These changes are usually embodied in a blade being able to do less turning of the fluid, hence, less work than theoretically possible.

Since the problem at hand is the indirect or design problem, however, the effect of losses is to require a blade shape with more turning than would be required for the same nonviscous flow. In a turbulent fluid, the quantification of viscous effects is nearly impossible and, hence, empirical data are required. The basic effects of viscosity are felt in three ways. First, an over-all total pressure loss occurs. This loss is distributed in some manner both through and across the blade-to-blade channel. Secondly, boundary layers on both blade surfaces, which are dependent on the blade surface pressure distribution, are generated. The effect of these boundary layers is to displace the streamlines near the blade some distance out into the flow. The final effect is that of the blade wake. At the trailing edge of each blade, a wake of low velocity boundary layer fluid is generated. This wake is propagated downstream and is gradually attenuated. The presence of the boundary layer and wake affect velocity terms in the momentum equation.

The continuity equation is the final condition to be satisfied. The purely two-dimensional solution for cascade flow presents little problem so far as satisfying continuity is concerned. However, when generating a quasi-three-dimensional solution for a blade row, account must be made for variations in stream sheet thickness in both the chordwise and channelwise direction. Additionally, the solution of the blade-to-blade flow will affect the meridional plane flow, i.e., the effects of thickness and boundary layers on the blade cause blockage accelerations in the meridional plane solution.

The following chapter presents a detailed solution of the equations of motion to determine a camber line given the blade loading and thickness distribution and specified inlet and exit fluid angles. An iterative numerical process involving the three equations of motion and the constraints discussed here was developed to determine the camber line of a cascade blade section. A test program was conducted to help ascertain the validity of the analysis and design method.

CHAPTER VIII

CASCADE BLADE SECTION DESIGN USING THE STREAMLINE CURVATURE METHOD--THE NUMERICAL METHOD

8.1 Development of the Numerical Method

This chapter describes an analytical method of prescribing a camber line for blades in a cascade. The flow is basically a two-dimensional or plane flow and is assumed steady, inviscid, and incompressible. The blade shape which results from the analysis has prescribed inlet and exit angles, loading and thickness distributions, and uses a correlational model for the blade surface boundary layer effects and downstream wake structure. The result of the analysis is a detailed description of the flow field in the vicinity of the blades, and, in particular, the velocities and pressures inside the blade channel are calculated.

The solution of the flow field requires that the three equations of motion be satisfied. These are the momentum equation, the continuity equation, and the conservation of total pressure. The method of solution is the Streamline Curvature Method and the derivation of the equations is similar to that reported in an earlier chapter. The basic difference in their solution is that the specification of the boundary conditions for the flow is considerably different.

The boundary conditions that are related to the blade-to-blade performance are shown graphically in Figure 32. The three most important boundary conditions are the inflow angle (ϕ_1), the exit flow angle (ϕ_2), and the blade projected length and spacing. Together, these flow and

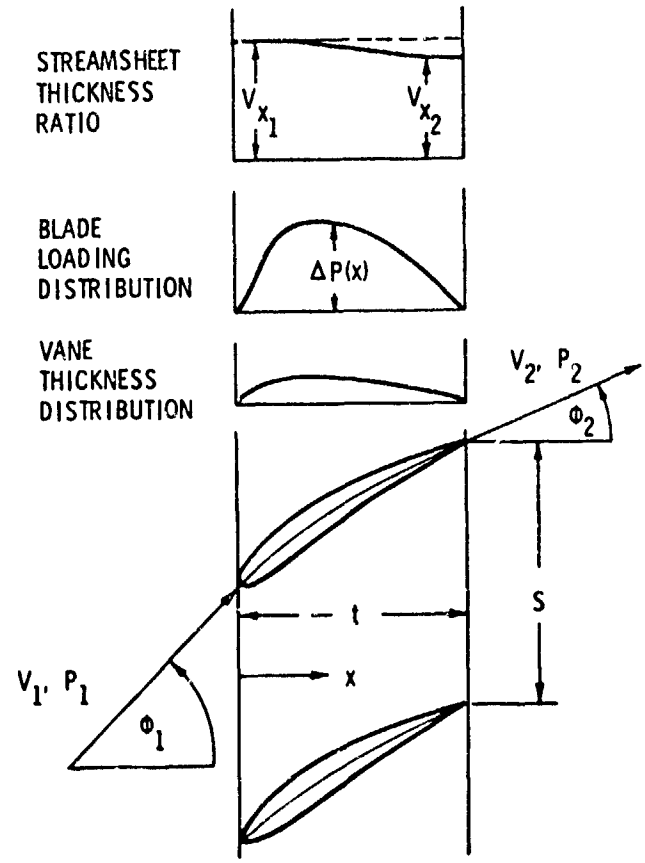

Figure 32. Design Boundary Conditions Input to the Two-Dimensional Cascade Design Procedure.

geometric properties determine the loading that is required of each blade in the cascade.

There are additional conditions which must be met in order to obtain a valid solution of the flow field. When a solution for the momentum equation is obtained, the momentum averaged in the direction of the cascade axis must be equivalent to that determined by the one-dimensional mean flow streamline, insuring that the blade surface pressure distribution exactly balances the momentum changes that occur. Because the cascade of blades extends to infinity in both directions parallel to the cascade axis, the flow must be periodic with a wave length equal to the blade spacing. In addition, in the flow external to the blade row, there can be no net momentum changes.

The momentum and continuity equations are both integral equations and require data to start their solution. Therefore, to start the iterative computation cycle, an approximate solution is required. This approximation may be generated by specifying the angular momentum changes as a function of location through the blade row and the continuity equation. In essence, the entire flow is given the properties of the mean flow streamline. The blade thickness and boundary layer are ignored in the initial approximation. Thus, the starting solution is an inviscid, thin airfoil theory with two-dimensional acceleration effects in the momentum equation neglected. The initial solution is shown schematically in Figure 33.

As the computation cycle progresses, blade thickness, boundary layer and loss models, and terms in the momentum equation are "turned on" gradually, so that each pass through the analysis represents a converged

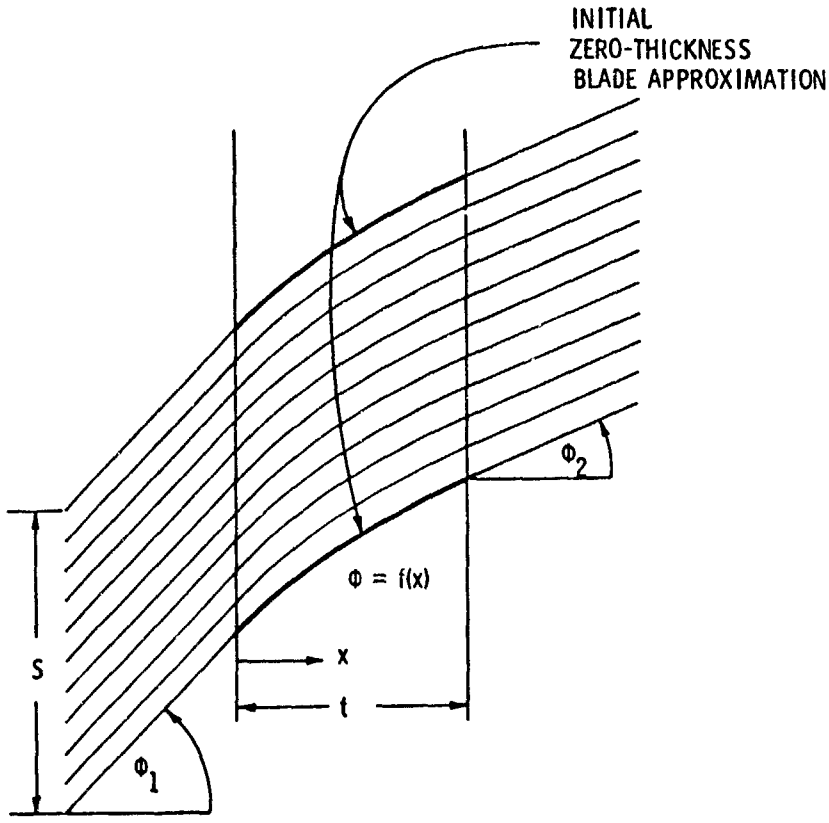

Figure 33. Initial Solution Geometry Consisting of a Number of Parallel Mean Streamlines Between Ideal, Zero Thickness Blades.

solution satisfying the modified equations in use for that pass. This prevents the solution from diverging numerically, due to the introduction of large perturbations on a single pass. In essence, the input to the equations on any pass represents a valid solution and, hence, only small changes in the solution are required on any particular pass. The required velocities on the streamlines are approximated by use of the following equations. The velocity parallel to the cascade axis at some point inside the blade row is

$$Vy(x) = Vy_1 + \Delta Vy \frac{\int_1^x \Delta P(x)\, dx}{\int_1^2 \Delta P(x)\, dx} \quad , \tag{8.1}$$

where ΔVy is the change in velocity parallel to the cascade axis from inlet to exit. The velocity normal to the cascade axis is calculated by use of the continuity equation, which is written for a one-dimensional flow with constant distance between the stagnation streamlines (i.e., plane flow with no accelerations due to flow field curvatures or blockage effects). This equation is

$$V_x(x) = Vx_1 \; f[sst(x)] \quad ,$$

where $f[sst(x)]$ is a function describing the average stream sheet thickness effect through the cascade. Normally, this function is unity for two-dimensional plane flows.

Functions describing both components of velocity $[V_x(x)$ and $V_y(x)]$ now exist, and a streamline satisfying these velocities may be constructed. This is the so-called mean flow streamline. The following equation is used to geometrically construct a mean flow streamline:

$$y(x) = y(x_1) + \int_{x_i}^{x} \frac{Vy(x)}{Vx(x)}\, dx \quad . \tag{8.2}$$

Normally, (x_1) would be a value several chord lengths upstream of the cascade leading edge, and the calculation of $[y(x)]$ would proceed until (x) values several chord lengths downstream of the cascade trailing edge were attained. This method is the construction of a streamline from its tangents.

Taking a number of these streamlines and repeating them in the defined spacing between adjacent blades in the cascade, as seen in Figure 33, yields a geometric solution that can be utilized to calculate the geometric derivatives necessary to start the iterative solution of the momentum equation. The velocity field also allows calculation of the required velocity derivatives. The solution as it stands satisfies the continuity and momentum balance equations averaged parallel to the cascade axis.

The equations of motion are now written in a manner that makes them applicable to the flow field geometry shown in Figure 34. The equations are solved along lines parallel to the cascade axis and that are generally perpendicular to the direction of flow. Usually, the term quasi-orthogonal is given to these solution paths; however, the angle of the flow to that of the quasi-orthogonal can be much less than 90

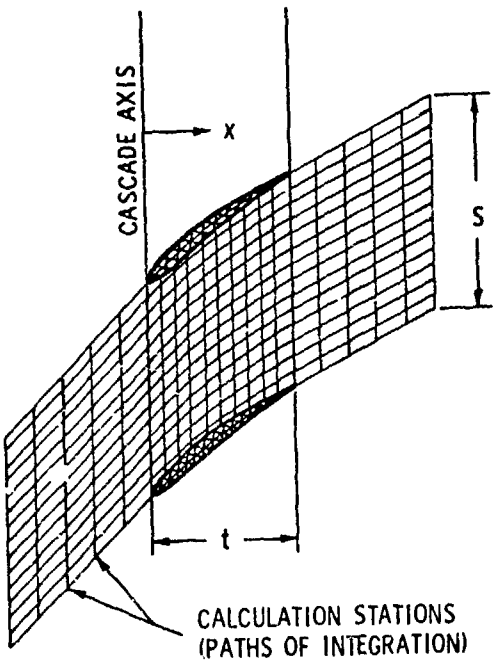

Figure 34. Generalized Cascade Flow Field Geometry.

degrees. The equations are solved at a number of positions along the axis perpendicular to the cascade axis. The solutions along these paths are linked through the geometric properties of the streamlines passing by each computing station. Euler's equation of motion applicable along each quasi-orthogonal in the above defined geometry is

$$-\frac{1}{\rho}\frac{\partial p}{\partial y} = V_x \frac{\partial V_x}{\partial x} + V_y \frac{\partial V_x}{\partial y} \quad . \tag{8.3}$$

This equation is modified in a manner similar to that used in the Streamline Curvature through-flow calculations in Chapter IV. The form used for computation is

$$-\frac{1}{\rho}\frac{\partial p}{\partial y} = \frac{V_m^2}{R_k}\cos\phi + V_m \frac{\partial V_m}{\partial s}\sin\phi \quad . \tag{8.4}$$

The term (R_k) is the streamline radius of curvature and is computed from the first and second geometric derivations of the streamline traces. These terms are shown in Figure 35. The term ($\frac{\partial V_m}{\partial s}$) is obtained from a finite difference approximation from the velocity field and the geometry of the streamlines.

The effect of this equation is to calculate the pressure gradient throughout the flow field based on the local acceleration due to streamline curvature ($\frac{Vm^2}{R_k}$) and the local convective acceleration ($V_m \frac{\partial V_m}{\partial s}$).

The simultaneous application of the continuity equation and conservation of total pressure completes the essential portions of the calculation. The following equation combines the two equations used in this analysis:

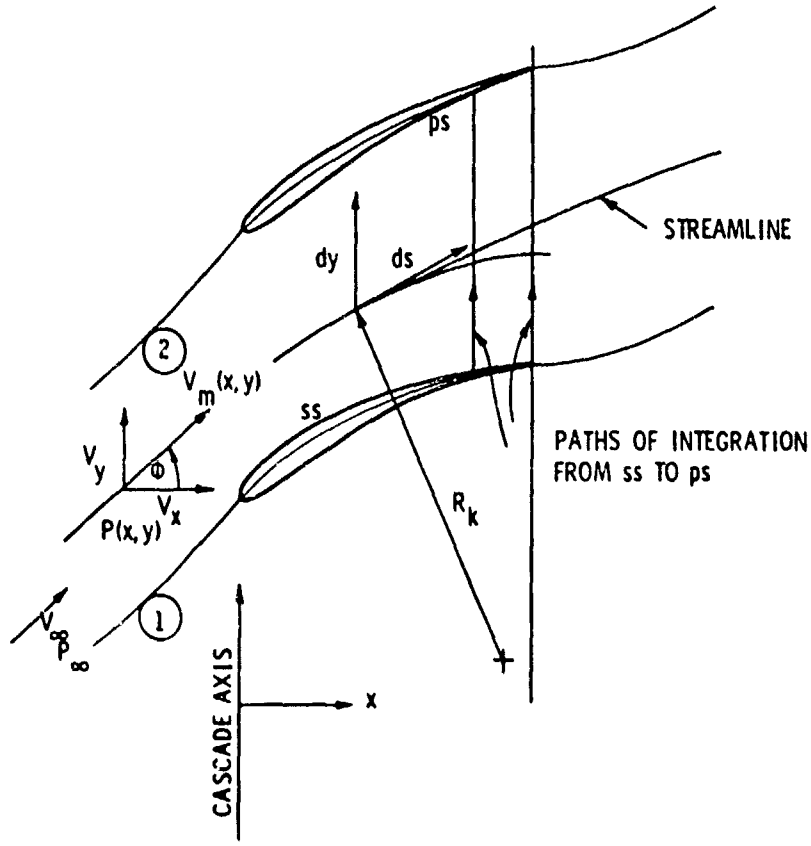

Figure 35. Geometric and Physical Variables Required for the Integration of the Momentum Equation.

$$\text{Const} = \int_1^2 \left\{ P_\infty(x,y) - \int_1^y \frac{1}{\rho} \frac{\partial P}{\partial \beta}(x,\beta)\, d\beta - V_y(x,y)^2 - P_{x_1} \right\} dy \,. \quad (8.5)$$

The term P(x) is the static pressure on the surface of one blade or on the stagnation streamline and must be solved. Once found, the static pressure determines the velocity field that satisfies both continuity and the conservation of total pressure.

Once the static pressure field has been determined, Bernoulli's equation may be used to recalculate the velocity field. The following equation is used to this end:

$$V_m^2 = P_\infty(x,y) - \int_1^y \frac{\partial \rho(x)}{\partial y}\, dy - P_{s_1} \,, \quad (8.6)$$

where $P_\infty(x,y)$ is the total upstream pressure for any streamline.

Having redefined the velocity field, it becomes necessary to reposition the streamlines. This is accomplished by integrating the new velocity profiles along a quasi-orthogonal and, at prescribed percentages of the total flow, positioning a new streamline. In practice, it is necessary to use damping of these streamline shifts to prevent numerical instabilities from growing at this point. Generally, only a small percentage (0.1) of the calculated streamline shift is allowed to help speed convergence. The above process may be repeated until changes in velocity and streamline shape are deemed negligible. At this point, the solution is converged. The entire process described is very similar to that discussed in more detail in Chapter IV.

The effect of these calculations in the blade space will show an increase in velocity near the blade suction surface and a corresponding decrease in velocity on the blade pressure side. The effect of the streamline relocation will be propagated both upstream and downstream as well. The important point to be made here is that, under the above circumstances, the one-dimensional values of momentum in the direction parallel to the cascade axis will no longer be satisfied. In general, the integrated pressure force parallel to the cascade axis derived from the blade pressure diagram will be less than that required to produce the fluid deflection specified by the inlet and exit flow angles. Additional inspection of the stagnation streamlines will show a pressure difference between corresponding points for two successive blades. This indicates that the required condition of periodicity has not been achieved.

The solution to the above inconsistency is to assure that the one-dimensional value of average momentum parallel to the cascade axis is maintained, balancing the specified blade pressure forces. This is accomplished in the following manner.

Integration of the momentum along each quasi-orthogonal after each iteration will yield the local value of total momentum. This value can be compared to the theoretical value, which is based solely on the desired loading distribution. After each iteration, a correction can be made to the shape of the stagnation streamline and the blade camber line to cause an increment of momentum equal to the difference calculated above to be added. This is caused by a small change in the angle of flow for each streamline. Figure 36 gives a geometric interpretation of the results of this procedure. The required change in the direction of flow can be calculated by the following equation:

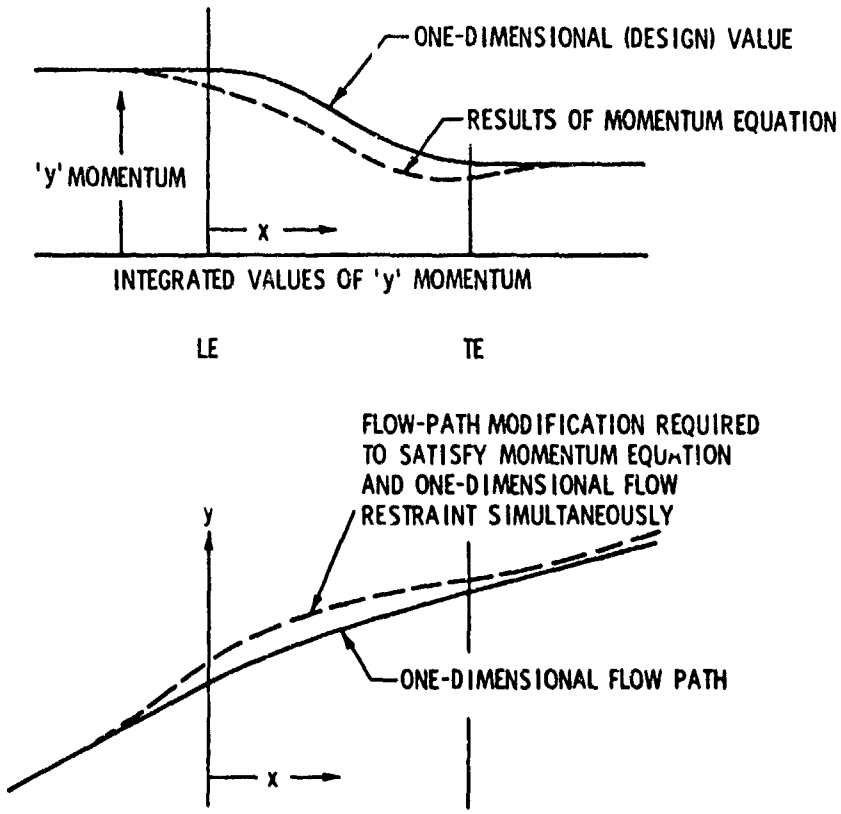

Figure 36. Initial Differences Between the One-Dimensional or Averaged Flow and the Results of the Exact Integration of the Momentum Equation.

$$\Delta\phi(x) = \phi(x) - \tan\left[\frac{V_y(x) + \Delta V_y(x)}{V_x(x)}\right] , \qquad (8.7)$$

where $\Delta V_y(x)$ is the increment in velocity along each quasi-orthogonal required to satisfy the one-dimensional momentum requirement. This relationship is approximate in that it is used for finite size regions of the flow. However, at convergence, the required stagnation streamline shift or angular change is zero and, therefore, the method converges to the exact solution.

The effect of the use of the above method is to produce a solution which is consistent in the following. First, the integrated values of momentum in the direction parallel to the cascade axis are consistent with the design criteria, i.e., the sum of all the forces is equal to the total momentum change through the cascade. Furthermore, the pressure distribution is consistent with the prescribed loading distribution. The condition of periodicity or repeated flow conditions along the cascade axis will be met. Finally, there can be no net momentum changes anywhere upstream or downstream of the cascade. The actual streamline pattern and the velocity field will satisfy the three equations of motion: momentum, continuity, and conservation of total pressure. Thus, an inviscid, two-dimensional, thin airfoil design is produced that has a specified loading distribution. The effects of finite blade thickness viscosity and turbulence must now be included to complete the blade-to-blade flow analysis.

The incorporation of the blade thickness distribution is straightforward, although care must be taken not to make the numerical method unstable by causing large perturbations to the flow field as discussed above. The thickness distribution is chosen by the designer to fit

whatever criteria are required, i.e., cavitation resistance, low drag, strength or maximum thickness, and so forth. For practical purposes, one could use the method of Abbot and Von Dohenhoff [33] to add the thickness distribution to the already defined thin airfoil camber line and subsequently correct the surface pressure distribution in the same manner. However, due to effects of the blades being in cascade, the data used in Reference [33] are not applicable, and additional potential flow effects may be present that will cause additional perturbations to the flow field and pressure distribution. This effect may actually require a different camber distribution to produce the same turning. Therefore, the effect of the finite thickness must be added to the flow field solution.

The effect of the thickness distribution is a major perturbation on the flow field calculation. Because of this, the following procedure is used to gradually add the thickness over a large number of iterations. This is demonstrated graphically in Figure 37. As each iteration is started, the maximum thickness is increased slightly from zero to its full value after some number of iterations. In this way, the pass-by-pass variation in the flow field is small and convergence is enhanced. An equal portion of the thickness is added to the pressure and suction sides of the camber line on each pass. Because of the thickness, the stagnation streamline is separated into two separate streamlines corresponding to the pressure and suction surfaces of the blade.

An area of particular difficulty is encountered with the thickness distribution at this point. This problem is common with Streamline Curvature Methods and is related to the leading and trailing edge stagnation points. Figure 38 helps to clarify this problem at the leading edge. With a finite radius thickness distribution, the

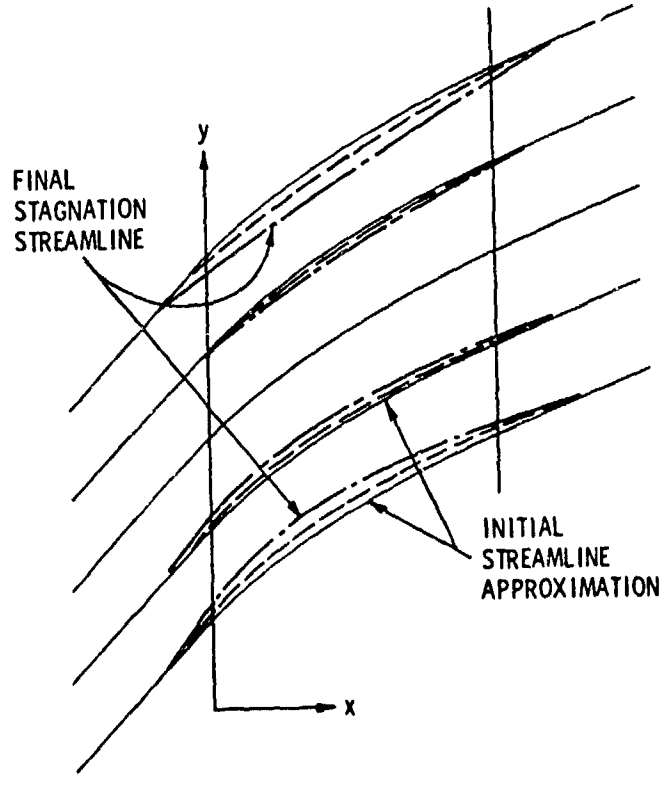

Figure 37. The Effects of the Gradual Addition of Blade Thickness to the Analytical Solution.

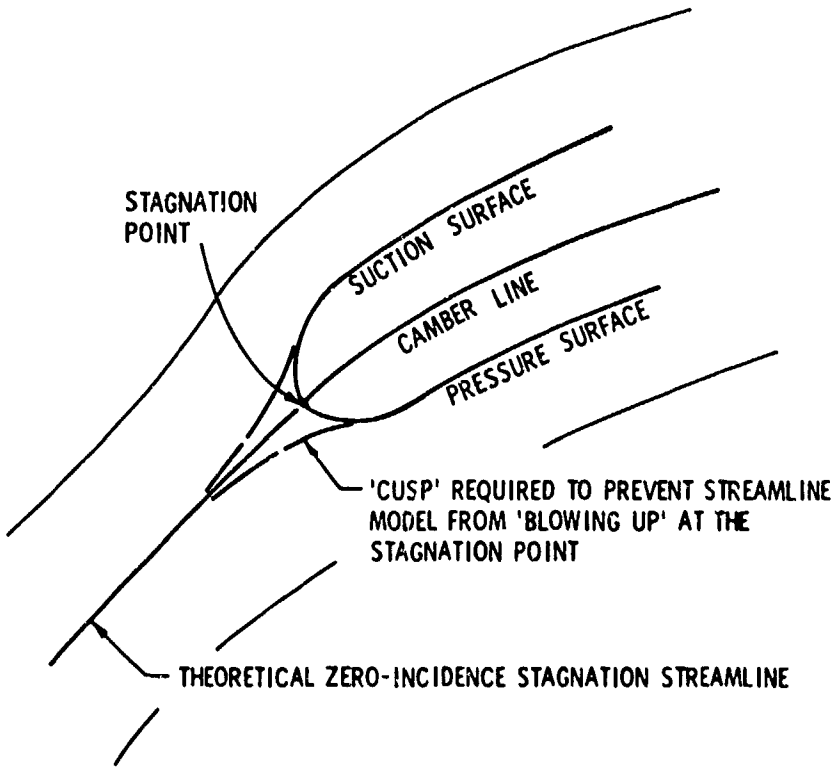

Figure 38. Illustration of Singular Point at Blade Leading Edge.

stagnation streamline is forced into a singular point. In almost all cases, polynomial functions that model the streamlines will fail or "blow up" at this point. In the present method, the streamline was separated into three segments: the upstream portion up to the leading edge, the blade surfaces, and the portion downstream of the trailing edge. In the integration of the momentum equation, the radius of curvature was neglected at the leading and trailing edge points and the velocity set equal to zero at the singular points. This procedure neglects the problems associated with the singularities without affecting the majority of the solution. While this method has little physical justification, no other practical method could be found to solve the problem.

The final portion of the cascade model deals with the problems of viscosity and turbulence. The total pressure change encountered in a two-dimensional cascade arises from boundary layer growth on the blade surfaces. This does not lend itself readily to theoretical treatment, and when a calculation of the viscous effects on rotating blade rows is necessary, the problem is intractable. The viscosity effect must then be represented by an empirical correlation. This correlation for a two-dimensional cascade must include the boundary layer on the blade surfaces, the wake shed from the blades, and total pressure loss considerations over the entire flow field. The physical nature of cascade boundary layers is quite clearly indicated by Raj and Lakshminarayana [17] where the wake structure is shown by experimental data.

The cascade analysis described here incorporates the gross effects of the boundary layers and wake in the following manner. A boundary layer calculation due to Truckenbrodt [34] gives the displacement thickness as a function of distance along the blade surface. This

method, though not as accurate as modern methods, is quite fast computationally. This displacement thickness is used to modify the stagnation streamline as indicated in Figure 39. This modified boundary is included in the momentum equation calculations and results in a general acceleration of the flow around the cascade trailing edge. In addition, the wake is approximated by allowing the displacement thickness to proceed downstream and gradually vanish at one blade chord downstream.

The equation for the conservation of total pressure must also be modified to include the effect of viscosity. This is accomplished by use of a distributed total pressure loss whose magnitude is determined empirically. The energy thickness of a boundary layer is approximately one-half the displacement thickness as given by Schlicting [35]. At each station in the blade row, the boundary layer calculation gives the displacement thickness, and the integrated reduction of total pressure can be calculated. The distributed reduction of pressure is accomplished by "smearing" the loss across the duct, weighting the loss as the square of the distance from each blade surface, and as the square of the local velocity. In this way, the majority of the loss is concentrated in an energy boundary layer near each blade surface.

A major item of concern in the cascade design procedure is the possibility of linking the blade-to-blade solution and the meridional plane solution. At present, no analysis exists which can solve either a true three-dimensional solution using all the equations of motion or a properly coupled set of two-dimensional solutions, such as proposed by Wu [1]. However, progress has been made in the direct or analysis case as exemplified by Novak [23]. Novak uses a coupled set of

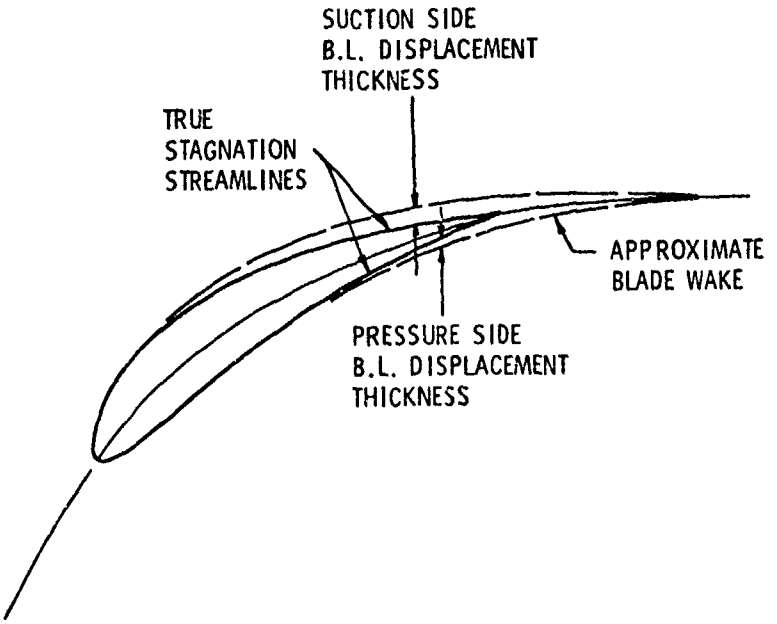

Figure 39. Modification of the Stagnation Streamline to Account for Boundary Layer Displacement Thickness and the Blade Wake.

two-dimensional Streamline Curvature solutions to produce a quasi-three-dimensional analysis of compressor or turbine blade rows.

No previous attempt at coupling solutions for the indirect or design problem is known. However, in the analysis described here, the possibility of a coupled, indirect solution exists. The technique used is essentially that of Wu. However, it is still approximate in that a circumferentially-averaged meridional plane solution must be used. The coupling of the solutions requires carrying the local stream sheet thickness from the meridional plane solution to the blade-to-blade solution and vice versa. In this way, effects of the blade spanwise loading distribution are carried into the blade-to-blade solution, and body forces generated by the surface geometry of the blading are carried into the meridional plane solution.

The current indirect blade-to-blade analysis allows input of the stream sheet thickness variations determined from the meridional plane solution for purely axial flow turbomachinery. This is accomplished in the continuity equation shown earlier. For mixed or radial turbomachinery, a conformal transformation of the stream surface is necessary but is not pursued here.

To summarize, the analysis presented here is an indirect or design method for two-dimensional airfoils in cascade. The method solves the equations of motion for incompressible, steady flow by use of the Streamline Curvature Method while satisfying a number of required boundary conditions. An airfoil camber line is developed for given inlet and exit angles, loading distribution, and thickness distribution. The solution satisfies conservation of momentum everywhere and periodicity in the inlet and exit flows, as well as the continuity equation. A boundary

layer and wake model are included to accommodate the viscous and turbulent flow effects found in turbomachine blade rows.

8.2 Definition of a Cascade Design Test Case

A program was conducted to test the validity of the Streamline Curvature Method of airfoil section design discussed in this chapter. An airfoil design was performed using a computer program developed to implement this procedure. The design was purely two-dimensional, i.e., no effects of acceleration of the through-flow were investigated. The design was conducted on an airfoil section of high solidity and moderate loading. The chordwise loading distribution was chosen to be elliptical. The thickness distribution was one with maximum thickness at 60 percent of the chord in an effort to minimize the blockage effects encountered in a high solidity cascade. The following discussion explains the actual design parameters in more detail.

The airfoil design parameters, Figure 40, were chosen as: the inlet fluid angle, 45 degrees, and the exit flow angle, 26.5 degrees; hence, the turning angle, 19.5 degrees, and the solidity as 1.0. Therefore, the lift coefficient per blade is

$$C_L = 2 \frac{\Delta V_y}{W_\infty} \frac{S}{C} = 0.707 \quad , \tag{8.8}$$

where $\Delta Vy = V_{y_2} - V_{y_1}$ as shown in Figure 40. Experience shows that this is a moderate value of C_L and, therefore, the flow should not separate. The blade section was designed for an operating Reynolds number of 240,000 based on W_∞ and C, which, according to Horlock [36], makes it unlikely to suffer from laminar separation. An elliptical loading distribution was used to make the section more nearly conform to the

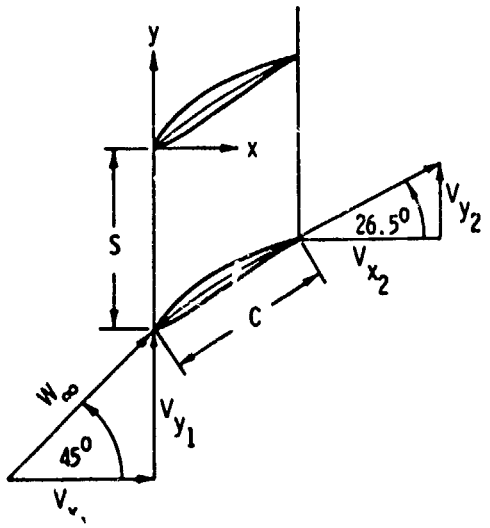

Figure 40. Prescribed Performance Requirements for the Design Cascade Blade Analysis.

ideal flow blade loadings employed in thin airfoil theory. The thickness distribution used is similar to that reported in Erwin [24] and has its maximum thickness (10 percent of chord) at the 60 percent chord position.

8.3 Results of Cascade Airfoil Design Calculations

The computerized blade-to-blade solution produces as output a plot of the streamline pattern through the cascade, the camber line and blade surface coordinates, and a comparison with the initial approximation to the streamlines. A plot for the test case reported here is presented in Figure 41. Additionally, the velocity and pressure profiles along each solution station are outputed. These profiles are compared to experimental data in a later chapter for this test case.

An important observation to be made from Figure 41 is that the blade camber line has more curvature than the mean streamline approximation to the camber line used to start the procedure. Second, in the upstream and downstream flow, curvature of the stagnation streamline is required to satisfy the condition of periodicity. The boundary layer displacement thickness can be seen on both surfaces, as well as the approximate wake structure used in this analysis. Flow separation was predicted by the boundary layer analysis at 70 percent of the chord in the suction side and at 90 percent of the chord on the pressure side. This is due, in part, to the choice of thickness distribution and the sharp curvature and bluntness caused by it at the trailing edge.

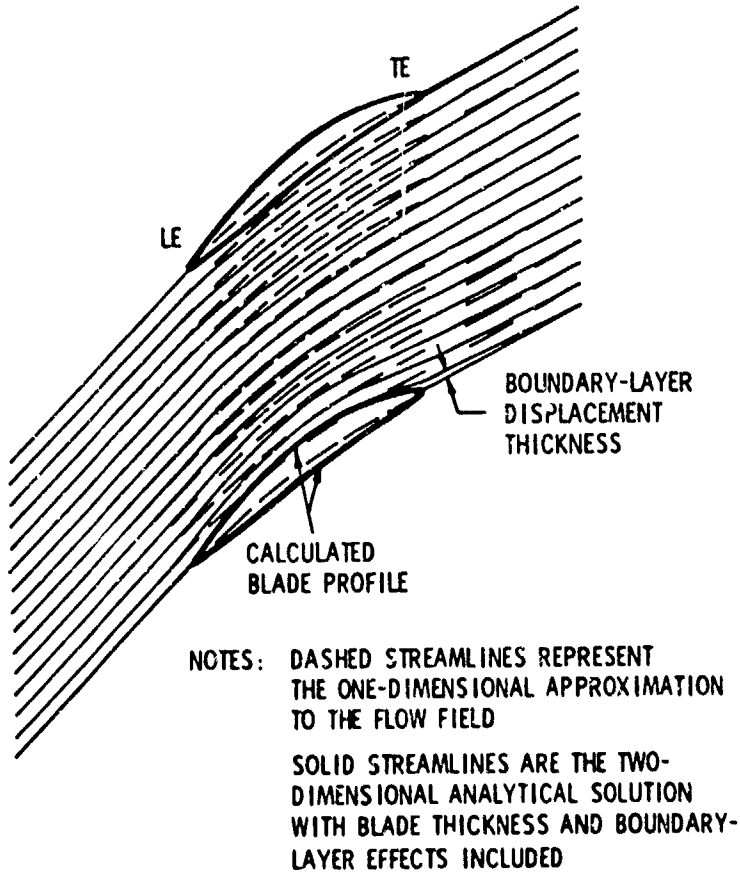

Figure 41. Computer Generated Plot of the Initial and Final Analytical Solution for the Cascade Blade Test Case.

CHAPTER IX

EXPERIMENTAL PERFORMANCE VERIFICATION OF THE STREAMLINE CURVATURE CASCADE BLADE DESIGN METHOD

A test program was conducted in an effort to verify the performance of a cascade of blades designed by the Streamline Curvature Method discussed in an earlier chapter. The program consisted of the design and fabrication of the cascade of blades, the experimental determination of the blade surface pressure distribution, the experimental determination of the flow field, and the direct comparison of these data with the theoretical flow field determined during the blade section design. The experiment was conducted in the cascade blade test facility located at the Applied Research Laboratory (ARL).

The theoretical flow field determined by the Streamline Curvature blade design procedure is shown graphically in Figure 42. This figure indicates the geometric shape and relative position of two blades in an infinite cascade. Also shown is the theoretical streamline distribution and the effects of the boundary layer modeling on the blade surface streamlines and the blade wake. As output from the analysis, the static pressure and velocity profiles along each indicated reference line were obtained. The blade surface static pressure distribution and the intra-blade velocity profiles were compared directly to data derived from the experiment.

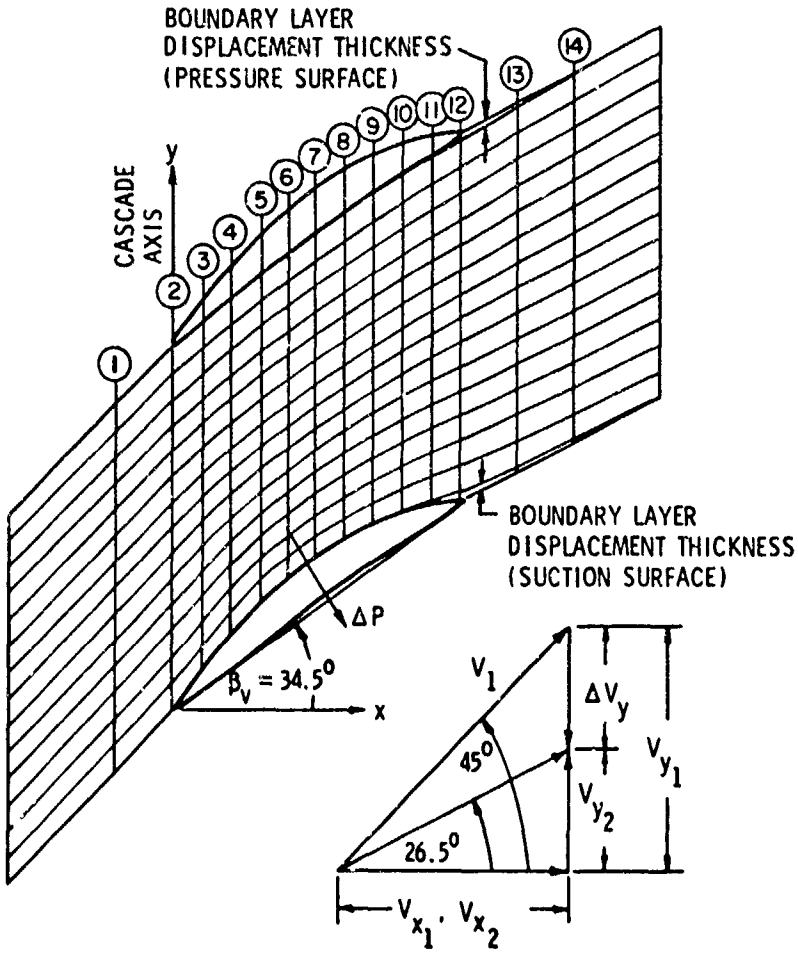

Figure 42. Theoretical Streamline Distribution and Blade Shape Determined by the Streamline Curvature Blade Design Method.

9.1 Cascade Blade Test Experimental Apparatus

Five blades with surfaces numerically machined to the ordinates specified by the design analysis were manufactured and installed in the ARL cascade test facility. The blade chord was 4.65 inches, the blade span was 14.50 inches, and the blade-to-blade spacing was 4.65 inches. The arrangement of these blades in the test facility is shown in the photograph of Figure 43. The central blade was instrumented with surface static pressure taps which are located as indicated in Figure 44. The pressure taps were located so as to correspond to the computation stations indicated in Figure 42. In addition, the holes were located in a manner that assured that wakes shed from each hole would not affect readings taken at downstream locations. The tubing required to transfer pressures from the blade surface to an external transducer was located within the blade, thus eliminating the need to mar the blade surface, possibly disturbing the flow.

The pressure in the cascade tunnel settling section, the approach section to the test cascade, the blade surface taps, and the ambient pressure were measured with a Validyne variable reluctance differential pressure transducer and averaged for 10 seconds to eliminate variations in the output voltages. The data were repeatable to within 1 percent, while the calibration of the transducer was repeatable to within 0.3 percent.

The ARL cascade test facility is equipped with boundary layer suction screens at both ends of the cascade blades. In practice, these screens remove the boundary layer on the tunnel walls, thereby assuring two-dimensional flow in the cascade itself. During the test of the cascade, a suction setting was maintained that gave no change in static

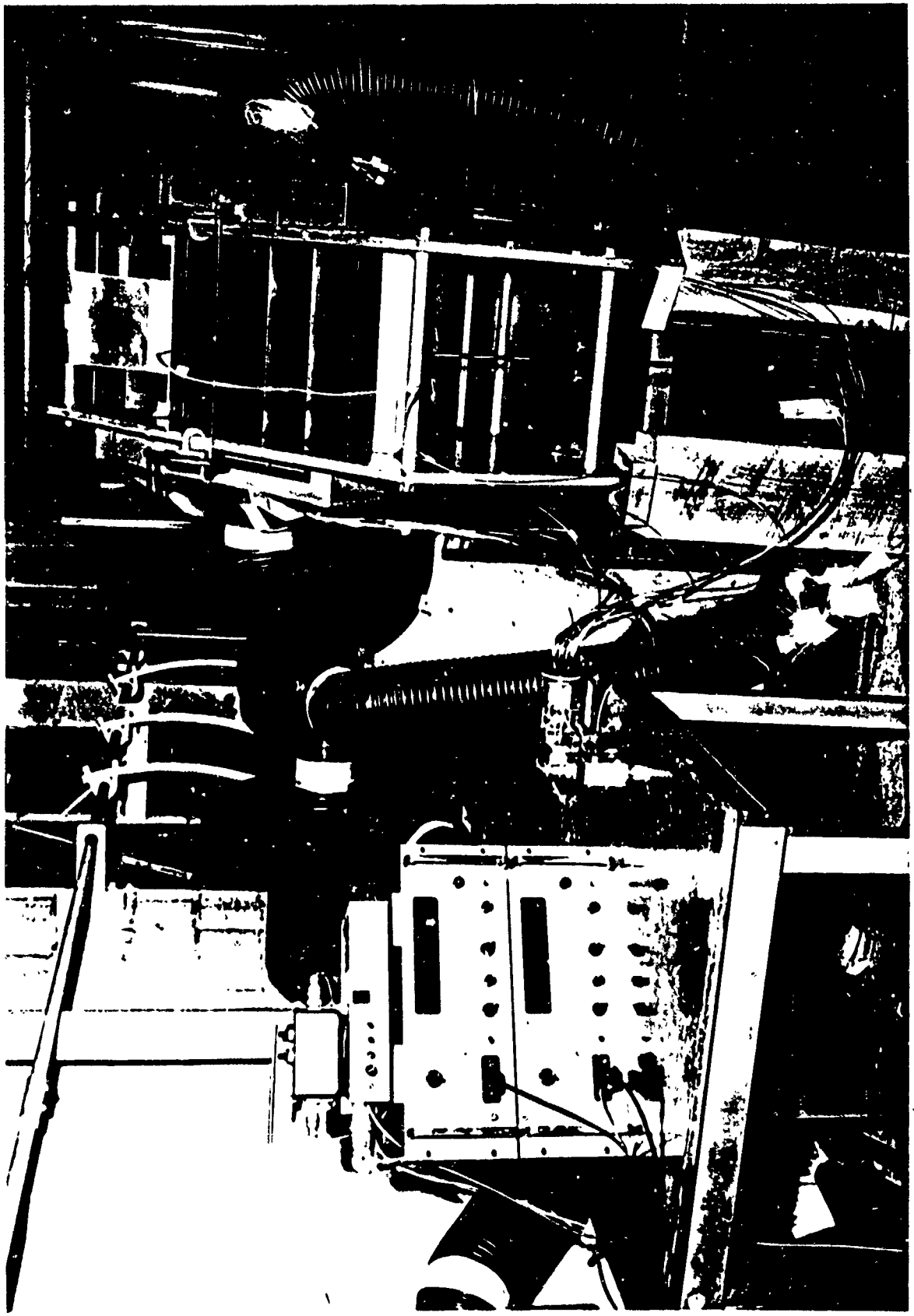

Figure 43. Photograph of Cascade Tunnel with Test Blades and Three-Hole Probe Mounted.

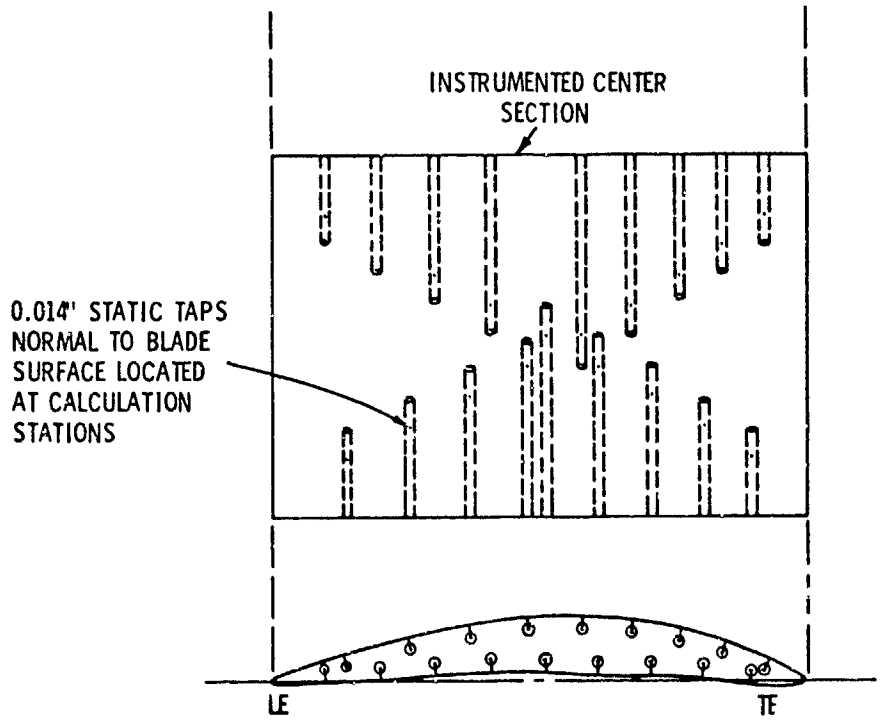

Figure 44. Detail of Airfoil Section Shape and Location of Holes for Surface Pressure Measurements.

pressure along the approach duct to the cascade, indicating that two-dimensional flow was maintained.

A comparison of the flow field in the test cascade with the theoretical flow field requires obtaining the velocities (V_y) and (V_x) parallel and perpendicular to the cascade axis, respectively, and the local static pressure (P_{s_ℓ}) at various locations in the flow field. A three-hole probe was fabricated and calibrated for use in this experiment. The mounting arrangement of the probe in the ARL cascade facility is shown in Figure 43 and schematically in Figure 45. An expanded schematic view of the probe tip is shown in Figure 46. The basis for the design and calibration of this probe is presented in Treaster and Yocum [37].

Calibration of the three-hole probe was accomplished in the following manner. The probe was mounted in a retaining collar with the probe tip located at the center of a 1.0 foot diameter, low turbulence, open jet. This arrangement is shown schematically in Figure 47. The jet velocity was maintained at 103 feet per second, the maximum capability of the facility. The probe Reynolds number, based on the hole diameter, was 1080. The angle of the probe was systematically varied in small increments from a flow angle relative to the probe of -20 degrees to +20 degrees. At each setting, the pressures (P^+, P_t, P^-) from the probe were recorded. Additionally, the settling section total pressure (P_T) and the jet face (atmospheric) pressure P_S were recorded. These pressures are represented schematically in Figure 46. The Validyne variable reluctance differential pressure transducer was used so that each recorded pressure was the pressure difference above the atmospheric referenced pressure.

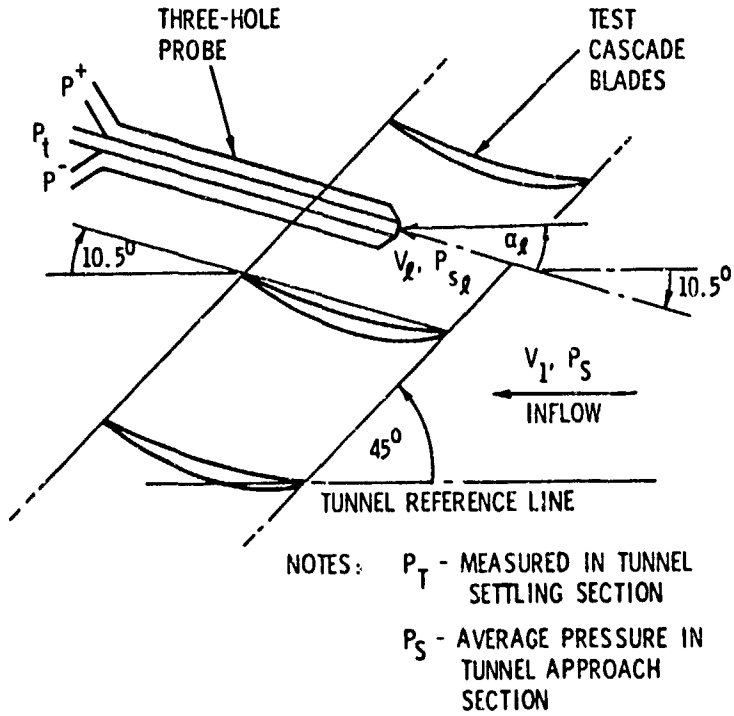

Figure 45. Three-Hole Probe and Cascade Blade Test Geometry.

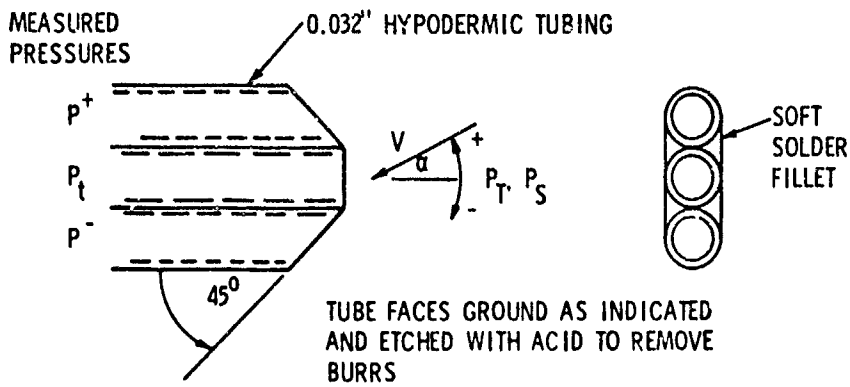

Figure 46. Expanded View of Three-Hole Probe Tip.

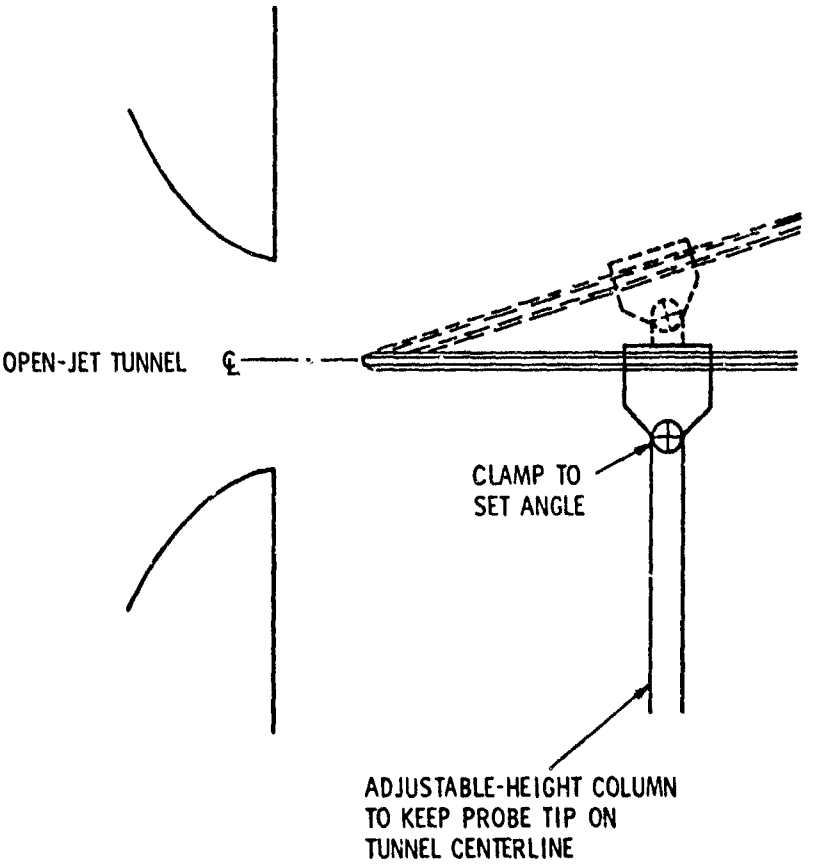

Figure 47. Three-Hole Probe Calibration in Open Jet Tunnel.

The pressures were averaged for 10 seconds to reduce variability, leading to a repeatibility of 1 percent.

Three calibration coefficients are required to determine the two velocity components and the static pressure at the probe tip. To determine the flow angle, the difference in pressure between the two side pressure tubes P^+ and P^- is used. The angularity correlation coefficient (C_{p_α}) is defined as

$$C_{p_\alpha} = \frac{(P^+ - P^-)}{P_t - 1/2(P^+ + P^-)} \quad , \tag{9.1}$$

where the measured pressures are defined as in Figure 46. The result of this calibration is plotted on Figure 48 as a function of flow angle (α) relative to the probe axis.

Determination of the total pressure that exists at the probe location is accomplished by a correlation of the measured total pressure P_t and the actual total pressure P_T. During calibration, P_T is measured in the calibration facility settling section. The total pressure correlation coefficient (C_{p_t}) is defined as

$$C_{p_t} = \frac{P_T - P_t}{P_t - 1/2(P^+ + P^-)} \quad . \tag{9.2}$$

These calibration data are plotted in Figure 49 as a function of the flow angle (α).

The final calibration coefficient is used to determine the static pressure at the probe tip. The correlation relates the average measured

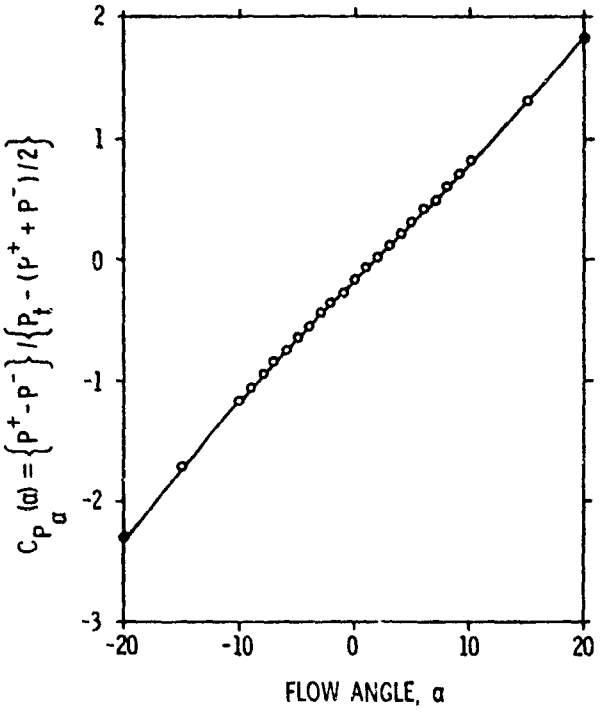

Figure 48. Three-Hole Probe Calibration (C_{P_α} vs α).

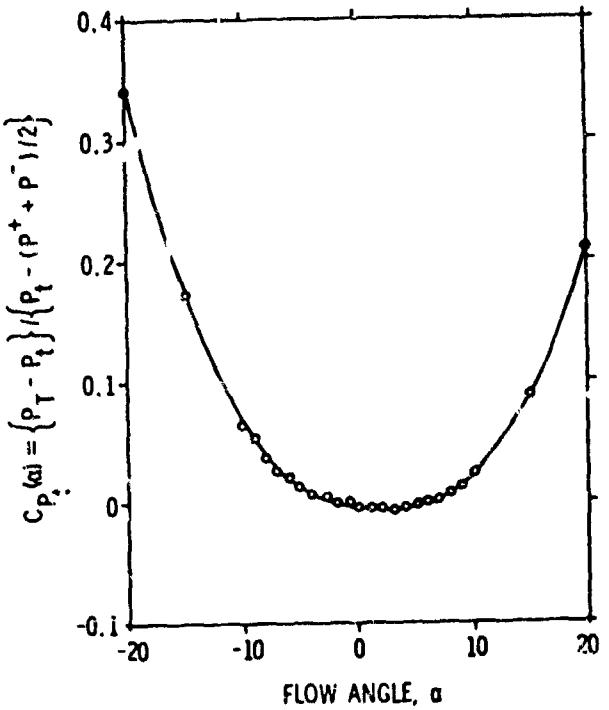

Figure 49. Three-Hole Probe Calibration (C_{P_t} vs α).

static pressures $(P^+ + P^-)/2$ to the true static pressure P_S. During calibration, the actual static pressure P_S is measured at the edge of the open jet of air. The static pressure correlation coefficient is defined as

$$C_{P_s} = \frac{(P^+ + P^-)/2 - P_S}{P_t - 1/2(P^+ + P^-)} \quad . \tag{9.3}$$

These calibration data are plotted in Figure 50 as a function of the flow angle (α).

All measured pressures used during this calibration are referenced to atmospheric pressure.

Calculation of the velocity components and static pressure at some point in an unknown flow field requires use of the calibration data summarized in Figures 48 through 50. The experimental determination of the local flow angle (α_ℓ), the local velocity (V_ℓ), and the local static pressure (P_{s_ℓ}) is accomplished in the following manner.

Experimentally determined pressure P^+, P^-, and P_t from the probe are determined. Calculation of the flow angle is accomplished by using Equation (9.1) to determine the local value of (C_{P_α}). Once known, an interpolation on the curve fit of Figure 48 yields the local flow angle (α).

Determination of the local total pressure is achieved by determining the value of C_{P_t} for the corresponding value of flow angle already determined. This is accomplished with the aid of the curve fit shown in Figure 49. Having determined the local value of C_{P_t}, Equation (9.2) is rearranged to give

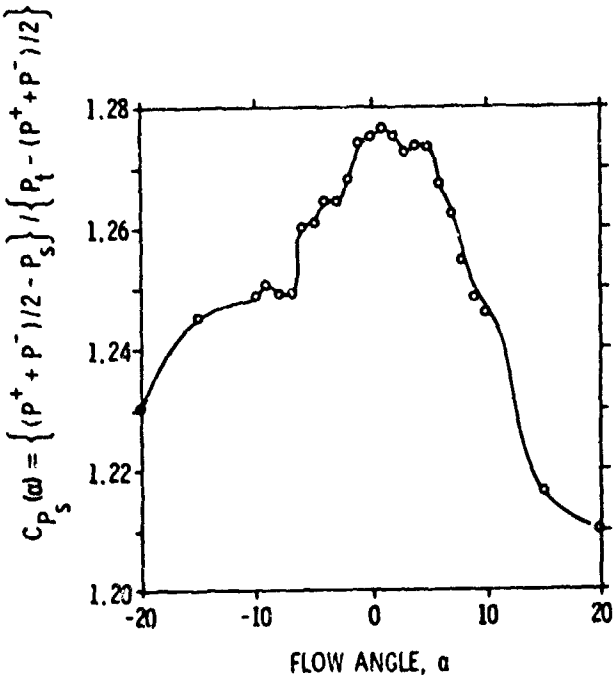

Figure 50. Three-Hole Probe Calibration (C_{P_s} vs α).

$$P_{t_\ell} = C_{P_t} \cdot \left[P_t - 1/2(P^+ + P^-)\right] + P_t \quad , \tag{9.4}$$

where P_{t_ℓ} is the desired value of the local total pressure.

Determination of the local static pressure is achieved by determining the value of C_{P_s} for the corresponding value of flow angle already determined. This is accomplished with the aid of the curve fit shown in Figure 50. Having determined the local value of C_{P_s}, Equation (9.3) is rearranged to give

$$P_{s_\ell} = (P^+ + P^-)/2 - C_{P_s} \cdot \left[P_t - 1/2(P^+ + P^-)\right] \quad , \tag{9.5}$$

where P_{s_ℓ} is the desired value of the local static pressure.

The flow may have experienced a loss in total pressure between the upstream reference conditions and the point at which measurements are being made. This loss of total pressure (P_L) may be determined from the difference between the indicated local total pressure and the total pressure measured at the upstream reference conditions. The loss of total pressure is

$$P_L = P_T - P_{t_\ell} \quad . \tag{9.6}$$

Bernoulli's equation may now be used to determine the local velocity (V_ℓ). This equation is

$$V_\ell = \left\{(P_T - P_L - P_{s_\ell})\frac{2}{\rho}\right\}^{1/2} \quad . \tag{9.7}$$

A reference velocity (V_1) is defined as

$$V_1 = \left\{(P_T - P_S)\frac{2}{\rho}\right\}^{1/2} , \qquad (9.8)$$

where P_S is the reference static pressure measured upstream and beyond the influence of the test cascade. The location of P_S is shown schematically in Figure 45. The local velocity ratio (V_ℓ/V_1) is easily determined by combining Equations (9.7) and (9.8).

The local static pressure coefficient $C_{P_{s_\ell}}$ is defined as

$$C_{P_{s_\ell}} = \frac{P_{s_\ell}}{P_T - P_S} . \qquad (9.9)$$

Using this calibration and analysis technique, a three-hole probe can be used to map the velocity and pressure field in a cascade of blades. Subsequent tests of the cascade of blades were run at a reference velocity of 100 feet per second and a corresponding blade chord Reynolds number of 240,000. The Reynolds number corresponds to the calibration Reynolds number of the three-hole probe. Results of the flow field measurements when averaged for 10 seconds were repeatable to within 1 percent.

9.2 Comparison of the Analytical and Experimental Pressure Distribution

Blade surface pressure distributions for the cascade geometry designed by the Streamline Curvature Method were obtained from three sources. The principle distribution is that shown in Figure 51 and is

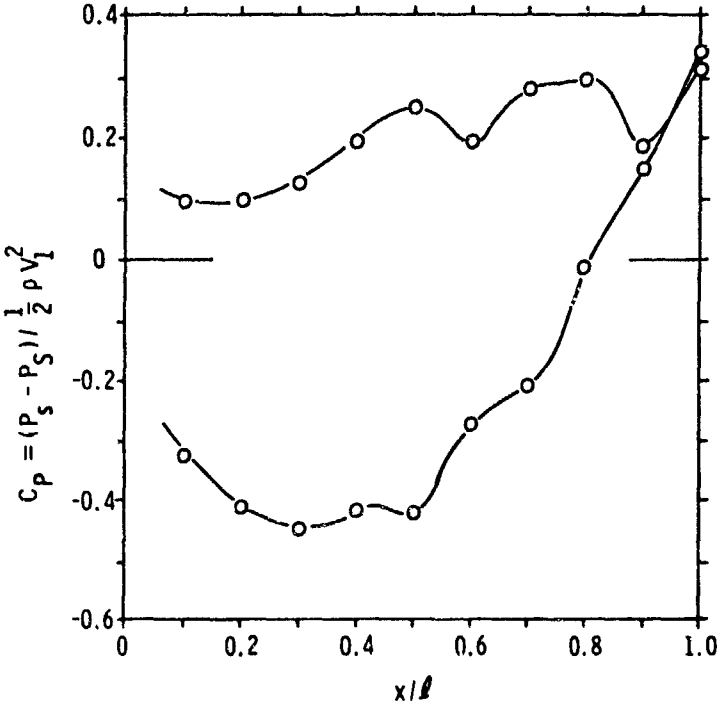

Figure 51. Theoretical Cascade Blade Pressure Distribution from the Streamline Curvature Analysis.

predicted by the design analysis. The design requires a fluid turning angle of 18.43 degrees and a nondimensional flow diffusion, (V_2/V_1), of 0.790, where V_1 is the velocity upstream of the cascade and V_2 is the velocity far downstream. The balance of blade forces to fluid momentum changes requires that the average blade force per blade, in the direction parallel to the cascade axis, be equal to the momentum change of the fluid in the blade passage in the same direction. The equation

$$\Delta P \cdot C \cos(\beta) = \rho S V_x \Delta V_y \qquad (9.10)$$

expresses this balance. (ΔP) is the average pressure difference across the blade. Because the force parallel to the cascade axis is required, the pressure acts on the projection of the blade chord (C) perpendicular to the cascade axis $(C \cdot \cos(\beta))$. (β) is the angle of the vane relative to the (x) direction and can be seen in Figure 42. The mass of fluid acted on by the blade force per unit time is $(\rho S V_x)$, where (ρ) is the density, (S) is the blade spacing, and (V_x) is the velocity across the cascade. The fluid momentum change is embodied in the term (ΔV_y), the change in velocity parallel to the cascade axis, between the leading and trailing edges. The quantities used in this discussion are depicted in Figure 42.

If the average blade pressure difference, (ΔP), is nondimensionalized by the upstream dynamic pressure, as in the following relations,

$$\overline{Cp} = \Delta P/(1/2\rho V_1^2) = 2 \frac{S}{C \cos \beta} \frac{V_x}{V_1} \frac{\Delta V_y}{V_1} \quad , \qquad (9.11)$$

a blade average loading or pressure coefficient $(\overline{Cp})$ is formed. The test case specified a design value of $(\overline{Cp})$ of 0.6067. Integration of the pressure distribution that is output of the design analysis yields a

value of $\overline{Cp}$ = 0.440. Using Equation (9.10), the flow turning angle would be 12.5 degrees using the reduced value of $\overline{C_p}$. This angle is 5.9 degrees less than the 18.43 degrees called for by the design.

As a check on the design geometry, the Douglass-Neumann potential flow analysis method of Giesing [38] was performed. The pressure distribution of Figure 52 was generated. In this case, the value of $\overline{Cp}$ = 0.580, indicating a fluid turning angle of 17.4 degrees, was 1.0 degrees less than called for by the design. Experience has shown that the Douglass-Neumann analysis usually overestimates the turning that can be performed by a cascade.

The Douglass-Neumann analysis indicated that the geometry was close to conforming to the design but that the pressure distribution calculated by the Streamline Curvature Method was in error.

A final comparison with the results from testing the design cascade was made. The experimentally obtained pressure distribution is plotted in Figure 53. The integrated value of $\overline{C_p}$ at the design conditions was found to be 0.504, giving a flow turning angle of 14.7 degrees, 3.7 degrees less than design and 7.7 degrees less than predicted by the Douglass-Neumann method.

Inspection of the pressure distributions shown in Figures 51, 52, and 53 reveals that good agreement is obtained among the various comparisons for the pressure side of the blade. On the suction side, fair agreement is maintained for the first 50 percent of the blade surface, but at mid chord, the theoretical distribution from the Streamline Curvature design analysis shows poor agreement with both comparison cases. The conclusion here is that the lack of proper momentum force balance noted previously is due to this discrepancy. Examination of the

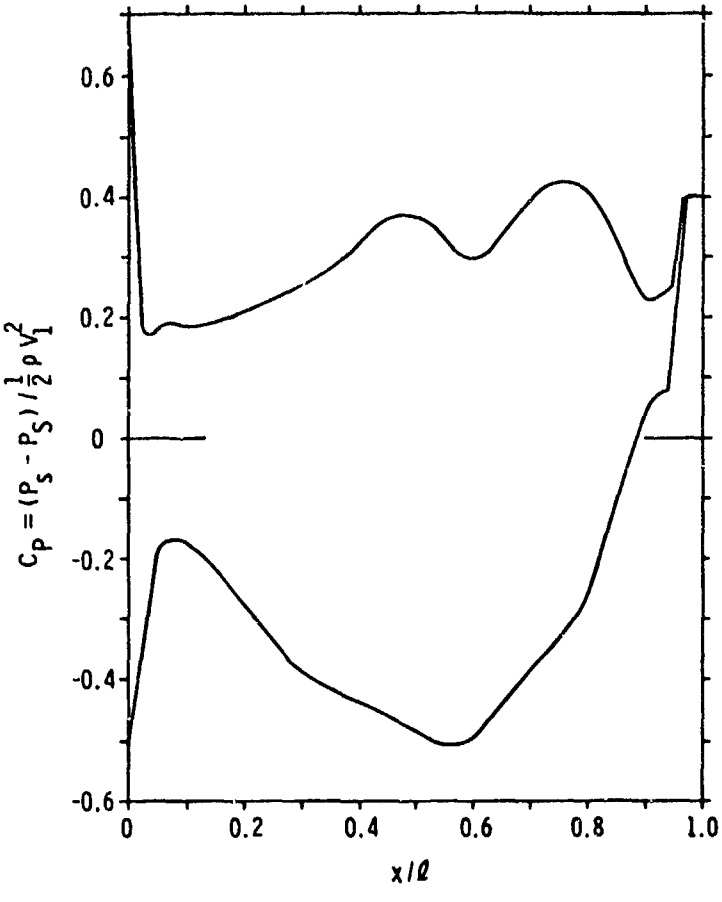

Figure 52. Theoretical Cascade Blade Pressure Distribution from the Douglass-Neumann Potential Flow Analysis.

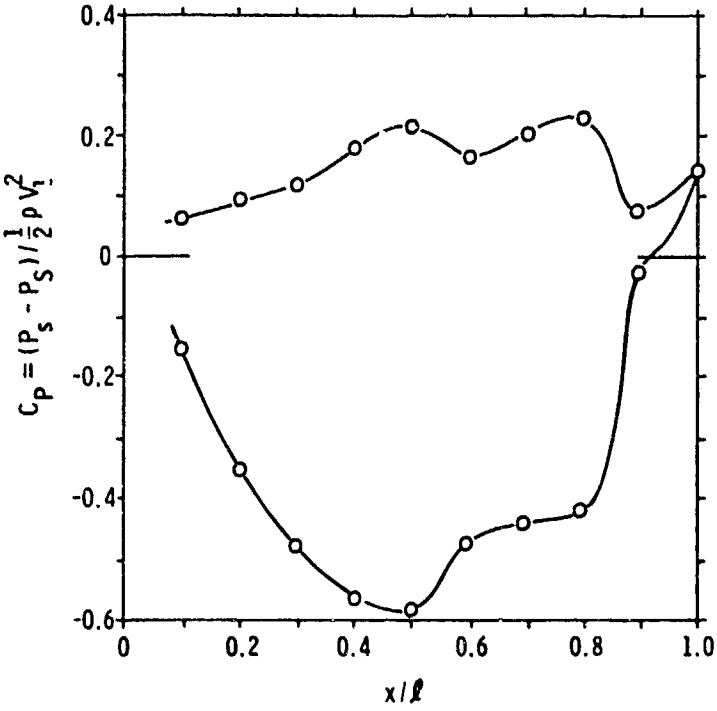

Figure 53. Experimental Cascade Blade Pressure Distribution.

boundary layer calculations performed during the design indicated the possibility of flow separation at 70 percent of the chord on the suction surface, making the boundary layer and wake model inaccurate. Additionally, experimental visual observations with tufts indicated that the experimental blade was indeed separated in this area, possibly increasing the observed underturning of the flow.

9.3 Comparison of the Analytical and Experimental Flow Fields

The velocity and pressure fields for the cascade design were determined analytically upstream, within, and downstream of the blade row. An experimental program using a three-hole probe determined the corresponding flow field for the actual cascade. The results of the experimental program are partially represented by the computer generated plot of Figure 54. This figure shows the location of each data point acquired, with the resulting velocity and direction shown.

Figure 54 shows the more important features of the flow field in the cascade. First is an indication of a separated flow region on the suction surface trailing edge. This region was also indicated by tufts attached to the blade surface. The second most visible feature is an indication of the extent and structure of the wake of low velocity fluid shed from the blade trailing edges. Finally, the averaged fluid deflection angle at the downstream station is 13.5 degrees, agreeing fairly well with the value determined by use of the pressure distribution.

More specific comparison of the analytical and experimental flow fields are made in Figures 55 through 68. These figures are velocity profile comparisons at each indicated reference station in Figure 42.

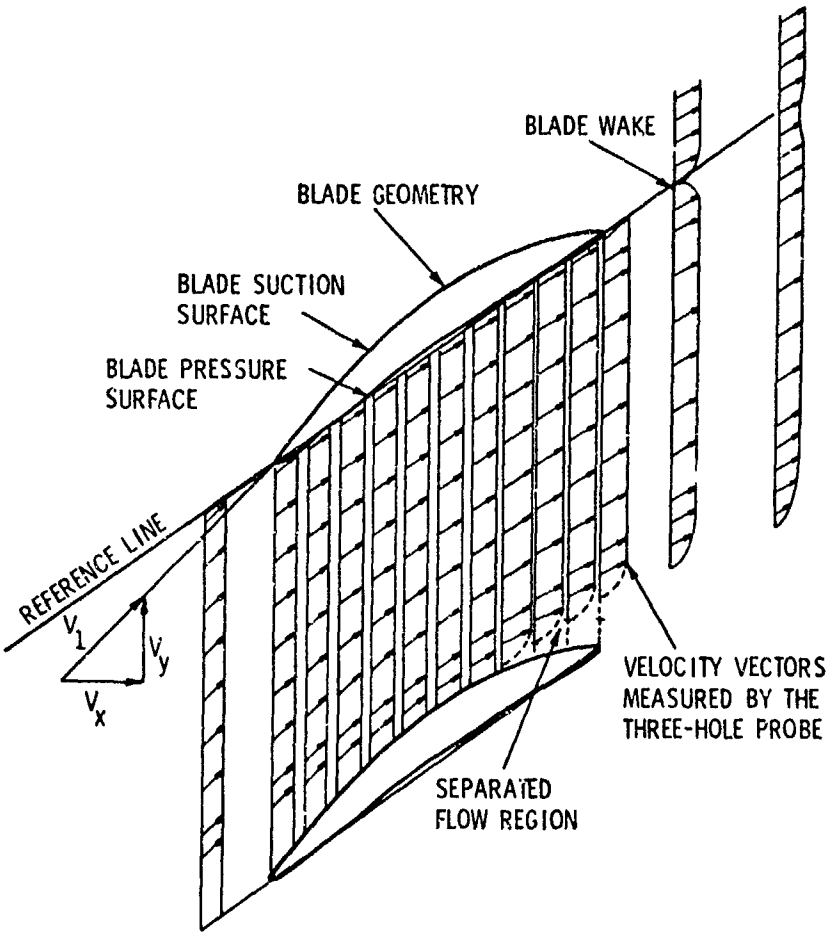

Figure 54. Experimentally Determined Velocity Field in the Test Cascade.

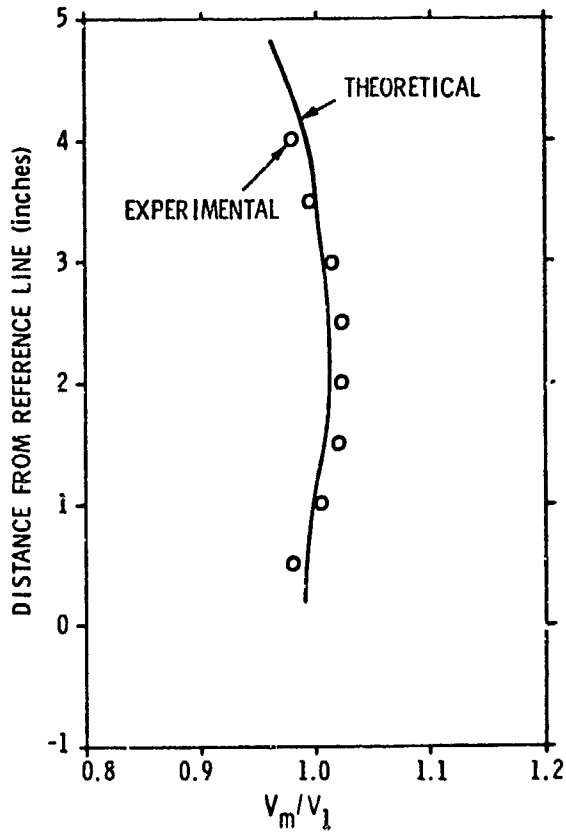

Figure 55. Comparison of the Theoretical and Experimental Velocity Profiles in the Test Cascade Reference Station 20 Percent Blade Chord Upstream.

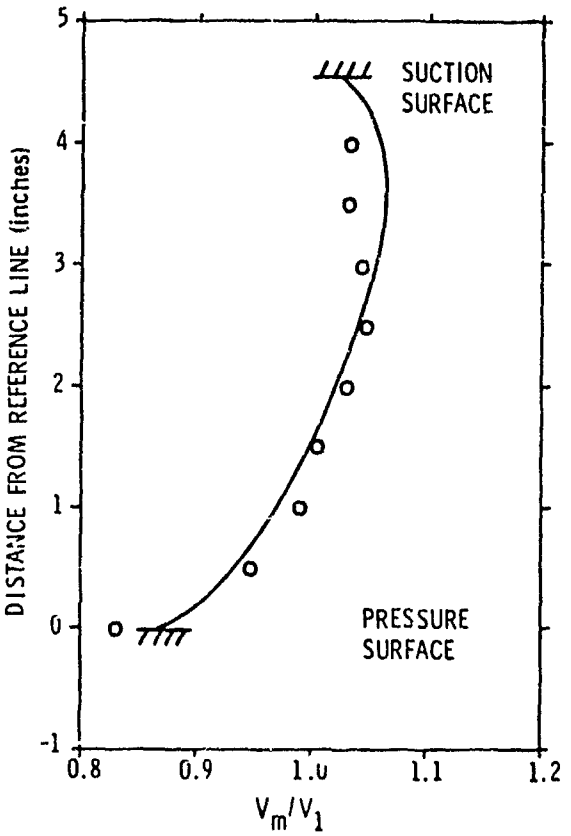

Figure 56. Comparison of the Theoretical and Experimental Velocity Profiles in the Test Cascade Reference Station Coincident with Leading Edge.

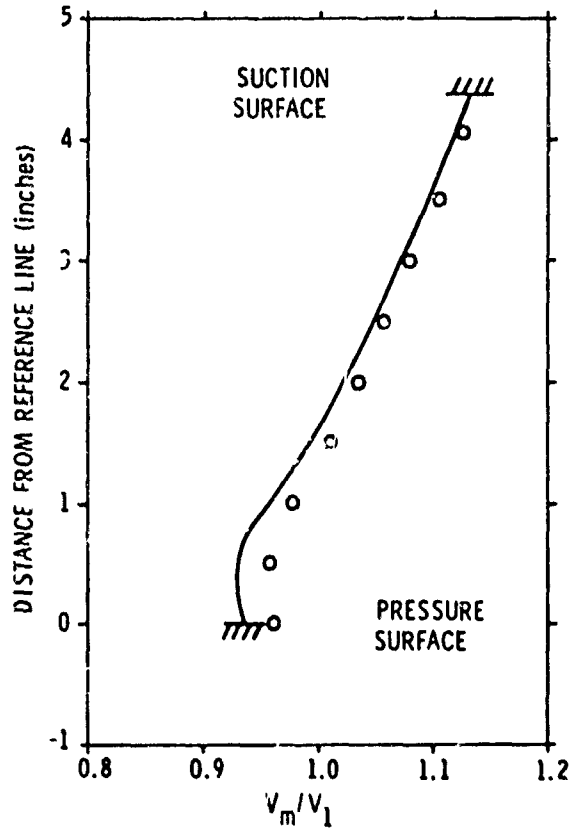

Figure 57. Comparison of the Theoretical and Experimental Velocity Profiles in the Test Cascade Reference Station at 10 Percent of the Blade Chord.

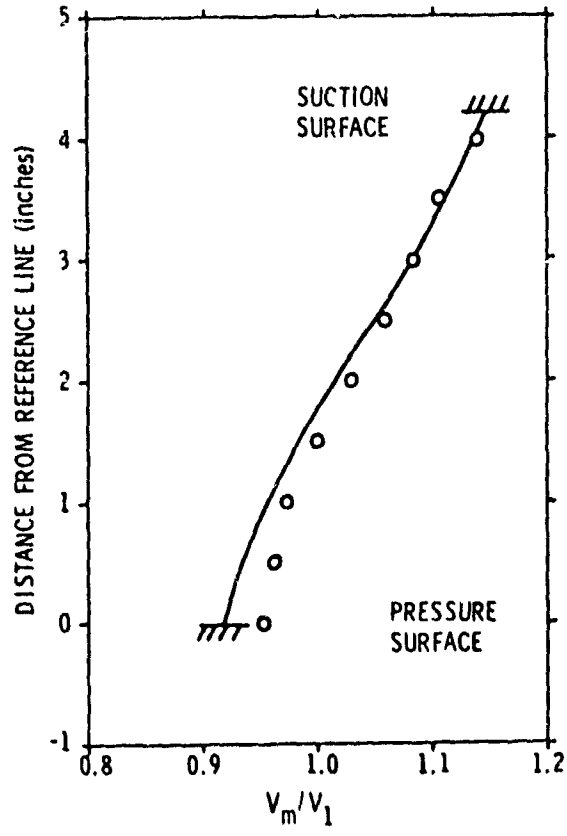

Figure 58. Comparison of the Theoretical and Experimental Velocity Profiles in the Test Cascade Reference Station at 20 Percent of the Blade Chord.

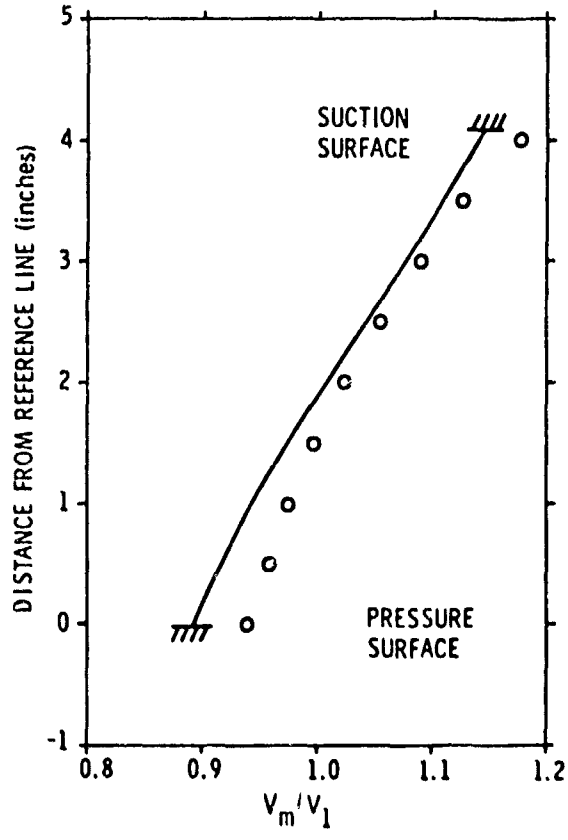

Figure 59. Comparison of the Theoretical and Experimental Velocity Profiles in the Test Cascade Reference Station at 30 Percent of the Blade Chord.

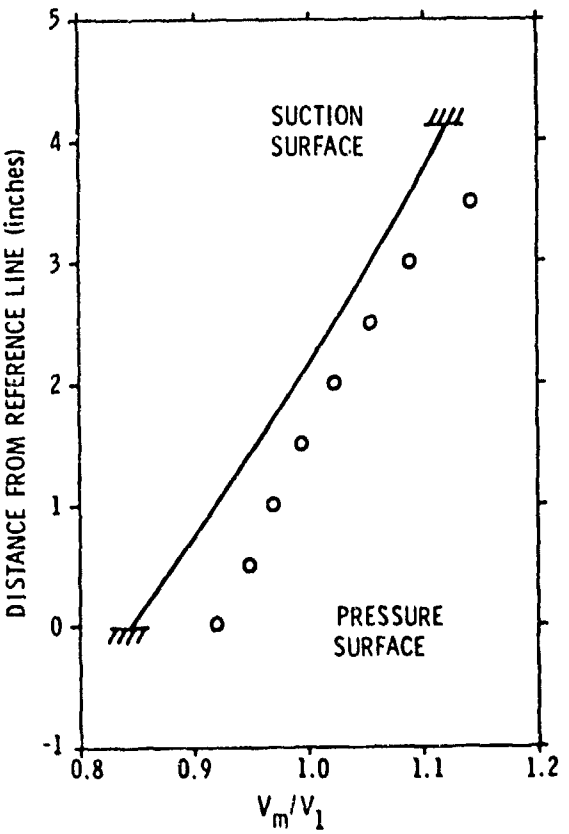

Figure 60. Comparison of the Theoretical and Experimental Velocity Profiles in the Test Cascade Reference Station at .0 Percent of the Blade Chord.

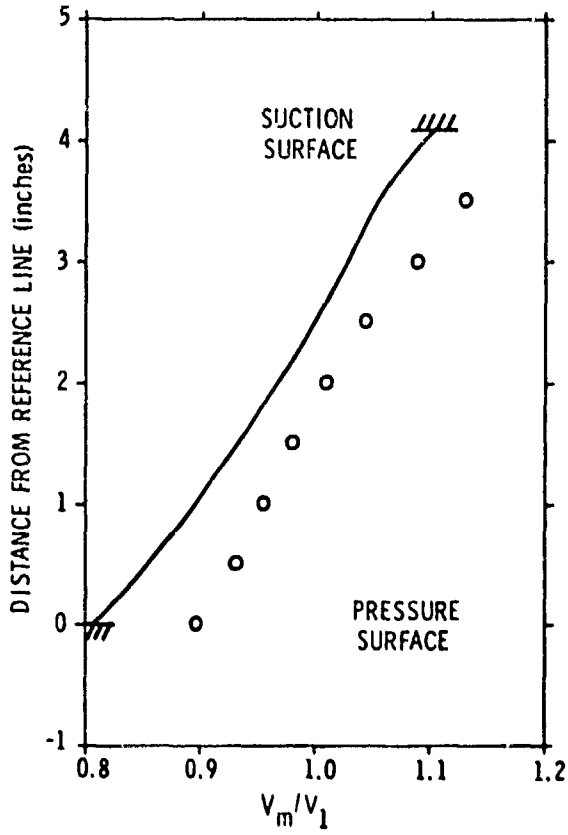

Figure 61. Comparison of the Theoretical and Experimental Velocity Profiles in the Test Cascade Reference Station at 50 Percent of the Blade Chord.

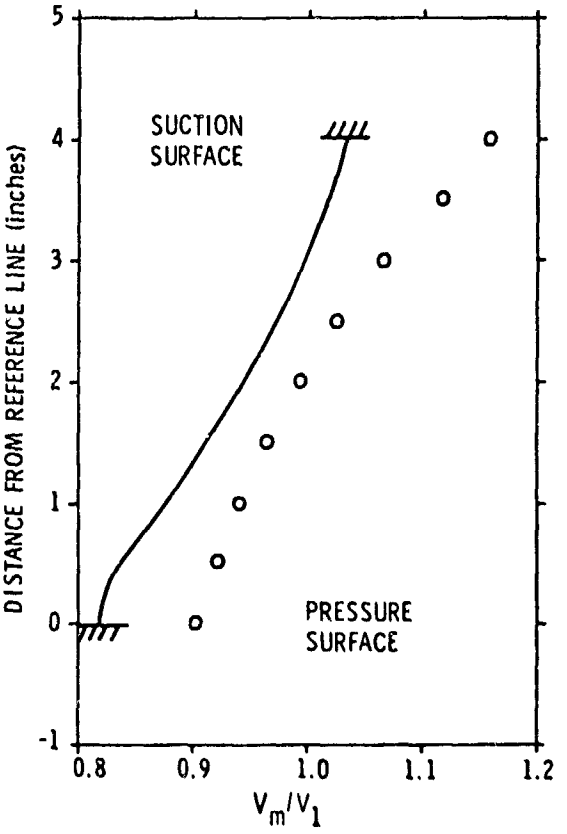

Figure 62. Comparison of the Theoretical and Experimental Velocity Profiles in the Test Cascade Reference Station at 60 Percent of the Blade Chord.

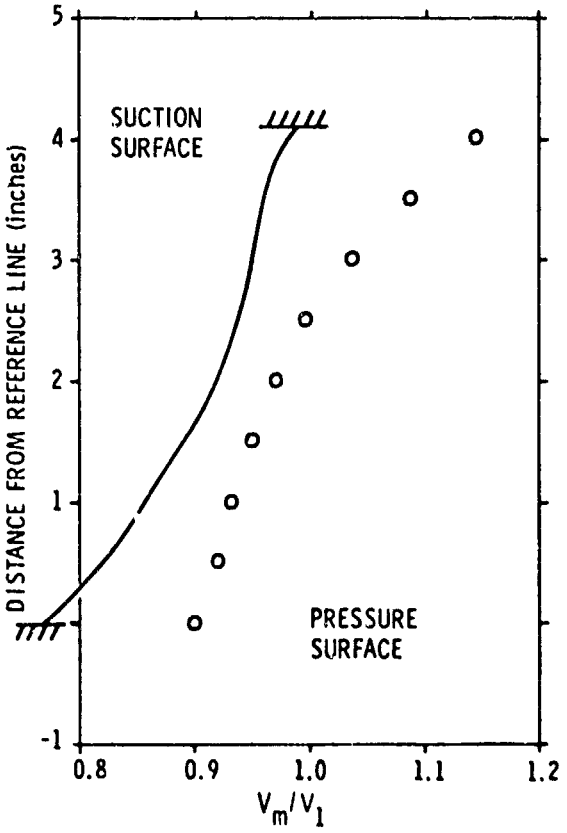

Figure 63. Comparison of the Theoretical and Experimental Velocity Profiles in the Test Cascade Reference Station at 70 Percent of the Blade Chord.

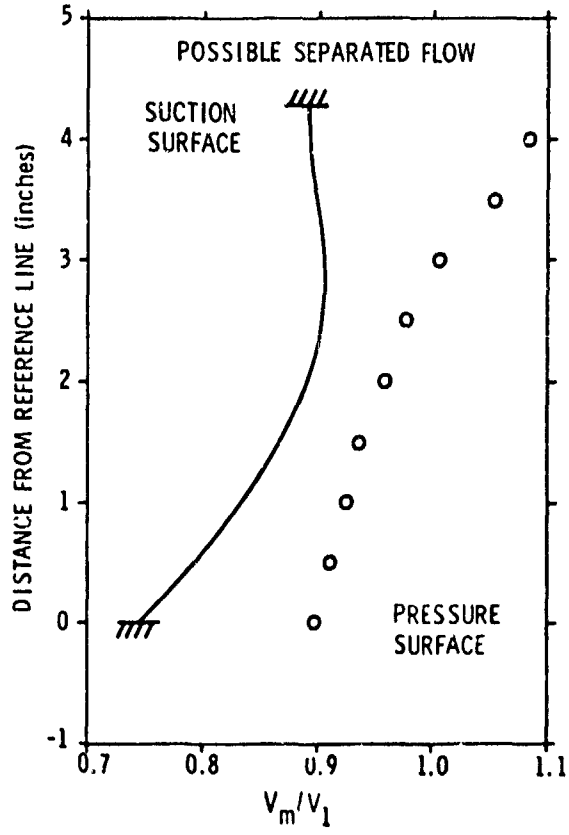

Figure 64. Comparison of the Theoretical and Experimental Velocity Profiles in the Test Cascade Reference Station at 80 Percent of the Blade Chord.

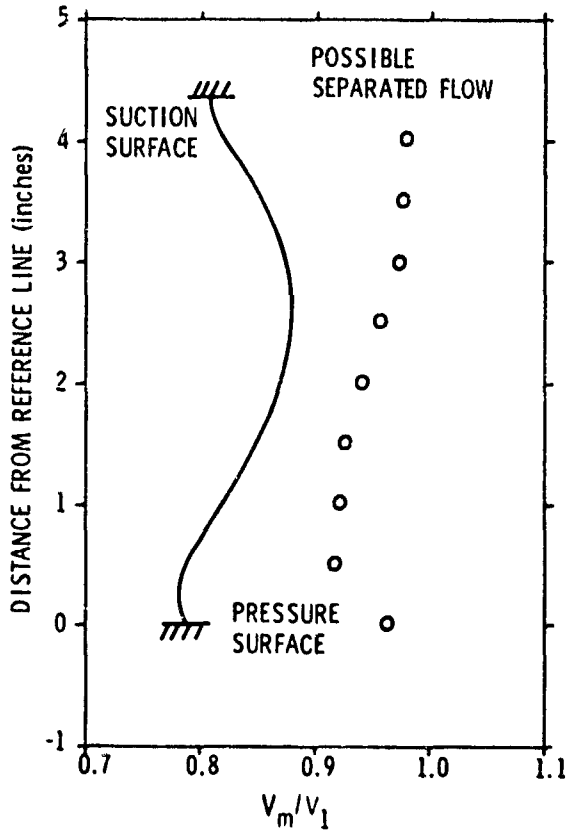

Figure 65. Comparison of the Theoretical and Experimental Velocity Profiles in the Test Cascade Reference Station at 90 Percent of the Blade Chord.

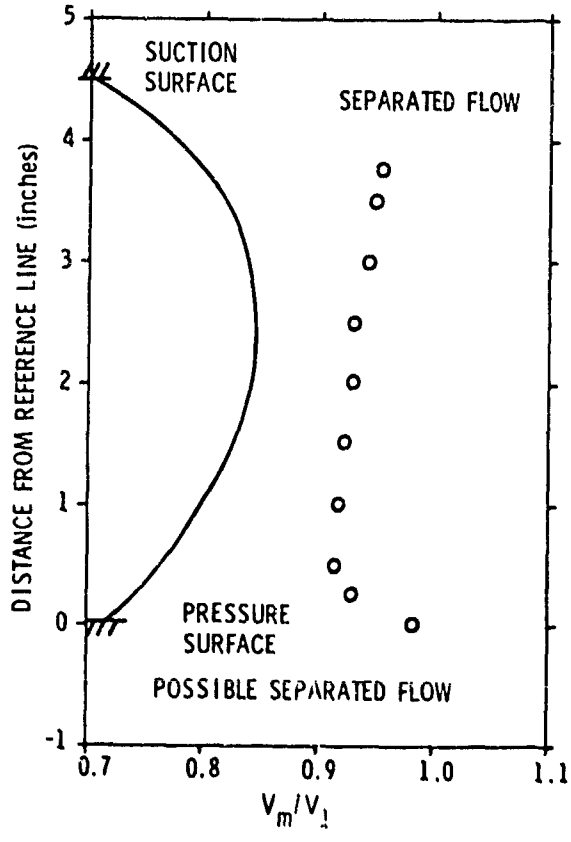

Figure 66. Comparison of the Theoretical and Experimental Velocity Profiles in the Test Cascade Reference Station Coincident with Trailing Edge.

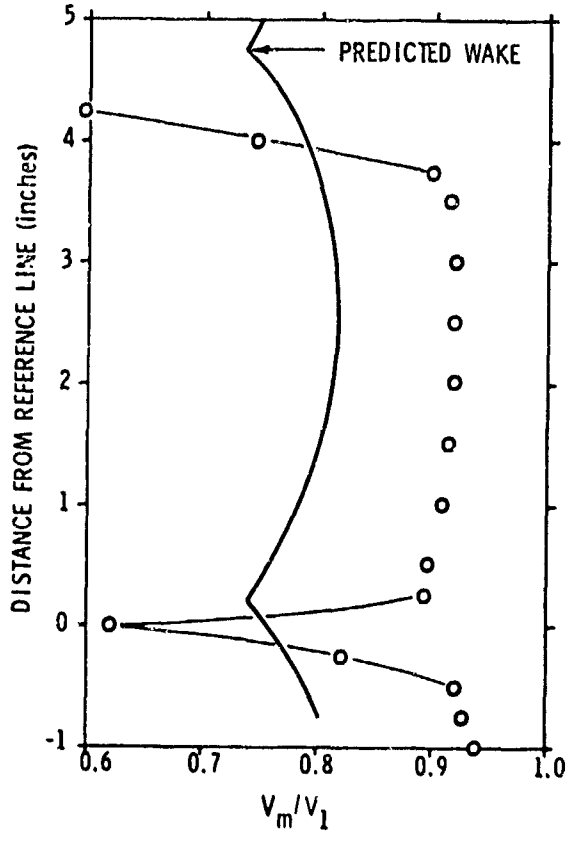

Figure 67. Comparison of the Theoretical and Experimental Velocity Profiles in the Test Cascade Reference Station 20 Percent Blade Chord Downstream.

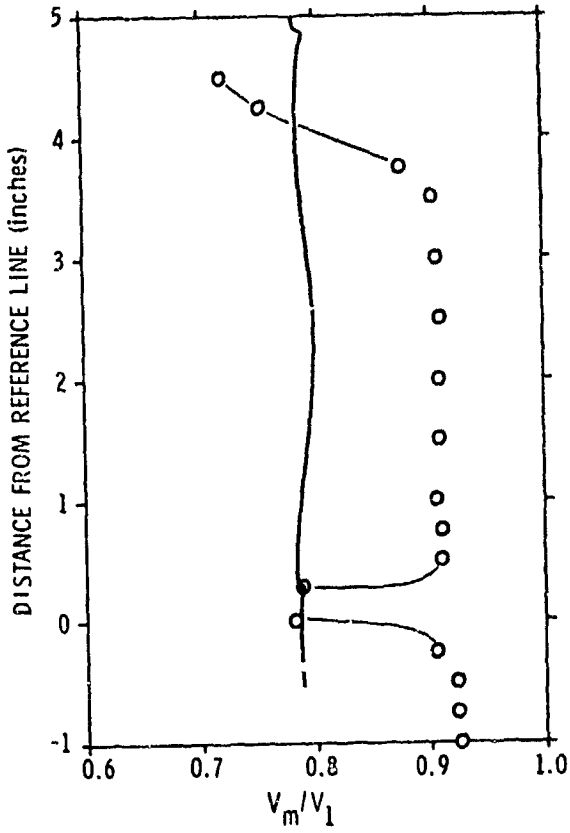

Figure 68. Comparison of the Theoretical and Experimental Velocity Profiles in the Test Cascade Reference Station 50 Percent Blade Chord Downstream.

Examination of the velocity profiles on each reference station reveals the following. Agreement between experiment and analytical results is good up to 40 percent of the blade chord. Figure 55 represents a station 20 percent of the chord upstream of the blade row. The significant feature of this plot is that there are induced velocity effects propagated upstream which are represented by the analysis method. Also seen in this plot is an indication that the periodic nature of the flow is not precisely maintained at this station, due to the required cusping of the stagnation streamline at the blade leading edge. The localized error, however, is only on the order of 3 percent.

Figures 56 through 59 show excellent agreement of the predicted and experimental velocity profiles, both in magnitude and form.

Between 40 percent and 60 percent of the blade chord (Figures 60 through 67), some divergence in magnitude of the profile is seen. The differences increase to the point where, at 60 percent of the chord, the measured velocity is uniformly 5 percent high. This is due to the blade row underturning, because the blade row design is diffusing, rather than accelerating, the flow.

From 70 percent to 100 percent of the chord, substantial (10 percent) errors in the velocity profiles are seen. A definite indication is present of the flow separation seen both on the pressure distribution and by the tuft method. Again, due to the blade row underdiffusing the flow, the indicated measured velocities are uniformly high.

Downstream of the cascade, the measured data clearly indicate the extent of the shed wake (Figures 67 and 68). Also seen is the failure of the analytical method to accurately model the wake structure. In

general, the measured velocities are 13 percent too high, due again to the blade row underturning.

An additional investigation was performed to help gain insight into the physical phenomenon associated with the cascade underturning. A tuft approximately 2 feet long was attached to the trailing edge pressure side of the central blade in the cascade. A protractor was used to measure the exit flow angle of the cascade relative to the inflow direction. These measurements were accurate to 1/2 degree and result in the plot of Figure 69. In the case of the as-designed data, there are three distinct flow regimes. Below a Reynolds number of 210,000, severe underturning is seen. This is probably due to a laminar separation at the minimum pressure point on the blade suction surface. Above this condition, the turning angle steadily increases to a steady value at a Reynolds number of 300,000, indicating a partial turbulent separation that moves toward the trailing edge as the velocity increases. As a test of the separation theory, a cloth tape trip, one-eighth inch wide was attached to each blade at 60 percent of the blade chord. Testing yielded the second curve on Figure 69. The turning angle with the tripped boundary layer is nearly constant, indicating that a separated boundary layer is responsible for the variation in turning angle with velocity or Reynolds number. The test cascade was designed to operate at a Reynolds number of 240,000, as indicated on Figure 69. The turning angle at this velocity agrees with that determined by the pressure distribution measurements and by the flow field surveys.

Pressure distributions were determined in each of the major flow regimes noted on Figure 69. These pressure distributions are plotted on Figure 70, and their corresponding velocities noted. The most

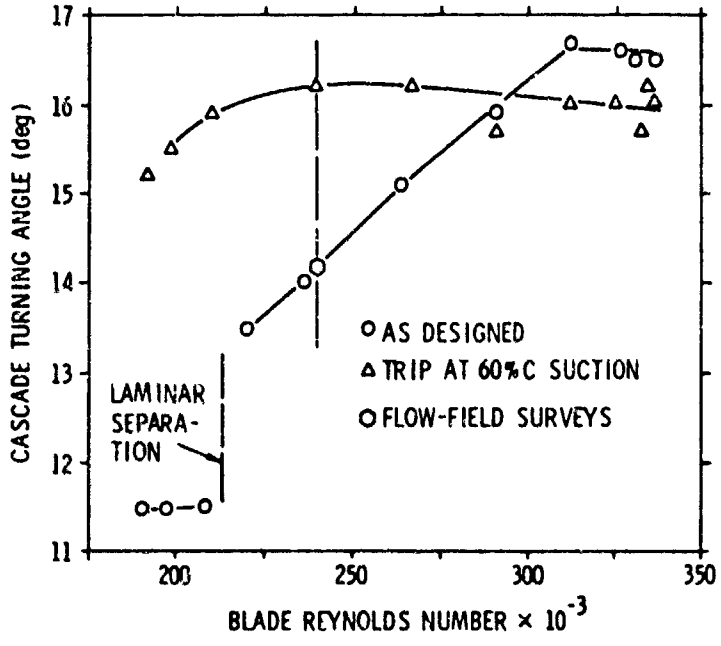

Figure 69. Cascade Turning Angle as a Function of Blade Chord Reynolds Number.

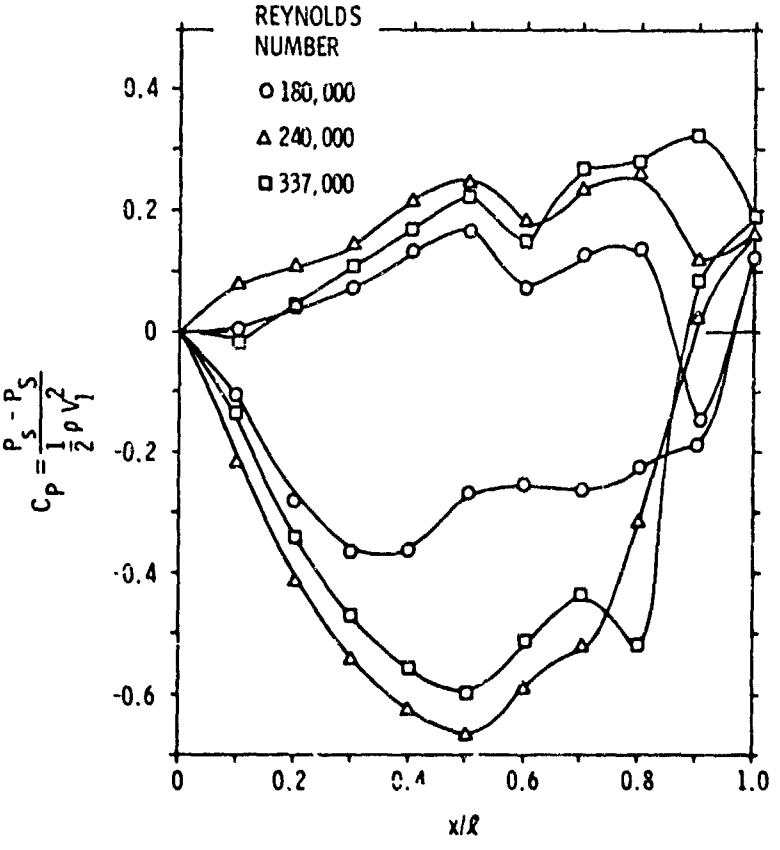

Figure 70. Experimental Cascade Blade Pressure Distribution as a Function of Blade Chord Reynolds Number.

interesting feature of this plot involves the pressure distribution for the lowest velocity case. Compared to the two higher velocity pressure distributions, a severe difference in pressure on the suction side can be seen. This indicates again the possibility of flow separation, perhaps initiated at 40 percent of the blade chord. At the highest velocity, the pressure distribution at the trailing edge is somewhat fuller, accounting for the additional turning noted previously.

Because of the possibility of laminar separation affecting the performance of the cascade, the turbulence level of the cascade test facility was measured with a hot wire annemometer and found to be on the order of 0.5 percent of the free stream velocity, which is quite low. This could account for the unexpected laminar separation and for the effect of the trip on the cascade performance. Additionally, the correlations used in the development of the boundary layer model used on the design process give no insight into the effect of the over-all turbulence level on the shape or extent of the boundary layer.

9.4 Summary of the Analytical and Experimental Comparisons

Examination of the analytical and experimental data available points to a major source of the problems encountered in this design. The ability to accurately predict the boundary layer characteristics on the suction side of the blades led to serious performance degradation. In addition, the wake model, influenced by the boundary layer, was unacceptable. A more accurate boundary layer model usable for boundary layers in an increasing pressure zone must be developed and included in the Streamline Curvature blade design method before a critical judgement of its usefulness can be made.

Further examination of the output of the blade design analysis, specifically Figure 42, shows that some refinements to the computational scheme are in order. To assure that the far upstream and downstream flow is uniform and parallel, the calculations should be performed to several chord lengths in both directions. Figure 42 indicates some convergence of the streamlines at the last calculation station, due to the presence of the wake. This region should be extended to achieve parallel flow. Increasing the number of calculation stations, streamlines, and cycles to convergence should improve the over-all accuracy of the method.

CHAPTER X

SUMMARY, CONCLUSIONS, AND RECOMMENDATIONS FOR FURTHER RESEARCH

10.1 Summary and Conclusions

The design and analysis of a turbomachine requires a method for predicting the three-dimensional flows which occur, along with methods of designing blade rows which produce the desired performance. A large class of turbomachines operate in flows which can be considered as being incompressible. These include axial, mixed, and radial flow pumps and turbines and low speed fans. The intent of this study is the development of a rational engineering solution for the analysis and design of these turbomachines.

The over-all performance of a turbomachine is related to the axisymmetric through-flow field within it. Various parameters affect the through-flow, including the duct or casing geometry, the fluid velocity and pressure at the inlet of the turbomachine, the geometric characteristics of the blade rows which change the total energy of the fluid, and the losses in energy due to viscous and turbulence effects. The accurate predicting of this through-flow field must consider all of these boundary conditions and satisfy the laws of fluid motion. A computerized numerical analysis has been developed to solve the equations of motion and satisfy these boundary conditions.

A Streamline Curvature Method is utilized as the basic solution for the through-flow. Equations for a steady, inviscid, incompressible flow

in an arbitrary shaped turbomachine are derived and a numerical method developed for their solution.

The equations of motion are developed in a way that allows the effects of blade spanwise and chordwise loading distributions to be included in the solution. This is an improvement over some earlier methods that treat a blade row as a thick actuator disk with uniform chordwise loading.

The effects of the blade thickness distribution and blade surface boundary layers may be incorporated into the solution. This point is important when high solidity blade rows are used.

The effects of viscosity and turbulence on the through-flow are very difficult to determine analytically; therefore, correlational data for specific types of turbomachines are used to correct the through-flow solution for these effects. The effects of viscosity and turbulence are included as a distributed total pressure loss. Determination of the specific distribution must rely on tests of turbomachines having a similar geometric form.

Blade rows whose surfaces are not perpendicular to the axisymmetric streamsurfaces in the turbomachine produce a component of blade force normal to the streamsurfaces. In some cases, this component can produce a significant effect on the through-flow. The magnitude of this force may be determined from the solution of the blade-to-blade flow fields on the individual streamsurfaces and included in the through-flow solution as a circumferentially-averaged pressure gradient normal to the streamsurfaces.

Several examples show the through-flow solution based on the Streamline Curvature Method to be accurate in predicting the

axisymmetric properties of the flow in turbomachines. The design of blade rows to provide a specified performance is difficult because of the effects of viscosity and turbulence. As with the through-flow analysis, it is necessary to include these effects in an empirical fashion. The Mean Streamline Method of Wislicenus uses correlations developed from experimental data to specify airfoil sections with a specified chordwise loading distribution and includes the effects on fluid turning due to viscosity and turbulence. The original correlation as developed by Wislicenus is based on a small number of experimental investigations A computerized method of analyzing the data generated by the testing of airfoils in two-dimensional cascades is developed.

A large volume of data for airfoil sections tested in a cascade are analyzed, the results are compared to the original data prepared by Wislicenus, and a new correlation is developed which extends the range of applicability of the Mean Streamline Method.

The improved Mean Streamline Method is adapted to the digital computer and can be used rapidly and reliably by a designer. Due to the complex nature of the flow between individual blades in a cascade, an analytical approach to the solution of the blade-to-blade flow field is desirable. This solution allows the effect of each of the geometric and flow parameters to be determined separately. Several methods for the analysis of the blade-to-blade flow field for defined geometries exist. However, an indirect or design solution which prescribes a blade shape which will provide a specified performance has been elusive.

A Streamline Curvature Method is developed to solve the indirect or design blade-to-blade flow problem. The solution relies on the numerical solution of the steady, inviscid, incompressible equations of fluid

motion, with the results corrected for the effects of viscosity and turbulence. The solution starts with a blade shape defined by the Mean Streamline Method and iteratively adjusts the camber line and thickness distribution to satisfy the prescribed boundary conditions. These boundary conditions include the specification of the chordwise loading and thickness distributions and the periodicity of the flow field upstream and downstream of the cascade. An empirical correction to the flow field is made to account for the effects of the blade surface boundary layers and the blade wake. The result of this analysis is a cascade blade geometry and the associated flow field in the blade-to-blade plane, which provides a specified performance.

An empirical cascade of blades was designed and tested in a cascade wind tunnel to verify this analysis. The experimental results indicate the potential of the design method to predict the flow field when the effects of viscosity and turbulence are small. However, serious difficulties were encountered in the boundary layer and wake regions of the flow field and suggested that more sophisticated models of these regions must be used.

The blade-to-blade flow solutions allow the computation of pressure gradients normal to the streamsurfaces in a turbomachine. These terms may be input to the through-flow solution to improve its accuracy in the region of the blade row and, thus, produce a three-dimensional model of the flow field in the blade row.

An axial flow pump stage was designed by the Streamline Curvature Method and the Mean Streamline Method and tested in a pump loop. Test results indicate that the total pressure rise through the stage is 13 percent higher than predicted. Analysis of the results reveals that the

experimental inflow velocity distribution is not the same as the design inflow or that anticipated for the actual application of the pump. Additionally, the estimated efficiency of the pump was probably too low during the preliminary design phase, contributing to the increased value of total pressure rise observed in the experimental results.

10.2 Recommendations for Further Research

The Streamline Curvature Method for predicting the axisymmetric through-flow in turbomachines can be improved and extended by considering the following areas of future research. The empirical correlations which are employed to include real flow effects can be made more general for axial flow units. This will require the testing and analysis of different configurations of axial flow pumps and turbines. Radial and mixed flow turbomachines are more difficult to design and their internal flow processes, especially boundary layer flows, are poorly understood. The Streamline Curvature Method developed in this study can be used for the prediction of the flow in a radial flow pump or turbine. Tests should be designed to provide the analysis with the same type of correlation data as used in the axial flow case.

The Mean Streamline Method of blade section design has been reliably employed for axial flow turbomachinery and two-dimensional cascades. A major improvement, including the capability to design blade sections in conformal planes would allow the application of this design method to mixed flow and perhaps radial flow turbomachinery. Experimental verification of the design method will be necessary to prove its usefulness and accuracy.

The Streamline Curvature Method developed in this study to design cascade airfoil sections will require a great deal of additional effort before reliable designs can be produced. The numerical solution of the equations can be improved by increasing the density of the calculation stations and number of streamlines used in the solution. The empirical data used to predict the boundary layer and wake effects will require a test and analysis program, along with an advanced theoretical approach to produce useful design correlations that properly account for Reynolds number effects. A series of two-dimensional cascade tests with accurate measurements of the boundary layer and wake profiles will help to produce the required correlations.

The development of a three-dimensional design solution for turbomachinery is required if maximum possible performance is to be obtained. An important part of this solution is the blade-to-blade flow solution. The Streamline Curvature Method of blade section design produces this flow field as a part of the design process. Improvements will have to be made, however, before the solution is reliable. Again, experimental comparisons of the flow fields in two-dimensional cascades will be necessary to improve the solution. Of great importance here is the experimental determination and comparison of the blade-to-blade flows in a rotating blade row.

The effects of blade body forces on the through-flow solution should be studied in greater depth. Occasionally, the blade geometry leads to significant components of the blade force normal to the streamsurfaces. This causes redistribution of the through-flow and, consequently, changes the performance of the turbomachine. A large rotating blade row, which exhibits a geometry leading to a streamsurface normal

force should be fully instrumented and its through-flow analyzed and compared to a theoretical solution.

When the blade-to-blade and through-flow solutions have been developed, a three-dimensional design solution can be developed by analytically coupling the two-dimensional solutions. In this solution, the blade row design is produced as a result of the specification of the through-flow. All effects of blade row forces, loading distributions, blade thickness, and the effects of viscosity and turbulence will be included and solved simultaneously. The output of such a procedure is the three-dimensional flow field in the blade-to-blade space and a blade geometry required to produce the flow field. If five blade-to-blade and meridional planes are specified as a minimum, the problem will require at least twenty times the computer power and complexity currently required. However, as testing of turbomachinery becomes more expensive and performance is pushed to higher levels, numerical design, modeling, and testing will become more attractive and more important. Comparison with experimental data will always be necessary to assure that the physical processes involved are understood and that the empirical data necessary to refine calculated flow models are accurate.

Improvement of the performance of turbomachinery operating in steady incompressible flow will require the continued refinement and expansion of numerical and mathematical flow models. The basic means of analysis and design presented in this study can be used and improved and will lead ultimately to the design of turbomachines that are more systematic and reliable and with improved levels of performance.

REFERENCES

1. Wu, C. H., "A General Theory of Three Dimensional Flow in Subsonic and Supersonic Turbomachines of Axial, Radial, and Mixed Flow Types," National Advisory Committee on Aeronautics, NACA TN 2604, 1952.

2. Wislicenus, G. F., Fluid Mechanics of Turbomachinery, New York, N. Y., Dover Publications Inc., 1965.

3. NASA Staff, Aerodynamic Design of Axial Flow Compressors, NASA SP-36, 1965.

4. Smith, L. H., Jr., "The Radial Equilibrium Equation of Turbomachinery," Trans. ASME, J. Eng. Power, 88A, 1, 1966.

5. Marsh, H., "A Digital Computer Program for the Through Flow Fluid Mechanics in an Arbitrary Turbomachine Using a Matrix Method," Aeronautical Research Council, ARC R&M 3509, 1966.

6. Katsanis, T., "Use of Arbitrary Quasi-Orthogonals for Calculating Flow Distribution in the Meridional Plane of a Turbomachine," NASA TN D-2546, December 1964.

7. Novak, R. A., "Streamline Curvature Computing Procedures for Fluid Flow Problems," Trans. ASME, J. Eng. Power, Vol. 89, 1967.

8. Bosman, C., and H. Marsh, "An Improved Method for Calculating the Flow in Turbomachines, Including a Consistent Loss Model," J. Mech. Eng. Sci., 1974.

9. Davis, W. R., and D. A. J. Millar, "A Comparison of the Matrix and Streamline Curvature Methods of Axial Flow Turbomachinery Analysis, from a User's Point of View," Trans. ASME, J. Eng. Power, January 1975.

10. McBride, M. W., "A Streamline Curvature Method of Analyzing Axisymmetric Axial, Mixed, and Radial Flow Turbomachinery," Applied Research Laboratory TM 77-219, The Pennsylvania State University, July 1977.

11. Billet, M. L., "An Approximate Method for the Solution of the Direct Problem of an Open Rotor," Applied Research Laboratory TM 78-161, The Pennsylvania State University, May 1978.

12. Brophy, M. C., Computer Assisted Design of Pump Impellers," Applied Research Laboratory TM 78-02, The Pennsylvania State University, January 1978.

13. Katsanis, T., "Use of Arbitrary Quasi-Orthogonals for Calculating Flow Distribution on a Blade-to-Blade Surface in a Turbomachine." NASA TN D-2809, May 1965.

14. Wilkenson, D. H., "Calculation of Blade-to-Blade Flow in a Turbomachine by Streamline Curvature," Aeronautical Research Council, ARC R&M 3704, 1972.

15. Thompson, D. S., "Finite Element Analysis of the Flow Through a Cascade of Aerofoils," University of Cambridge Department of Engineering, CUED/A-Turbo/TR 45, 1973.

16. McBride, M. W., "Refinement of the Mean Streamline Method of Blade Section Design," Trans. ASME, J. Fluids Eng., Vol. 99, September 1977.

17. Raj, R., and B. Lakshminarayana, "Characteristics of the Wake Behind a Cascade of Airfoils," J. Fluid Mechanics, Vol. 61, Part 4, 1973.

18. Smith, L. H., and H. Yeh, "Sweep and Dihedral Effects in Axial Flow Turbomachinery," Trans. ASME, J. Basic Eng., September 1963.

19. Lewis, R. I., and J. M. Hill, "The Influence of Sweep and Dihedral in Turbomachinery Blade Rows," J. Mech. Eng. Sci., Vol. 13, No. 4, 1971.

20. Howels, R., and B. Lakshminarayana, "Blade Dihedral in Axial Flow Propeller Pumps," Trans. ASME, J. Fluids Eng., March 1977.

21. Katsanis, T., and W. D. McNally, "Quasi-Three-Dimensional Flow Solution by Meridional Plane Analysis," NASA TM X-71593.

22. Katsanis, T., "Quasi-Three-Dimensional Calculation of Velocities in Turbomachine Blade Rows," Trans. ASME, J. Eng. Power, February 1973.

23. Novak, R. A., and R. M. Hearsey, "A Nearly Three-Dimensional Intra Blade Computing System for Turbomachinery," Part I and II, Trans. ASME, J. Fluids Eng., March 1977.

24. Erwin, J. R., et al, "Two Dimensional Low-Speed Cascade Investigation of NACA Compressor Blade Sections Having a Systematic Variation in Mean-Line Loading," National Advisory Committee on Aeronautics, NACA TN 3816, November 1956.

25. Gearhart, W. S., "Two-Dimensional Tests of a Compressor Blade Designed by the Mean Streamline Method," Applied Research Laboratory TM 71-32, The Pennsylvania State University, February 1971

26. McCormick, B. W., Jr., The Aerodynamics of VSTOL Flight, New York, N. Y., Academic Press, 1967.

27. Schlicting, H., "Application of Boundary Theory in Turbomachinery," Trans. ASME, J. Basic Eng., Series D, Vol. 91, pp. 543-551, 1959.

28. McBride, M. W., "Computerization of the Mean Streamline Blade Design Method," Applied Research Laboratory TM 73-22, The Pennsylvania State University, February 1973.

29. Wislicenus, G. F., and L. R. Smith, "Hydraulic Jet Propulsion and Incipient Cavitation," Internal Flow Research Report I-6, Part A, The Johns Hopkins University, Mechanical Engineering Department, March 21, 1952.

30. Shephard, D. G., Principles of Turbomachinery, 6th printing, The Macmillan Company, 1965.

31. Vennard, J. K., Elementary Fluid Mechanics, 4th ed., New York, N. Y., John Wiley and Sons, 1961.

32. Davis, R. F., "Marine Propulsor Blade Section Definition," Ordnance Research Laboratory TM 513-3531-04, The Pennsylvania State University, February 1969.

33. Abbott, I. H., and A. E. Von Doenhoff, Theory of Wing Sections, New York, N. Y., Dover Publications Inc.

34. Truckenbrodt, E., "A Method of Quadrature for Calculation of the Laminar and Turbulent Boundary Layer in Case of Plane and Rotationally Symmetric Flow," National Advisory Committee on Aeronautics, NACA TN 1397, May 1955.

35. Schlicting, H., Boundary Layer Theory, New York, N. Y., McGraw-Hill Book Co., Inc., 1960.

36. Horlock, J. H., Axial Flow Compressors, Butterworths, London, 1958.

37. Treaster, A. L., and A. M. Yocum, "The Calibration and Application of Five-Hole Probes," Proceedings of the 24th International Instrumentation Symposium, Albuquerque, N. M., 1978, Instrument Soc. of America.

38. Geising, J. P., "Extension of the Douglass-Neumann Computer Program of Problems of Lifting Finite Cascades," U. S. Dept. of Commerce, Report No. AD 605207.

DISTRIBUTION LIST FOR UNCLASSIFIED TM 79-33 by Mark W. McBride, dated February 13, 1979

Commander
Naval Sea Systems Command
Department of the Navy
Washington, DC 20362
Attn: Library
Code NSEA-09G32
(Copy Nos. 1 and 2)

Naval Sea Systems Command
Attn: E. G. Liszka
Code SEA 63R-1
(Copy No. 3)

Naval Sea Systems Command
Attn: T. E. Peirce
Code SEA 63R-31
(Copy No. 4)

Naval Sea Systems Command
Attn: A. R. Paladino
Code SEA 05H
(Copy No. 5)

Defense Documentation Center
5010 Duke Street
Cameron Station
Alexandria, VA 22314
(Copy Nos. 6 - 17)

Commanding Officer
Naval Underwater Systems Center
Newport, RI 02840
Attn: J. F. Brady
(Copy No. 18)

Naval Underwater Systems Center
Attn: Library
Code 54
(Copy No. 19)

Commanding Officer
Naval Ocean Systems Center
Department of the Navy
San Diego, CA 92152
Attn: J. W. Hoyt
Code 2501
(Copy No. 20)

Naval Ocean Systems Center
Attn: A. W. Fabula
Code 5311
(Copy No. 21)

Naval Ocean Systems Center
Attn: D. Nelson
Code 6343
(Copy No. 22)

Commander
Naval Ship Engineering Center
Department of the Navy
Washington, DC 20361
Attn: D. V. Burke
Code NSEC 6140B.1
(Copy No. 23)

Commander
Naval Surface Weapon Center
Silver Spring, MD 20910
Attn: Library
(Copy No. 24)

Commander
David W. Taylor Naval Ship R&D Center
Department of the Navy
Bethesda, MD 20084
Attn: R. J. Boswell
Code 1544
(Copy No. 25)

David W. Taylor Naval Ship R&D Center
Attn: R. A. Cumming
Code 1544
(Copy No. 26)

David W. Taylor Naval Ship R&D Center
Attn: W. K. Blake
Code 1942
(Copy No. 27)

David W. Taylor Naval Ship R&D Center
Attn: W. B. Morgan
Code 154
(Copy No. 28)

David W. Taylor Naval Ship R&D Center
Attn: M. Sevik
Code 19
(Copy No. 29)

Officer-in-Charge
David W. Taylor Naval Ship R&D Center
Department of the Navy
Annapolis Laboratory
Annapolis, MD 21402
Attn: J. G. Stricker
Code 2721
(Copy No. 30)

DISTRIBUTION LIST FOR UNCLASSIFIED TM 79-33 by Mark W. McBride, dated February 13, 1979

David W. Taylor Naval Ship R&D Center
Annapolis Laboratory
Attn: M. C. Brophy
Code 2721
(Copy No. 31)

Naval Postgraduate School
Monterey, CA 93940
Attn: Library
Code 0212
(Copy No. 32)

Philadelphia Naval Shipyard
U. S. Naval Base
Philadelphia, PA 19112
Attn: F. Halpin
Code 260.6
(Copy No. 33)

Bureau of Reclamation
U. S. Department of the Interior
Engineering and Research Center
Room 28, Bldg. 56
P. O. Box 25007
Denver Federal Center
Denver, CO 80225
Attn: Dr. Henry T. Falvey
(Copy No. 34)

NASA Lewis Research Center
21000 Brookpark Road
Cleveland, OH 44135
Attn: N. C. Sanger
MS 5-9
(Copy No. 35)

NASA Lewis Research Center
Attn: M. J. Hartmann
MS 5-9
(Copy No. 36)

NASA Lewis Research Center
Attn: D. M. Sandercock
MS 5-9
(Copy No. 37)

NASA Lewis Research Center
Attn: W. M. McNally
MS 5-9
(Copy No. 38)

NASA Lewis Research Center
Attn: Library
(Copy No. 39)

NASA Ames Research Center
Moffett Field, CA 94985
Attn: Library
(Copy No. 40)

NASA Ames Research Center
Attn: S. Bodapati
MA 227-9
(Copy No. 41)

NASA Langley Research Center
Hampton, VA 23365
Attn: Library
(Copy No. 42)

Air Force Aero Propulsion Laboratory
Wright-Patterson Air Force Base
Ohio 45433
Attn: Library
(Copy No. 43)

Air Force Office of Scientific Research
1400 Wilson Boulevard
Arlington, VA 22209
Attn: Dr. J. F. Masi
(Copy No. 44)

National Technical Information Service
Department of Commerce
5285 Port Royal Road
Springfield, VA 22151
Attn: Chief Input Section
(Copy No. 45)

Office of Naval Research
Department of the Navy
Arlington, VA 22217
Attn: J. Patton
(Copy No. 46)

Detroit Diesel Allison Division
P. O. Box 894
Indianapolis, IN 46206
Attn: Library
(Copy No. 47)

Garrett Corporation
AiResearch Manufacturing Company
Sky Harbor Airport
402 South 36th Street
Phoenix, AZ 85034
(Copy No. 48)

General Electric Company
Cincinnati, Ohio 45215
Attn: Library
(Copy No. 49)

DISTRIBUTION LIST FOR UNCLASSIFIED TM 79-33 by Mark W. McBride, dated February 13, 1979

General Electric Company
Corporate Research and Development
P. O. Box 8
Schenectady, NY 12301
Attn: Library
(Copy No. 50)

LTV Vought Aeronautics Company
P. O. Box 5907
Dallas, TX 75222
Attn: Library
(Copy No. 51)

Lockheed Propulsion Company
Scientific and Technical Library
P. O. Box 111
Redlands, CA 92373
Attn: Library
(Copy No. 52)

McDonald Aircraft Company
P. O. Box 516
St. Louis, MO 63166
Attn: Res. & Eng. Library
Dept. 218 - Bldg. 101
(Copy No. 53)

Pratt and Whitney Aircraft Division
Florida Res. & Dev. Ctr.
P. O. Box 2691
West Palm Beach, FL 33402
(Copy No. 54)

Pratt and Whitney Aircraft Division
United Aircraft Company
400 S. Main Street
East Hartford, CT 06108
Attn: Library
(Copy No. 55)

Allis-Chalmers Corporation
Hydro-Turbine Division
Box 712
York, PA 17405
Attn: R. K. Fisher
(Copy No. 56)

Allis-Chalmers Corp.
Attn: W. Whippen
(Copy No. 57)

Calspan Corporation
4455 Genessee Street
Buffalo, NY 14221
Attn: Head Librarian
(Copy No. 58)

MS-16 United Technologies
Research Center
Silver Lane
E. Hartford, CT 06118
Attn: E. M. Greitzer
(Copy No. 59)

Creare, Inc.
Box 71
Hanover, NH 03755
Attn: W. Swift
(Copy No. 60)

Rocketdyne Division
North American Aviation
6633 Canoga Avenue
Canoga Park, CA 91303
Attn: E. Jackson
Hydrodynamics Group
(Copy No. 61)

Aerojet General
Post Office Box 15847
Sacramento, CA 15813
Attn: Library
(Copy No. 62)

Hydronautics, Inc.
Pindell School Road
Laurel, MD 20810
Attn: J. Bohn
(Copy No. 63)

California Institute of Technology
Jet Propulsion Laboratory
4800 Oak Grove Drive
Pasadena, CA 91109
Attn: Library
(Copy No. 64)

California Institute of Technology
Division of Engineering for
Applied Sciences
Pasadena, CA 91109
Attn: Dr. Allan J. Acosta
(Copy No. 65)

DISTRIBUTIC" LIST FOR UNCLASSIFIED TM 79-33 by Mark W. McBride, dated February 13, 1979

Dr. George F. Wislicenus
351 Golf Court (Oakmont)
Santa Rosa, CA 95405
(Copy No. 66)

Massachusetts Institute of Technology
77 Massachusetts Avenue
Cambridge, MA 02139
Attn: Technical Reports
MIT Libraries
Room 14 E-210
(Copy No. 67)

Massachusetts Institute of Technology
Attn: Eng. Tech. Reports
Room 10-408
(Copy No. 68)

Virginia Polytechnic Inst. & State Univ.
Blacksburg, VA 24061
Attn: Library
(Copy No. 69)

Iowa State University
Mechanical Engineering Department
Ames, IA 50010
Attn: Dr. G. K. Serovy
(Copy No. 70)

Purdue University
Thermal Science & Prop. Center
West Lafayette, IN 47907
Attn: Dr. S. N. B. Murthy
(Copy No. 71)

University of Pennsylvania
Towne School of Civil & Mech. Eng.
Room 113 Towne, 220 S. 33rd St.
Philadelphia, PA 19104
Attn: Dr. Hsuan Yeh, Director
(Copy No. 72)

Stevens Institute of Technology
711 Hudson Street
Castle Point Station
Hoboken, NJ 07030
Attn: S. Tsakonas
(Copy No. 73)

Stevens Institute of Technology
Attn: Dr. Bruce D. Cox
(Copy No. 74)

Professor J. H. Horlock
Vice-Chancellor
University of Salford
Salford, M5, 4WT
England
(Copy No. 75)

Dr. John Foxwell
Admiralty Research Laboratory
Teddington, Middlesex
England
(Copy No. 76)

Whittle Turbomachinery Laboratory
Madingley Road
Cambridge
England
Attn: Library
(Copy No. 77)

Whittle Turbomachinery Laboratory
Attn: Sir William Hawthorne
(Copy No. 78)

Whittle Turbomachinery Laboratory
Attn: Dr. D. S. Whitehead
(Copy No. 79)

Dr. D. S. Thompson
Turbine Research Department
Rolls Royce Ltd.
P. O. Box 31
Derby
England
(Copy No. 80)

Professor R. E. Peacock
School of Mechanical Engineering
Cranfield Institute of Technology
Cranfield, Bedford MK430AL
England
(Copy No. 81)

Dr. Allen Moore
Admiralty Marine Technology Establishi
Teddington, Middlesex
England
(Copy No. 82)

J. Lewis
University of Newcastle
Newcastle
England
(Copy No. 83)

DISTRIBUTION LIST FOR UNCLASSIFIED TM 79-33 by Mark W. McBride, dated February 13, 1979

Dr. Peter van Oossanen
Haagsteeg 2
Postbox 28
6700 AA Wageningen
The Netherlands
(Copy No. 84)

Von-Karman Institute for Fluid Dynamics
Turbomachinery Laboratory
Rhode-Saint-Genese
Belgium
Attn: Library
(Copy No. 85)

Professor J. P. Gostelow
School of Mechanical Engineering
NSW Institute of Technology
Broadway
Sidney
Austrailia
(Copy No. 86)

Dr. rer. nat. Horst Merbt
Forschungsbeauftragter für Hydroakustik
8012 Ottobrunn B Munchen
Waldparkstr. 41
Munich
Germany
(Copy No. 87)

Carl-Anders Johnsson
Statens Skeppsprovningsanstalt
Box 24001
S-400 22 Goetborg
Sweden
(Copy No. 88)

Dr. V. H. Arakeri
Department of Mechanical Engineering
Indian Institute of Science
Bangalore 560 012
India
(Copy No. 89)

The Pennsylvania State University
Applied Research Laboratory
Post Office Box 30
State College, PA 16801
Attn: W. S. Gearhart
(Copy No. 90)

Applied Research Laboratory
Attn: B. Lakshminarayana
(Copy No. 91)

Applied Research Laboratory
Attn: M. W. McBride
(Copy No. 92)

Applied Research Laboratory
Attn: J. R. Ross
(Copy No. 93)

Applied Research Laboratory
Attn: A. L. Treaster
(Copy No. 94)

Applied Research Laboratory
Attn: Garfield Thomas Water Tunnel Files
(Copy No. 95)